ISJET

INTERNATIONAL SCIENTIFIC JOURNAL OF ENGINEERING AND TECHNOLOGY

Volume 6 No. 1 January-June 2022

ISSN 2586-8527 (Online)

Panyapiwat Institute of Management

Indexed in the Thai-Journal Citation Index (TCI 2)

INTERNATIONAL SCIENTIFIC JOURNAL OF ENGINEERING AND TECHNOLOGY (ISJET)

Volume 6 No. 1 January-June 2022

ISSN 2586-8527 (Online)
PANYAPIWAT INSTITUTE OF MANAGEMENT

INTERNATIONAL SCIENTIFIC JOURNAL OF ENGINEERING AND THCHNOLOGY (ISJET)
Volume 6 No. 1 January-June 2022
ISSN 2586-8527 (Online)

Panyapiwat Institute of Management
85/1 Moo 2, Chaengwattana Rd.,
Bang Talat, Pakkred,
Nonthaburi, 11120, Thailand
Tel. +66 2855 1560
Fax +66 2855 0392
E-mail: isjet@pim.ac.th
Website: https://ph02.tci-thaijo.org/index.php/isjet/index

INTERNATIONAL SCIENTIFIC JOURNAL OF ENGINEERING AND THCHNOLOGY (ISJET)

Volume 6 No. 1 January-June 2022 ISSN 2586-8527 (Online)

Objective:
International Scientific Journal of Engineering and Technology will be dedicated to serving as a forum to share knowledge on research advances in all fields of sciences: Engineering, Technology, Innovation, Information Technology, Management Information System, Logistics and Transportation, Agricultural Science and Technology, Animal Science and Aquaculture, Food Science, and other areas in Sciences and Technology. Submissions are welcomed from both PIM as well as other Thai and foreign institutions.

Scope:
Engineering, Technology, Innovation Technology, Management Information System, Logistics and Transportation, Agricultural Science and Technology, Animal Science and Aquaculture, Food Science, and other areas in Sciences and Technology

Type of Article:
• Research article
• Academic article
• Book review
• Review article

Languages of academic works:
Article written in either English languages are accepted for publication.

Reviewing Policy:
1. Any manuscript to be accepted for publication must have been reviewed and approved by at least three peer reviewers in that particular field or related fields.
2. The submitted manuscript must have never been published in any other periodical, and must not be in the approving process for publication by any other periodical. Also, the author must not plagiarize the work of other people.
3. The article, expression, illustrations, and tables that are published in the Journal are the sole responsibility of the author, and definitely not that of Panyapiwat Institute of Management.
4. The Editorial Board of International Scientific Journal of Engineering and Technology reserves right for decision making on publishing any article in the Journal.

Frequency of Publication:
Twice a year
• The first issue: January-June
• The second issue: July-December

Publication and Access Charges:
There are no charges to submit and publish all types of articles. Full articles in pdf format can be downloaded freely from the journal website at https://ph02.tci-thaijo.org/index.php/isjet/index

ISJET Journal Editorial Board
The office of Research and Development
Panyapiwat Institute of Management
85/1 Moo 2, Chaengwattana Rd.,
Bang Talat, Pakkred, Nonthaburi, 11120, Thailand
Tel. +66 2855 1560
Fax +66 2855 0392
E-mail: isjet@pim.ac.th
Website: https://ph02.tci-thaijo.org/index.php/isjet/index

INTERNATIONAL SCIENTIFIC JOURNAL OF ENGINEERING AND TECHNOLOGY (ISJET)
Volume 6 No. 1 January-June 2022
ISSN 2586-8527 (Online)

INTERNATIONAL SCIENTIFIC JOURNAL OF ENGINEERING AND TECHNOLOGY (ISJET)
Volume 6 No. 1 January-June 2022
ISSN 2586-8527 (Online)

Peer Reviewers

Assoc. Prof. Dr. Nattapon Chantarapanich	Kasetsart University, Sriracha Campus, Thailand
Assoc. Prof. Dr. Parinya Sanguansat	Panyapiwat Institute of Management, Thailand
Assoc. Prof. Dr. Patomsok Wilaipon	Naresuan University, Thailand
Assoc. Prof. Dr. Thananya Wasusri	King Mongkut's University of Technology Thonburi, Thailand
Assoc. Prof. Dr. Wilaiporn Lee	King Mongkut's University of Technology North Bangkok, Thailand
Asst. Prof. Dr. Adisak Joomwong	Maejo University, Thailand
Asst. Prof. Dr. Kanyarat Lueangprasert	Burapha University Sa Kaeo, Thailand
Asst. Prof. Dr. Nipat Jongsawat	Rajamangala University of Technology Thanyaburi, Thailand
Asst. Prof. Dr. Panomkhawn Riyamongkol	Naresuan University, Thailand
Asst. Prof. Dr. Phannachet Na Lamphun	Panyapiwat Institute of Management, Thailand
Asst. Prof. Dr. Weerawit Lertthaitrakul	Sripatum University Chonburi Campus, Thailand
Asst. Prof. Dr. Weerawut Thanhikam	Panyapiwat Institute of Management, Thailand
Dr. Kwankamon Dittakan	Graduate School, Prince of Songkla University, Thailand
Dr. Sanparith Marukatat	National Electronics and Computer Technology Center (NECTEC), Thailand

INTERNATIONAL SCIENTIFIC JOURNAL OF ENGINEERING AND TECHNOLOGY (ISJET)
Volume 6 No. 1 January-June 2022
ISSN 2586-8527 (Online)

PANYAPIWAT INSTITUTE OF MANAGEMENT
85/1 Moo 2, Chaengwattana Rd.,
Bang Talat, Pakkred, Nanthaburi,11120 Thailand

Dear Colleagues,

For more than half a decade now, many scientific articles have been published in this journal and I look forward to its continued success.

This new issue of ISJET highlights multidisciplinary contents, which include six original research articles, as follows: A Review of Object Detection Based on Convolutional Neural Networks and Deep Learning, Application of Analytic Hierarchy Process for Fulfillment Warehouse Location Selection, Automated Single-Pole Double-Throw Toggle Switch Pin Inspection using Image Processing and Convolutional Neural Network Techniques, Development of Business Intelligence System and Prediction with Data Mining of Lam Sam Kaeo Town Municipality, Thailand, Materials on Wheels: Batteries for Electric Vehicles, and Trend Analysis Based AMDF for Robust Pitch Detection of Speech Signals.

All authors and readers from around the world are invited to visit the website https://ph02.tci-thaijo.org/index.php/isjet/index. This link will grant you to submit your research to publish in our journal or will access to electronic versions of all issues of our journal. On behalf of the Editorial Board, I would like to take this opportunity to thank everyone who has complemented our goal by contributing to the ISJET.

With kind regards,

Assoc. Prof. Dr. Parinya Sanguansat
Editor-in-chief
isjet@pim.ac.th

INTERANTIONAL SCIETIFIC JOURNAL OF ENGINEERIN AND TECHNOLOGY (ISJET)
Volume 6 No. 1 January-June 2022
ISSN 2586-8527 (Online)

CONTENTS


PIM
PANYAPIWAT
INSTITUTE OF MANAGEMENT
สถาบันการจัดการปัญญาภิวัฒน์

A Review of Object Detection Based on Convolutional Neural Networks and Deep Learning

MingYuan Wang[1] and Watis Leelapatra[2]

[1,2]Department of Computer Engineering, Khon Kaen University, Thailand
E-mail: wangmingyuan@kkumail.com, watis@kku.ac.th

Received: January 26, 2022 / Revised: June 6, 2022 / Accepted: June 17, 2022

***Abstract*—Object detection, as one of the three main tasks of computer vision, is of great importance for the development of artificial intelligence in the future. The rapid advancement of convolutional neural networks (CNNs) and deep learning have provided a broader arena for object detection. From traditional methods to state-of-the-art algorithms, numerous innovative technologies and methods have been proposed. This paper reviews the one-stage and two-stage object detection algorithms and compares their advantages and shortcomings from various aspects. Some applications in real life, such as self-driving, weeding robots, and face recognition are illustrated in this paper. Finally, current issues and future studies direction prospect.**

***Index Terms*—Object Detection, Deep Learning, Computer Vision**

I. Introduction

Object detection technology is a fundamental part of computer vision research and essential for the development of artificial intelligence. The core task is to process the image data, using various feature extraction and classification algorithms to obtain useful semantic and positional information, and ultimately to figure out the useful features in the image quickly, accurately, and reliably. But, the process of capturing images is inevitably affected by angle, light, equipment, and shading, which can cause distortion and noise results. To overcome and solve such problems, a great number of researchers have explored and proposed different algorithms from various aspects.

The basic process of a traditional algorithm consists mainly of region proposal selector, feature extraction, and classifier. Analysis of images that are stored in a computer, since images can be viewed mathematically as a data set with one or more matrices. The selector uses sliding windows of different sizes to slide sequentially from left to right and top to bottom on the image to find the region proposal. Then, feature extraction is performed on the region proposal. In traditional algorithms, Scale Invariant Feature Transform (SIFT) [1] and Histogram of Oriented Gradient (HOG) [2] are commonly used for feature extraction. The role of classifiers is to classify and identify the extracted features to achieve the purpose of object detection, and typical classifiers commonly used are Support Vector Machines (SVM) [3] and Deformable Part Model (DPM) [4].

Most state-of-the-art algorithms are based on convolutional neural networks (CNNs) and deep learning. The rapid development of CNNs and the Graphics Processing Units (GPU) have opened up new research directions for object detection. The ImageNet Large Scale Visual Recognition Challenge (ILSVRC) is one of the most popular and prestigious academic competitions in the field of machine vision in recent years. AlexNet [5] won the 2012 ILSVRC champion and was a milestone in computer vision for CNNs. Various structures were subsequently introduced, such as VGG [6], GoogLeNet [7], SPPnet [8], ResNet [9]. For different network structures, object detection algorithms can be divided into two categories, one is two-stage algorithms based on region proposals, such as R-CNN [10], Fast R-CNN [11], and Faster R-CNN [12]. The other is a regression-based end-to-end one-stage algorithm. The YOLO [13] and SSD [14] algorithms have performed very well. Both have their advantages and drawbacks. The one-stage algorithm is faster than the two-stage and has a higher Frames Per Second (FPS) in video detection, which can be applied to real-life situations, such as a self-driving car. The two-stage algorithm, on the other hand, is slower but has higher accuracy. So, it can be applied to situations where high accuracy is required.

II. Assessment Measures and Datasets

Popular measures used to evaluate object detection algorithms are Precision (P), Recall (R), F1 score, Average Precision (AP), Mean Average Precision (mAP), FPS, and the amount of parameters in the network. To better explain the above measures, we need to introduce the concept of Intersection over Union (IoU). IoU is a ratio of the area where the prediction box intersects the real box and the area where the two are combined, it reflects the deviation of the prediction result from the truth, the value is between 0 and 1, the closer to 1 the better the result. Thus, at a certain threshold level we can calculate the values of TP (True Positive), TN (True Negative), FP (False Positive) and FN (False Negative) according to the confusion matrix. The P shows the accuracy of detection, while the R shows the proportion of detected objects to the total number of true objects. The F1 is the summed average of the P and R. The values obtained at a specified threshold are rather lopsided in multiple classification tasks, so we calculate the corresponding P and R values of different thresholds and then plot the Precision-Recall curve (P-R curve). The area enclosed by the P-R curve with x and y axes is AP, which ranges from 0 to 1. The larger the AP, the better the model. Some models will predict several categories, and mAP is the value obtained by summing all AP values and then averaging.

Most algorithms use the principle of gradient descent to optimize the loss function and find optimal weight value. In order to optimize the result in the right direction, we need to feed our network with true results during the training process, this is supervised learning. Datasets play a crucial role in this kind of process. Popular data sets include VOC2007, VOC2012, Microsoft COCO [15], ImageNet [16] and Open Image Challenge Object Detection (OICOD). The VOC dataset was introduced in the PASCAL VOC Competition, the most important versions are VOC2007 and VOC2012, and they are the most widely used in the field of object detection. They split all images into three parts, the training set, the validation set, and the test set. As shown in Table I, VOC2007 and VOC2012 both consist of a large number of images. Each image has its corresponding xml file, which records the location and category information of those objects within an image.

TABLE I
Comparison of VOC2007 and VOC2012 Datasets

List	Train		Validation		Test	
	Image	Object	Image	Object	Image	Object
VOC2007	2501	6301	2510	6307	4952	12032
VOC2012	5717	13609	5823	13841	11540	27450
Total	8218	19910	8333	20148	16492	39482

III. Two-Stage Algorithms

A. R-CNN Model

Regions with CNN features (R-CNN) is one of the classical algorithms for two-stage object detection. The reason why it is called a two-stage algorithm is that in the object detection process, firstly, through some approaches, such as Selective Search [17], Multi-scale combinatorial grouping [18], or Edge Boxes method [19] to extract region proposal and then regression prediction is performed on the region proposal to obtain the predicted object, the whole detection consists of two stages. Compared to traditional object detection methods, R-CNN [10], proposed by Girshick in 2014, is the first to use CNNs to feature extraction of suggested region proposals.

This method achieves 58.5% mAP on the VOC2007 dataset, an improvement of 24.2% compared to DPMv5. However, R-CNN also faces many problems, the search method used is very time-consuming, which is one of the reasons why the whole network is not very time-efficient. Multiple models in the network have to be trained separately, which not only requires a lot of space to store those models but also increases training time. To solve the problem of inconsistent region proposal size, R-CNN directly changes the size of the input feature map, which inevitably loses some data from the original image.

B. Fast R-CNN Model

In 2015, the introduction of Fast R-CNN [11] improved the network structure of R-CNN and combined with SPPnet to propose a region of interest (RoI) pooling layer. This approach avoids the problem of repeated training of multiple suggestion boxes in R-CNN, and after RoI pooling, the problem of the inconsistent size of the fully connected layer that is obtained by Singular Value Decomposition (SVD) can be solved. The backbone network uses VGG-16 which has a deeper layer network. Testing on the VOC2007 dataset obtained mAP of 70%, while R-CNN and SPPnet were 66% and 63.1% respectively. The training time was also reduced from 84 hours in R-CNN to 9.5 hours, which is about 9 times faster than R-CNN. The whole detection process of Fast R-CNN still suffers some weaknesses.

1) *Using selective search methods to generate a large number of suggested regions proposal, resulting in a long training and prediction time, which has not yet achieved the purpose of real-time detection.*
2) *Multiple fully connected layers are used at end of the network and are calculated separately, the weights are not shared, which increases the number of parameters.*

C. Faster R-CNN Model

Ren et al. found that region proposal selection is a computational bottleneck during a two-stage algorithm, and therefore proposed the Faster R-CNN [12] in 2017 to address this problem. A new Region Proposal Network (RPN) is proposed to replace the sliding window in Fast R-CNN to generate regions proposal. RPN generates k anchor frames (k defaults is 9) in the convolutional feature layer. Anchor frames of different scales predict different sizes objects, and the location and classification are determined by category regression and anchor frame regression. This is also the advantage of Faster R-CNN, which improves the detection speed of whole network. Multi-channel convolutional layer, RPN layer, RoI pooling layer, classification and regression layer are responsible for feature extraction, region proposal selection, preventing images cropping distortion and optimization of results in its network respectively. A comparison with Fast R-CNN tested on different backbone networks revealed that Faster-RCNN with VGG-16 obtained 73.2% of mAP on the VOC2007 and the detection speed is 5 FPS. Due to large amount of down sampling in the network, however, the final anchor is less accurate for small objects, and the network also has more fully connected layers and a huge number of parameters, while the best FPS obtained from the test still does not meet the requirements of real-time detection.

TABLE II
PERFORMANCE COMPARISON OF TWO-STAGE ALGORITHMS

Model	Backbone	Speed/(f · s^{-1})	mAP/% VOC2007
R-CNN	AlexNet	0.03	58.5
Fast R-CNN	VGG-16	7	70
Faster R-CNN	VGG-16	5	73.2

IV. ONE-STAGE ALGORITHMS

A. YOLO Model

The YOLO method is one of the one-stage detection algorithms that has performed a number of modifications and improvements. Redmon et al. in 2016 innovated the idea of incorporating regression into the object detection task and proposed the YOLOv1 [13] model. A single convolutional network can predict the position of an object and its category from an image, while eliminating the need for regions proposal, resulting in a significant speed increase of up to 45 FPS. A smaller FAST YOLO network achieved 155 FPS, which was twice the speed of other real-time object detection models at the time.

The process of YOLOv1 is divided into three steps: (1) Reshape the input image to 448×448, while to prevent image distortion, filling in the edges around the image to maintain the original image ratio of width to height. (2) Feed images into the trained model for prediction, the Fully Connected Layer (FC) will output the predicted objects' position and category. (3) Finally, through the Non-Maximum Suppression (NMS) algorithm to filter the Bounding Box (bbox), select the best result, and plot bbox, category, and confidence on the image. The test result on the VOC2007 dataset was 63.4% mAP.

To compensate for some drawbacks in YOLOv1, Redmon et al. proposed YOLOv2 [20] model in 2017. The main improvement points include replacing the backbone network with DarkNet-19 and adding a batch normalization operation to each convolutional layer, allowing for as much reduction as possible in one direction during gradient descent, preventing the gradient from jumping back and forth. For multi-scale training, YOLOv2 changes the size of input images according to its own iteration process, thus meeting the requirements of multi-scale images for training. To some extent, these methods all benefit the detection speed and mAP, finally, with 40 FPS and 78.6% mAP on the VOC2007.

YOLOv3 [21], in 2018 Redmon et al. further optimized the network structure and loss function, etc., based on YOLOv2 to make the model more accurate and robust. In contrast to YOLOv2, the backbone of YOLOv3 is DarkNet-53, which has a deeper network structure and uses a residual structure to prevent gradient disappearance. The Feature Pyramid Networks (FPN) [22] structure is also used to extract multi-scale features from images, which effectively improves the detection accuracy of small objects.

Bochkovskiy et al. proposed YOLOv4 [23] model in 2020. YOLOv4 was designed to achieve goals of higher speed and accuracy. Various network optimization solutions are used to improve network performance, such as increasing receptive fields, data augmentation, and changing the loss function. The backbone network was replaced with CSPDarkNet-53, which was experimentally found to be more suitable for object detection networks. Multichannel fusion using Path Aggregation Network (PANet) discards the previous FPN to improve the receptive field of the input images.

B. SSD Model

SSD [14] was proposed by Liu et al. in 2016 as a new end-to-end and one-stage object detection model based on YOLOv1. To overcome the inaccurate problem of small objects in YOLOv1, the SSD network structure is based on the VGG network, replacing the fully connected layers with 6 different sizes CNNs. Small objects are predicted by the front convolutional network, while large objects are detected by the back convolutional network. Experiments have also demonstrated that mixed-scale feature images can effectively improve accuracy.

Also, data enhancement is essential and SSD improves whole network robustness by changing the scale size of images, with a result of 79.8% mAP on the VOC2007. Unlike YOLOv1 which uses a fully connected layer to output results, SSD removes the last fully connected layer and uses a convolutional network to output results directly, reducing the total amount of parameters in the network.

In 2017 Jeong et al. proposed the R-SSD [24] model by combining pooling with deconvolution rather than expanding the number of feature maps. This approach allows the entire network to be characterized by both low-and high-resolution feature maps. The result is an increase in detection accuracy and speed without increasing network parameters and a better score of 80.8% mAP on VOC2007.

Under the influence of SSD, the improved models DSSD [25] and FSSD [26] have also been proposed sequentially. DSSD changes backbone of SSD from VGG to ResNet-101 that is a residual structure and a deeper network, which can effectively improve the accuracy and prevent gradients from disappearing during backpropagation. The mAP reached 81.5% on the VOC2007 dataset, but DSSD detection speed was only 5.5 FPS, which is one of drawbacks of this model. Like YOLOv3, inspired and influenced by feature pyramid structure, Li et al. introduced FSSD, which up samples and down samples input images while fusing different layers to create a richer network. It was then tested on the VOC2007 and obtained results of 82.7% mAP and 65.8 FPS.

C. RetinaNet Model

Lin et al. 2017 first proposed that the extreme foreground-background class imbalance can also have an impact on the prediction results, and used a new focal loss function to address this problem, making the entire training process more focused on difficult samples, and subsequently proposed the RetinaNet [27] model. In RetinaNet, the ResNet network is first used as backbone network, then the feature pyramid structure is also used to obtain rich multi-scale feature maps, finally there are two sub-networks responsible for category regression and prediction box regression respectively. When compared to YOLOv2 and DSSD algorithms, RetinaNet-101 has a clear advantage, with a mAP of 17.5% higher than YOLOv2 and 6.1% higher than DSSD513 when tested on the COCO dataset.

TABLE III
PERFORMANCE COMPARISON OF OEN-STAGE ALGORITHMS

Model	Backbone	Speed/(f · s^{-1})	mAP/%		
			VOC2007	VOC2012	COCO
YOLOv1	VGG-16	45	63.4	57.9	-
YOLOv2	Darknet-19	40	78.6	73.5	21.6
YOLOv3	Darknet-53	51	-	-	57.9
YOLOv4	CSPDarknet-53	23	-	-	43.5
SSD	VGG-16	19.3	79.8	78.5	28.8
R-SSD	VGG-16	16.6	80.8	-	-
DSSD513	ResNet-101	5.5	81.5	80.8	33.2
FSSD	VGGNet	65.8	82.7	-	-
RetinaNet	ResNeXt-101+FPN	5.4	-	-	40.8

V. PRACTICAL APPLICATIONS

A. Self-Driving Cars

The ability to effectively and quickly recognize objects while driving is a key technology and challenge for self-driving cars, and one-stage object detection algorithms based on CNNs offer the possibility to achieve this. Real-time scene analysis and detection during driving can provide path planning and active safety measures. Fast and compact models are also a trend for the development of object detection on automotive platforms. In 2022, Li et al. proposed an EfficientDet-Gs [28] model with better efficiency and fewer network parameters based on the EfficientDet [29]. Based on YOLOv3, Zhang et al. [30] applied adaptive feature fusion and DSC approaches to improve network performance, and devised a technique to help drivers by automatically detecting vehicle license plates.

B. Weeding Robots

Although herbicides can be effective to eliminate weeds in agriculture, they also have many harmful effects. New weed control methods such as mechanical weeding, laser weeding and flame weeding are all based on the object detection. In 2018, Sun et al. [31] improved AlexNet to detect crops and weeds by using atrous convolution and global

pooling, finally achieved better results compared to the original AlexNet, with an accuracy of over 90%. Zhang et al. [32] applied three different backbone networks, VGG-16, ResNet-50 and ResNet-101, to the Faster R-CNN model for ablation experiments and successfully applied CNNs to the oilseed rape and weeds recognition, through using migration model and testing on the COCO dataset, achieving precision and recall of 83.90% and 81.30%, respectively.

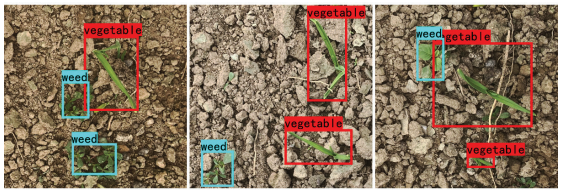

Fig. 1. Weeds detection results of weeding robot

C. Face Recognition

With the development of numerous detection algorithms, face recognition also is one of the great successful applications and provides many conveniences to your daily life. Face recognition can be used in a lot of industries, such as contactless payment, phone unlock, criminal investigation and pedestrian detection. As shown in Fig. 2, Jiang et al. [33] have found the sharing of convolutional layers would affect the effectiveness of face recognition using the Faster R-CNN. In 2021, Li et al. [34] proposed that illumination is an important factor for the performance of face recognition and established face datasets based on different light intensities, finally improved the detection accuracy to 98%.

Fig. 2. Face recognition results of Faster R-CNN

VI. Conclusion

This paper focuses on the evolution of object detection algorithms and their trends. Convolutional neural networks and deep learning algorithms stand out for their powerful feature extraction and excellent classification characteristics. Through a comprehensive overview to two kinds of object detection algorithms, we describe their concepts, network structure, and implementation methods, as well as evaluate their advantages and shortcomings, and then outline some applications in our daily lives. In general, the market for object detection is promising and potential. However, it also still faces many problems that need to solve such as:

1) Supervised learning requires a large number of data sets as support. It is only through tremendous training that the loss function can be optimally solved and weights can be optimized. However, due to confidentiality, capture difficulties and other reasons caused a lack of datasets in some industries.

2) Detection of small objects has always been a difficult problem, because the pixel data of small objects on the image is lacking, so training process cannot achieve a very satisfactory result. This is also one of the directions that need to be studied in the future.

3) For large datasets processing, only focusing on speed improvement is unrealistic since we should consider many factors, such as the parameter number, the performance of GPU, and the depth of the whole network. A reasonable strategy is to find out an acceptable balance between speed and economy according to our practical application.

REFERENCES

[1] G. Bingtao, W. Xiaorui, C. Yujiao et al., "High-Accuracy Infrared Simulation Model Based on Establishing the Linear Relationship between the Outputs of Different Infrared Imaging Systems," *Infrared Physics & Technology*, vol. 69, pp. 155-163, Mar. 2015.

[2] N. Dalal and B. Triggs, "Histograms of Oriented Gradients for Human Detection," in *Proc. 2005 IEEE Computer Society Conference on Computer Vision and Pattern Recognition (CVPR'05)*, 2005, pp. 886-893.

[3] S. R. Gunn, "Support Vector Machines for Classification and Regression," *ISIS Technical Report*, vol. 14, pp. 5-16, May. 1998.

[4] P. F. Felzenszwalb, R. B. Girshick, D. McAllester et al., "Object Detection with Discriminatively Trained Part-Based Models," *IEEE Transactions on Pattern Analysis and Machine Intelligence*, vol. 32, pp. 1627-1645, Sep. 2010.

[5] A. Krizhevsky, I. Sutskever, and G. E. Hinton, "Imagenet Classification with Deep Convolutional Neural Networks," *Advances in Neural Information Processing Systems*, vol. 25, pp. 1097-1104, 2012.

[6] K. Simonyan and A. Zisserman, "Very Deep Convolutional Networks for Large-Scale Image Recognition," *arXiv Preprint arXiv:1409.1556*, vol. 1, pp. 1-14, Sep. 2014.

[7] C. Szegedy, W. Liu, Y. Jia et al., "Going Deeper with Convolutions," in *Proc. IEEE Conference on Computer Vision and Pattern Recognition*, 2015, pp. 1-9.

[8] K. He, X. Zhang, S. Ren et al., "Spatial Pyramid Pooling in Deep Convolutional Networks for Visual Recognition," *IEEE Transactions on Pattern Analysis and Machine Intelligence*, vol. 37, pp. 1904-1916, Jan. 2015.

[9] K. He, X. Zhang, S. Ren et al., "Deep Residual Learning for Image Recognition," in *Proc. IEEE Conference on Computer Vision and Pattern Recognition*, 2016, pp. 770-778.

[10] R. Girshick, J. Donahue, T. Darrell et al., "Rich Feature Hierarchies for Accurate Object Detection and Semantic Segmentation," in *Proc. IEEE Conference on Computer Vision and Pattern Recognition*, 2014, pp. 580-587.

[11] R. Girshick, "Fast r-cnn," in *Proc. IEEE International Conference on Computer Vision*, 2015, pp. 1440-1448.

[12] S. Ren, K. He, R. Girshick et al., "Faster R-CNN: Towards Real-Time Object Detection with Region Proposal Networks," *Advances in Neural Information Processing Systems*, vol. 28, pp. 1137-1149, Jun. 2015.

[13] J. Redmon, S. Divvala, R. Girshick et al., "You Only Look Once: Unified, Real-Time Object Detection," in *Proc. IEEE Conference on Computer Vision and Pattern Recognition*, 2016, pp. 779-788.

[14] W. Liu, D. Anguelov, D. Erhan et al., "Ssd: Single Shot Multibox Detector," *European Conference on Computer Vision*, 2016, pp. 21-37.

[15] T. Lin, M. Maire, S. Belongie et al., "Microsoft COCO: Common Objects in Context," in *Proc. European Conference on Computer Vision*, 2014, pp. 740-755.

[16] J. Deng, W. Dong, R. Socher et al., "ImageNet: A Large-Scale Hierarchical Image Database," *IEEE*, pp. 248-255, Jun. 2009.

[17] J. R. Uijlings, K. E. Van De Sande, T. Gevers et al., "Selective Search for Object Recognition," *International Journal of Computer Vision*, vol. 104, pp. 154-171, Sep. 2013.

[18] P. Arbeláez, J. Pont-Tuset, J. T. Barron et al., "Multiscale Combinatorial Grouping," in *Proc. IEEE Conference on Computer Vision and Pattern Recognition*, 2014, pp. 328-335.

[19] C. L. Zitnick and P. Dollár, "Edge Boxes: Locating Object Proposals from Edges," in *Proc. European Conference on Computer Vision*, 2014, pp. 391-405.

[20] J. Redmon and A. Farhadi, "YOLO9000: Better, Faster, Stronger," in *Proc. IEEE Conference on Computer Vision and Pattern Recognition*, 2017, pp. 7263-7271.

[21] J. Redmon and A. Farhadi, "YOLOv3: An Incremental Improvement," *arXiv Preprint arXiv:1804.02767*, pp. 1-6, Apr. 2018.

[22] T. Lin, P. Dollár, R. Girshick et al., "Feature Pyramid Networks for Object Detection," in *Proc. IEEE Conference on Computer Vision and Pattern Recognition*, 2017, pp. 2117-2125.

[23] A. Bochkovskiy, C. Wang, and H. M. Liao, "YOLOv4: Optimal Speed and Accuracy of Object Detection," *arXiv Preprint arXiv:2004.10934*, pp. 1-17, Apr. 2020.

[24] J. Jeong, H. Park, and N. Kwak, "Enhancement of SSD by Concatenating Feature Maps for Object Detection," *arXiv Preprint Arxiv:1705.09587*, pp. 1-12, May. 2017.

[25] C. Fu, W. Liu, A. Ranga et al., "DSSD: Deconvolutional Single Shot Detector," *arXiv Preprint arXiv:1701.06659*, Jan. 2017.

[26] Z. Li and F. Zhou, "FSSD: Feature Fusion Single Shot Multibox Detector," *arXiv Preprint arXiv:1712.00960*, Dec. 2017.

[27] T. Lin, P. Goyal, R. Girshick et al., "Focal Loss for Dense Object Detection," in *Proc. IEEE International Conference on Computer Vision*, 2017, pp. 2980-2988.

[28] Y. LI, X. Zhang, M. Zhang et al., "Object Detection in Autonomous Driving Scene Based on Improved Efficient Diet," *Computer Engineering and Applications*, vol. 58, pp. 183-191, Mar. 2022.

[29] M. Tan, R. Pang, and Q. V. Le, "Efficientdet: Scalable and Efficient Object Detection," in *Proc. EE/CVF Conference on Computer Vision and Pattern Recognition*, 2020, pp. 10781-10790.

[30] J. Zhang, Y. Xiong, X. Sun et al., "License Plate Detection Using Siamese Feature Pyramid and Cascaded Positioning," *Computer Engineering and Applications*, vol. 12, no. 12, pp. 1-15, Nov. 2021.

[31] J. Sun, X. He, W. Tan et al., "Recognition of Crop Seedling and Weed Recognition Based on Dilated Convolution and Global Pooling In CNN," *Transactions of the Chinese Society of Agricultural Engineering*, vol. 34, pp. 159-165, 2018.

[32] L. Zhang, X. Jin, L. Fu et al., "Recognition Method for Weeds in Rapeseed Field Based on Faster R-Cnn Deep Network," in *Proc. IEEE International Conference on Automatic Face & Gesture Recognition*, 2020, pp. 304-312.

[33] H. Jiang and L. Erik, "Face Detection with The Faster R-CNN," in *Proc. IEEE International Conference on Automatic Face & Gesture Recognition*, 2017, pp. 650-657.

[34] W. Li, Y. Liu, and G. Xing, "Illumination Analysis of Deep Face Recognition," *Journal of Computer-Aided Design & Computer Graphics*, vol. 34, pp. 74-83, Nov. 2021.

MingYuan Wang received a B.Eng. degree in Mechanical Design, Manufacturing, and Automation from Henan University of Science and Technology, Henan, China, in 2013. Past work experience as an acting product designer at YTO Group Corporation from 2014 to 2020. He currently is a graduate student at the Department of Computer Engineering, Khon Kaen University, Thailand. His current research interests include computer vision and its applications to other science and engineering areas.

Watis Leelapatra received a B.Eng in Computer Engineering from Khon Kaen University, Khon Kaen, Thailand, an M.S. degree in Computer Science from the Case Western Reserve University, Cleveland, USA, and a D.Eng. degree in Computer Science from Asian Institute of Technology, respectively. He is concurrently a lecturer at the Department of Computer Engineering, Khon Kaen University.

Application of Analytic Hierarchy Process for Fulfillment Warehouse Location Selection

Anupong Thuengnaitham

Faculty of Logistics and Transportation Management, Panyapiwat Institute of Management, Nonthaburi, Thailand
E-mail: anupongthu@pim.ac.th

Received: July 23, 2021 / Revised: April 20, 2022 / Accepted: May 10, 2022

***Abstract*—The objective of this research is to apply the analytic hierarchy process to select the best fulfillment warehouse location for a 4PL (Fourth Party Logistics Service Provider) company that is seeking a new warehouse to support the growth of its business. The pairwise comparison judgments were collected from the company's management team by using a questionnaire to consider five location candidates in the Bangkok Metropolis Region and Vicinity. In the study, three main criteria and nine sub-criteria related to the facilities, transportation, market, and workforce were analyzed. The results show that the proposed model is able to determine the importance weights of criteria and sub-criteria for the fulfillment warehouse location selection. The highest priority criterion is transportation (41.7%). The subsequent priorities were assigned to facilities (37.6%) and market and workforce (20.7%) when selecting a fulfillment warehouse location according to the obtained weights. Finally, fulfillment warehouse location 2 (24.6%) is the first priority for location, followed by location 1, location 5, location 4, and location 3, respectively.**

***Index Terms*—Multi-Criteria Decision Making, Analytic Hierarchy Process, Warehouse Location Selection, Fulfillment Warehouse**

I. Introduction

The COVID-19 outbreak has disrupted the entire world in terms of health, society, economy, and business operations. In particular, COVID-19 has had a direct impact on the supply chains of goods and services [1]. The new normal of domestic and international consumption has quickly caused the common business model to be adjusted from offline to online on e-commerce platforms. Logistics entrepreneurs and startup companies have seen an opportunity to adapt their business model to B2C (business to customer) as well as to develop the business from C2C (customer to customer), which is just a provider of parcel delivery, to become a B2B2C (business to business to customer) business, which is an area where demand is increasing rapidly.

The logistics service provider is an integral part of any organization by providing the most efficient supply chain management and adding value to their client's business. Moreover, the logistics service provider having efficient logistics systems will help the organization that is using the service to compete with competitors in terms of speed of transportation, delivery accuracy, and quick response to the customers' needs with low-cost operations [2]. This research is a study of a logistics startup company located in Bangkok that provides 4PL (Fourth Party Logistics Service Provider) services between merchants and carriers, including warehouse rental service and delivery of goods service (fulfillment warehouse). Fulfillment warehouses are the places where converted online customer orders to parcel delivery packages, which are then transferred to the customers with the operational goal of fast fulfillment [3], [4]. Because fulfillment warehousing helps to yield the desired level of customer service at the least total cost, it is an essential component of any logistics system. The completion of warehouse activities is the bridge between the producer and the client, and it is becoming increasingly important in logistics operations. Due to the rapid growth of e-commerce during the COVID-19 outbreak, the company has gained more customers in both B2B and B2C. To avoid future difficulties, such as product delivery delays, a new warehouse location must be located to fulfill customer demands, promptly react to customer needs, and gain a competitive edge in terms of time and space. Such action also contributes to lower total logistics costs. Using Multiple Criteria Decision Making (MCDM), this study intended to identify a new warehouse location in Bangkok and vicinities to serve as the nation's distribution hub. The Analytic Hierarchy Process (AHP) is a decision-making tool

that can be used to conduct decision-making in cases through the use of a rating assessment having a scale from 1 to 9 through pairwise comparison of alternatives on each decision criteria. It uses a multi-level hierarchical structure of objectives, criteria, sub-criteria, and alternatives [5].

The majority of prior research has centered on robotic mobile fulfillment or dynamic demand fulfillment. The research on the placement of fulfillment warehouses is still in its early phases. As a result, the goal of this paper is to find the optimal fulfillment warehouse location for a startup company operating in the Bangkok metropolitan area to maintain a steady sales growth rate and avoid any uncertainties that might harm the company's overall performance. We utilized a common multi-criteria decision-making method, the Analytic Hierarchy Process (AHP), to decide the best alternative. There are five alternatives locations for the company to select from. The warehouses' name is not provided due to confidentiality reasons, but the location names will be shown.

II. Literature Review

A. Warehouse Location

Warehouses are a key link in a supply chain network in both regional and global markets [6]. With regard to supply chain networks, the speed and efficiency of supply chains are defined by the location of the warehouse [3], [7]. Alberto stated that the location of warehouses should be selected in an area where the overall efficiency of the company's supply chain can be increased and value can be added to the business [8]. Thus, the selection of warehouse location is a highly important undertaking due to the possibility of major losses, for example, increased production costs and delays in the delivery process, occurring for the company, due to an incorrect decision [6], [9]. There are several dimensions such as short lead-time, flexibility, and profitability, which are being achieved through warehousing. Especially in the globalized market and with the growth of e-commerce, warehouse location selection has become one of the most crucial strategic decisions for companies [10]. Onal et al. explained that order fulfillment is related to warehouse location decisions. If a warehouse is situated near the markets during high demand, it can deliver the products at the correct time [11]. The concept of warehouse location selection involves the travel distance between the warehouse and the markets [6]. Warehouse location parameters can be generated using both quantitative and qualitative requirements. The quantitative features can be measured using figures. Many of the most frequent geographical variables used in warehouse location are market, transportation, labor, site constraints, raw materials and services, utilities, government regulations, neighborhood, and ecology [12], [13]. Previous studies looked at the costs, labor qualities, facilities, markets, and taxes, as well as workforce feasibility [9]. Various critical factors have been used by researchers in the warehouse location selection process that broadly include four factors, proximity to market; proximity to transportation; building availability; and workforce availability [6], [8], [9], [12], [13].

B. Fulfillment Warehouse

Fulfillment warehouses also called 3PL or 4PL providers, are an essential part of the e-commerce business. These 3PL and 4PL service providers help e-commerce brands and retailers fulfill customers' orders. A fulfillment warehouse is utilized for the packing and delivery of a product to customers. Therefore, the structure and operations of fulfillment warehouses are different from those of traditional warehouses, which are used to store products or bulk inventory for long periods of time [14]. In contrast, a fulfillment warehouse is used to keep inventory for short time periods, until the e-commerce orders need to be shipped to customers. According to Hilletofth who explained that limited amounts of commodities are stored in fulfillment warehouses for brief periods [15]. Furthermore, fulfillment warehouses may handle various jobs, whereas traditional warehouses operate on a set schedule. The fulfillment time required to meet customer demands is fundamental to the fulfillment warehouse operation. Rapid fulfillment is the key aim of online merchants, with the mission of same-day, next-day, or two-day delivery [16]. As a result, fulfillment warehouse concepts are designed for rapid selection and precise delivery in order to maximize customer satisfaction. In addition, a substantial link between order fulfillment delays and consumer purchasing behavior was found by Nguyen et al. [17].

C. Analytical Hierarchy Process

Warehouse location is a strategic decision thus companies need to define the top criteria for selecting the best warehouse location based on their requirements. Multiple Criteria Decision Making (MCDM) is usually used when considering diverse categories of solutions to decision problems. The Analytical Hierarchy Process (AHP) is a method that considers a complicated multiple criteria decision-making problem as a system [18], [19]. The AHP is an effective tool for analyzing multiple criteria to support the decision-making process through a hierarchical structure that was proposed by Saaty.

This method takes into consideration both the tangible and intangible criteria by identifying the criteria and sub-criteria in a decision hierarchy and assigning rankings to the alternatives, criteria, and sub-criteria through pairwise comparison matrices in all the levels of the hierarchy [20], [21]. This analytical process can be divided into four steps: (1) structuring a hierarchy

prioritization model, (2) preparing a questionnaire for collecting data from experts, (3) constructing judgment matrices in all levels, and (4) checking the hierarchical single ordering and consistency [22]. However, the key step in the AHP process is a pairwise comparison to determine the weights of the criteria and provide ratings for alternatives. The weights of the criteria and sub-criteria used in the AHP process are based on the opinions of experts and/or stakeholders who helped in analyzing the critical factors in the warehouse location selection.

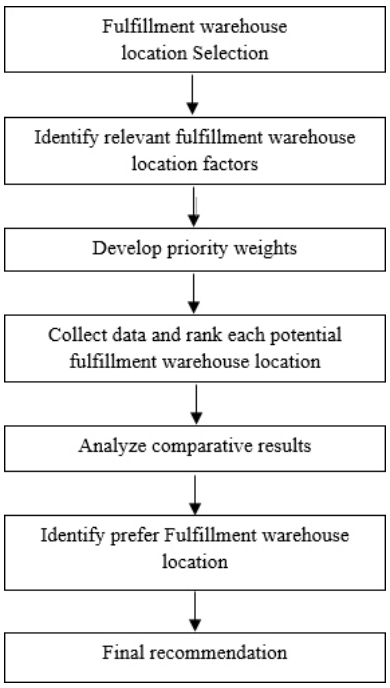

Fig. 1. Solution process of the AHP location model

III. Methodology

A. Judgment Aggregation and Rating of Decision Alternatives

Selecting a fulfillment warehouse location is a sophisticated process related to multiple locations, multiple criteria, multiple facilities, and multiple factors that can change over time due to crises such as the COVID-19 pandemic or natural disasters. No single location could be suitable under multiple criteria or factors because each location candidate may have a unique advantage in its favor. In this sense, the fulfillment warehouse placement location issue may be handled using the AHP solution technique, which is ideally suited in this case. AHP is a technique for assessing a variety of qualitative and quantitative factors. In the AHP paradigm, pairwise comparison is a crucial phase. The approach concentrates on two elements at the same time as well as their interactions. The relative significance of each element is assessed on a scale of 1 to 9, with 1 indicating that the two variables relate equally to the goal and 9 indicating that one variable is favored over the other to the greatest extent allowed [5], as seen in Table I. The creation of priority weights is a crucial stage in a pairwise comparison that is displayed as a matrix. Fig. 1 depicts the AHP fulfillment warehouse location decision model's technique. The AHP model is used in this study to examine the company's background and expectations before identifying the appropriate fulfillment warehouse location criteria. These variables are organized in a hierarchy that progresses from the overall goal to various criteria and sub-criteria in consecutive amounts [23].

B. Consistency Ratio: CR

The level to which a supposed link between components in a pairwise comparison is preserved is known as consistency. This is significant because a lack of consistency in comparisons might signal that respondents were unable to correctly calculate the impact of the items being evaluated or that they did not comprehend the distinctions between the options provided [24]. The consistency ratio (CR) is obtained by comparing the consistency index (CI) with an average random consistency index (RI), as shown in Table II [5]. The CR must be less than 0.1 to accept the computed weights. The CR is defined by using Equation (1) and the CI is determined using Equation (2).

Equation (1);

$$CR = \frac{CI}{RI}$$

Equation (2);

$$CI = \frac{\lambda \max - \mathrm{n}}{n-1}$$

where λmax = maximal eigenvalue

TABLE I
FUNDAMENTAL SCALES FOR PAIRWISE COMPARISONS

Scales	Degree of Preferences	Descriptions
1	Equally	Two activities contribute equally to the objective.
3	Moderately	Experience and judgment slightly or moderately favor one activity over another.
5	Strongly	Experience and judgment strongly or essentially favor one activity over another.
7	Very strongly	An activity is strongly favored over another and its dominance is showed in practice.
9	Extremely	The evidence of favoring one activity over another is of the highest degree possible of an affirmation.
2, 4, 6, 8	Intermediate values	Used to represent compromises between the preferences in weights 1, 3, 5, 7 and 9.

Source: Saaty [20]

TABLE II
RANDOM INDES (RI) TABLE

N (number of factors)	1	2	3	4	5	6	7	8	9	10
RI	0	0	0.52	0.89	1.11	1.25	1.35	1.4	1.45	1.49

C. Criteria and Sub-Criteria

To help with criteria selection, the researcher compiled the typical criteria and priority weights from past studies regarding warehouse location selection. Literature analysis and managerial conclusions were used to get the sub-criteria in this study.

There are five potential fulfillment warehouses proposed for location consideration. The reason for selecting these locations is because all of them passed the pre-requirements regarding the distance from the company to the candidate warehouses and the three key location criteria that are most relevant to fulfillment warehouse location [25]-[27]. Each of the key criteria is disaggregated into three major sub-criteria, which are based on company policy. The three key criteria and nine sub-criteria (two levels) are structured into a decision hierarchy, as shown in Fig. 2 and Table III.

The appropriateness of the decision order may be verified by a process that begins with small group meetings to establish research goals and outline the major criteria, sub-criteria, and alternatives in the decision model. The meeting is attended by a group of five assessors, comprising executives and staff from the company's warehouse department. The evaluators remarked on the model's suitability for selecting fulfillment warehouse locations.

Table III shows if the parameters are qualitative or quantitative. The nine site criteria are utilized as a decision matrix, and the AHP model requires the decision makers' evaluations for each site. The priority weights of each site criterion are calculated by comparing each parameter at a given level using pairwise comparisons.

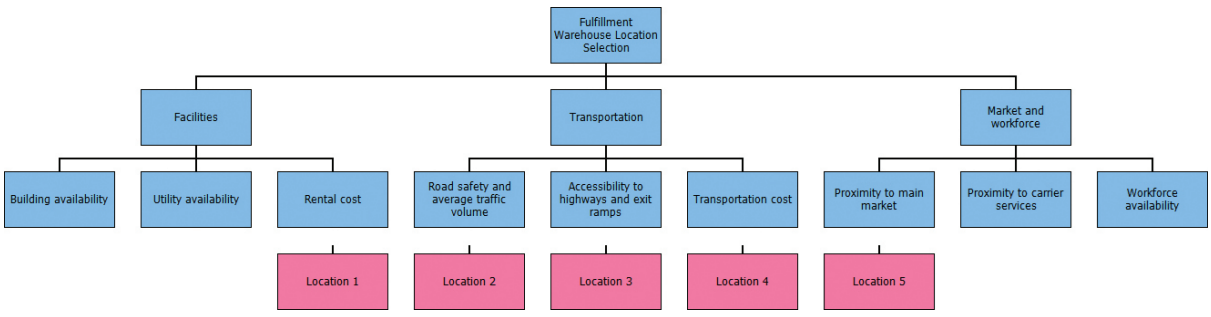

Fig. 2. Hierarchy structure

TABLE III
LOCATION CRITERIA AND SUB-CRITERIA TYPES

Criteria	Type
A. Facilities	
A1- Building availability	Qualitative
A2- Utility availability	Qualitative
A3- Rental cost	Quantitative
B. Transportation	
B1- Road safety and average traffic volume	Qualitative
B2- Accessibility to highways and exit ramps	Qualitative
B3- Transportation cost	Quantitative
C. Market and workforce	
C1- Proximity to main market	Qualitative
C2- Proximity to carrier services	Qualitative
C3- Workforce availability	Qualitative

D. Location Candidates

There are five potential fulfillment warehouses proposed for location consideration based on company criteria and policy. Location 1 is located in Pak Kret; location 2 is located in Muang Thong Thani; location 3 is located in Lat Phrao; location 4 is located in Ngamwongwan; and location 5 is located in Chatuchak.

G. Data Collecting and Analyzing

The company is expected to provide judgment data from decision-makers, company's management team, with knowledge, competence, and experience in logistics and warehouse services. The pairwise comparisons data were collected using the on-site questionnaire. There were 13 pairwise comparison matrices; 3 for the main criteria, 9 for the sub-criteria, and 1 for the alternatives. The aggregated pairwise comparison judgment is computed by the weighted geometric mean method. The researcher entered the data from the surveys into the Expert Choice software to calculate the Consistency Ratio for each person. The researcher scheduled another meeting with the assessor until the CR value was within an appropriate range if the value did not satisfy the requirements. The AHP approach was employed in this study, and the Expert Choice software was used in the assessment procedure.

IV. RESULTS

There are three key criteria in this research: (A) Facilities, (B) Transportation, and (C) Market and workforce. The nine sub-criteria are (A1) Building availability, (A2) Utility availability, (A3) Rental cost, (B1) Road safety and average traffic volume, (B2) Accessibility to highways and exit ramps, (B3) Transportation cost (C1) Proximity to main market, (C2) Proximity to carrier services and (C3) Workforce availability. Among the nine sub-criteria, two are quantifiable, but the others are not. The study was based on a pairwise evaluation of all of the sites concerning all criteria and sub-criteria.

The eigenvalue in the associated eigenvector of each matrix represents the priority weight of each condition. This eigenvector is graded with the greater element's weight, which is utilized as the pairwise comparison criteria. The weights of the sub-criteria are multiplied by the weight of the factor immediately in the hierarchy to get the composite weights of the location criteria. The results of the analysis of the composite weight are shown in Table IV.

TABLE IV
LOCATION CRITERION WEIGHT

Criteria	A	B	C
A. Facilities	**0.376**		
A1- Building availability	0.230		
A2- Utility availability	0.235		
A3- Rental cost	0.535		
B. Transportation		**0.417**	
B1- Road safety and average traffic volume		0.293	
B2- Accessibility to highways and exit ramps		0.262	
B3- Transportation cost		0.445	
C. Market and workforce			**0.207**
C1- Proximity to main market			0.389
C2- Proximity to carrier services			0.468
C3- Workforce availability			0.142

The results are shown in Table IV, and, with regard to the fulfillment warehouse location selection, transportation is the highest priority (0.417). The subsequent priorities are assigned to facilities (0.376) and market and workforce (0.207) according to the obtained weights. For the facilities criteria, the rental cost is the first priority sub-criteria (0.535), regarding the transportation criteria, transportation cost is the first priority sub-criteria (0.445), and for the market and workforce, proximity to carrier services is the first priority (0.468).

The total priority score for each site option is determined by multiplying the site's rating score for each provided criterion by the associated criterion's priority weight. The final results consist of the derived criteria weights and the class ratings, which are calculated using the consistency ration (CR). The CR of this model is less than 0.1, so the computed weights are accepted. As the results seen in Table V show, location 2 is the preferred location because it has the highest score (0.246) among the five candidate locations. The subsequent priorities are assigned to location 1 (0.212), location 5 (0.198), location 4 (0.174) and location 3 (0.168), according to the obtained weights.

TABLE V
OVERALL RATING OF FIVE LOCATIONS

Criteria	Location 1	Location 2	Location 3	Location 4	Location 5	CR
A. Facilities						
A1- Building availability	0.148	0.281	0.094	0.342	0.135	0.031
A2- Utility availability	0.114	0.281	0.087	0.380	0.138	0.036
A3- Rental cost	0.373	0.288	0.172	0.056	0.111	0.079
B. Transportation						
B1- Road safety and average traffic volume	0.227	0.300	0.137	0.159	0.177	0.068
B2- Accessibility to highways and exit ramps	0.151	0.370	0.136	0.126	0.217	0.018
B3- Transportation cost	0.140	0.098	0.264	0.202	0.296	0.045
C. Market and workforce						
C1- Proximity to main market	0.204	0.134	0.230	0.161	0.271	0.051
C2- Proximity to carrier services	0.229	0.321	0.125	0.119	0.206	0.029
C3- Workforce availability	0.265	0.326	0.140	0.148	0.121	0.009
Score	**0.212**	**0.246**	**0.168**	**0.174**	**0.198**	**0.045**

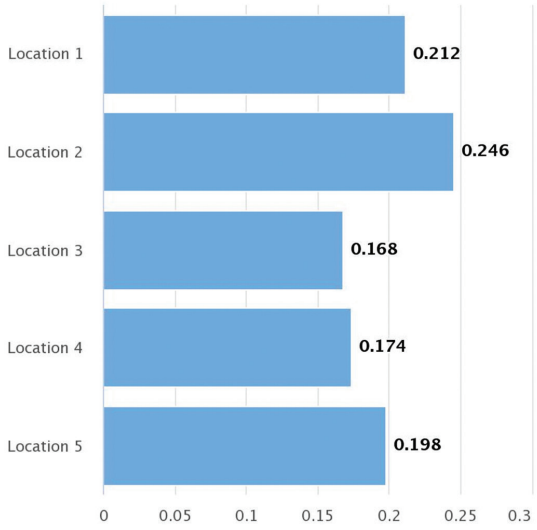

Fig. 3. Priorities with respect to fulfillment warehouse location selection

V. Summary and Managerial Implications

In the process of the optimization of a logistics system in 3PL and 4PL, the selection of the proper location for a fulfillment warehouse has always been considered as one of the most strategic and important challenges to overcome. Making good decisions is extremely important for startup companies because it is costly and difficult to reverse them and they give rise to long-term commitments [28]. Many quantitative and qualitative criteria affect the selection of the warehouse location as a long-term decision, such as markets, transportation, labor, and utilities [14]. The keys to the success of a fulfillment warehouse are speed and accuracy in responsiveness to customer demands [3], [4], [29]. This paper presents an Analytic Hierarchy Process (AHP) location decision model for the startup company seeking a location for expansion of their business. The main criteria consist of facilities, transportation, and market and workforce. Moreover, the nine sub-criteria are building availability, utility availability, rental cost, road safety and average traffic volume, accessibility to highways and exit ramps, transportation cost, proximity to main market, proximity to carrier services, and workforce availability. The highest priority criterion is transportation. The subsequent priorities are assigned to facilities, and market and workforce, respectively. Transportation is an important consideration factor because transportation costs are high and vary with distance and traffic conditions. Therefore, a location where transportation time, as well as transportation costs, can be reduced should be selected, which will increase transportation efficiency and facilitate a quick response to the needs of customers, in accordance with previous research [9], [30]. The operational goal of fulfillment warehouse is fast fulfillment. Proximity to key roadway is a key criteria when selecting the new warehouse location, according to previous research [3]. Based on the results of this research, it was found that fulfillment warehouse location 2 (Muang Thong Thani) is the first priority. The subsequent priorities are assigned to location 1, location 5, location 4, and location 3, respectively.

In this research, the analytical hierarchy process was applied to the fulfillment warehouse location selection, which allows decision-makers to compare the importance of the criteria and sub-criteria affecting the process when a decision is made. Furthermore, it can logically inform them about the importance of each of the location candidates in terms of the various criteria. In addition, the analytic hierarchy process can verify the inconsistency of the comparisons and analyze the accuracy of the information. However, Analytic Hierarchy Process cannot make decisions on behalf of humans; hence, the knowledge, experience, and expertise of the decision-makers will be the key factor in their decision making. These research outcomes can help a company's management to identify the important factors to consider when selecting the best fulfillment warehouse location. For further research, additional criteria related to warehouse management systems should be included in future studies.

References

[1] B. H. Meyer, B. Prescott, and X. S. Sheng, "The Impact of the COVID-19 Pandemic on Business Expectations," *International Journal of Forecasting*, vol. 38, no. 2, pp. 529-544, Apr. 2022.

[2] F. Chan and N. S. Kumar, "Global Supplier Development Considering Risk Factors Using Fuzzy Extended AHP-Based Approach," *Omega*, vol. 35, no. 4, pp. 417-431, Aug. 2007.

[3] J. Zhang, S. Onal, and S. K. Das, "The Dynamic Stocking Location Problem – Dispersing Inventory in Fulfillment Warehouses with Explosive Storage," *International Journal of Production Economics*, vol. 224, pp. 1-11, Jun. 2020.

[4] J. Zhang, S. Onal, R. Das et al., "Fulfilment Time Performance of Online Retailers – an Empirical Analysis," *International Journal of Retail & Distribution Management*, vol. 47, no. 5, pp. 493-510, Jun. 2019.

[5] T. L. Saaty, *Multicriteria Decision Making: The Analytic Hierarchy Process: Planning, Priority Setting, Resource Allocation*. Pittsburgh, PA: RWS Publications, 1990, pp. 1-24.

[6] R. K. Singh, N. Chaudhary, and N. Saxena, "Selection of Warehouse Location for a Global Supply Chain: A Case Study," *IIMB Management Review*, vol. 30, no. 4, pp. 343-356, Dec. 2018.

[7] S. Onal, J. Zhang, and S. K. Das, "Product Flows and Decision Models in Internet Fulfillment Warehouses," *Production Planning & Control*, vol. 29, no. 10, pp. 791-801, May. 2018.

[8] P. Alberto, "The Logistics of Industrial Location Decisions: An Application of the Analytic Hierarchy Process Methodology," *International Journal of Logistics Research and Applications*, vol. 3, no. 3, pp. 273-289, Nov. 2000.

[9] T. Demirel, N. Ç. Demirel, and C. Kahraman, "Multi-Criteria Warehouse Location Selection Using Choquet Integral," *Expert Systems with Applications*, vol. 37, no. 5, pp. 3943-3952, May. 2010.

[10] L. Devangan, "An Integrated Production, Inventory, Warehouse Location and Distribution Model," *Journal of Operations and Supply Chain Management*, vol. 9, no. 2, pp. 17-27, Jan. 2017.

[11] S. Onal, J. Zhang, and S. K. Das, "Modelling and Performance Evaluation of Explosive Storage Policies in Internet Fulfilment Warehouses," *International Journal of Production Research*, vol. 55, no. 20, pp. 5902-5915, Mar. 2017.

[12] F. Uysal, and Ö. Tosun, "Selection of Sustainable Warehouse Location in Supply Chain Using the Grey Approach," *International Journal of Information and Decision Sciences*, vol. 6, no. 4, pp. 338-353, Dec. 2014.

[13] T. Özcan, N. Çelebi, and S. Esnaf, "Comparative Analysis of Multi-Criteria Decision Making Methodologies and Implementation of a Warehouse Location Selection Problem," *Expert Systems with Applications*, vol. 38, no. 8, pp. 9773-9779, Aug. 2011.

[14] N. Boysen, R. Koster, and F. Weidinger, "Warehousing in the E-Commerce Era: A Survey," *European Journal of Operational Research*, vol. 277, no. 2, pp. 396-411, Sep. 2019.

[15] P. Hilletofth, "How to Develop a Differentiated Supply Chain Strategy," *Industrial Management & Data Systems*, vol. 109, no. 1, pp. 16-33, Jan. 2009.

[16] T. Laosirihongthong, D. Adebanjo, P. Samaranayake et al., "Prioritizing Warehouse Performance Measures in Contemporary Supply Chains," *International Journal of Productivity and Performance Management*, vol. 67, no. 9, pp. 1703-1726, Nov. 2018.

[17] D. Nguyen, S.D. Leeuw, and W. Dullaert, "Consumer Behaviour and Order Fulfilment in Online Retailing: A Systematic Review," *International Journal of Management Reviews*, vol. 20, no. 2, pp. 255-276, Nov. 2016.

[18] T. L. Saaty, "A Scaling Method for Priorities in Hierarchical Structures," *Journal of Mathematical Psychology*, vol. 15, no. 3, pp. 234-281, Jun. 1977.

[19] V. Rajput and A. C. Shukla, "Decision-Making Using the Analytic Hierarchy Process (AHP)," *International Journal of Scientific Research*, vol. 3, no. 6, pp. 135-136, Jun. 2012.

[20] T. L. Saaty, *The Analytical Hierarchy Process*. New York: McGraw-Hill, 1980, pp.1-50.

[21] B. L. Golden, E. A. Wasil, and P. T. Harker, "Applications of the Analytic Hierarchy Process: A Categorized, Annotated Bibliography," in *The Analytic Hierarchy Process: Applications and Studies*. Annotated edition. Springer, 1989, pp. 37-58.

[22] T. L. Saaty, "How to use the Analytic Hierarchy Process," in *Fundamentals of Decision Making and Priority Theory.* Pittsburgh, PA: RWS Publications, 2000, pp. 7-35.

[23] T. L. Saaty, "The Analytic Hierarchy Process," *Decision Making for Leaders: The Analytic Hierarchy Process for Decisions in a Complex World*, 3rd ed. Pittsburgh, PA: RWS Publications, 2013, pp. 12-26.

[24] A. Borade, G. Kannan, and S. Bansod, "Analytical Hierarchy Process-Based Framework for VMI Adoption," *International Journal of Production Research*, vol. 51, no. 4, pp. 963-978, Feb. 2013.

[25] I. Dogan, "Analysis of Facility Location Model Using Bayesian Networks," *Expert Systems with Applications*, vol. 39, no. 1, pp. 1092-1104, Jan. 2012.

[26] M. Brandeau and S. Chiu, "An Overview of Representative Problems in Location Research," *Management Science*, vol. 35, no. 6, pp. 645-674, Jun. 1989.

[27] B. MacCarthy and W. Atthirawong, "Factors Affecting Location Decisions in International Operations – A Delphi Study," *International Journal of Operations & Production Management*, vol. 23, no. 7, pp. 794-818, Jul. 2003.

[28] B. Malmir, R. Moein, and S. K. Chaharsooghi, "Selecting Warehouse Location by Means of the Balancing and Ranking Method with an Interval Approach," in *Proc. International Conference on Industrial Engineering and Operations Management (IEOM) held in Dubai, United Arab Emirates*, 2015, pp. 1-7.

[29] M. Fisher, S. Gallino, and J. Xu, "The Value of Rapid Delivery in Online Retailing," *SSRN Electronic Journal*, vol. 56, no. 5, pp. 732-748, Oct. 2015.

[30] M. Ashrafzadeh, F. M. Rafiei, N. Isfahani et al., "Application of Fuzzy TOPSIS Method for the Selection of Warehouse Location: A Case Study," *Interdisciplinary Journal of Contemporary Research in Business*, vol. 3, no. 9, pp. 655-671, Jan. 2012.

Anupong Thuengnaitham is a lecturer in the faculty of Logistics and Transportation Management, Panyapiwat Institute of Management. He received M.Sc. in Technopreneurship and Innovation Management, Chulalongkorn University. He also received his Ph.D. in Engineering (Management Science and Engineering) from Huazhong University of Science and Technology, Wuhan, China.

Automated Single-Pole Double-Throw Toggle Switch Pin Inspection using Image Processing and Convolutional Neural Network Techniques

Tamnuwat Valeeprakhon[1], Penpun Chaihuadjaroen[2], Chakapan Chanpilom[3], and Pairat Sroytong[4]

[1,2,4] Department of Computer Engineering, Faculty of Engineering at Sriracha, Kasetsart University Sriracha Campus, Chonburi, Thailand
[3] Department of Industrial Engineering, Faculty of Engineering at Sriracha, Kasetsart University Sriracha Campus, Chonburi, Thailand
E-mail: tamnuwat@eng.src.ku.ac.th, penpun@eng.src.ku.ac.th, chakapan@eng.src.ku.ac.th, pirat@eng.src.ku.ac.th

Received: August 23, 2021 / Revised: October 5, 2021 / Accepted: October 11, 2021

***Abstract*—The single-pole double-throw toggle switch bent pin inspection is an indispensable step in the switch production process. However, the traditional inspection process is conducted in manual work, and this may result in misunderstanding and reduces the manufacturing efficiency due to exhausted humans. To overcome these problems, the automated single pole-double throw toggle switch bent pin inspection method by using image processing and convolutional neural networks is proposed. Our proposed method can be achieved to inspect whether normal or abnormal bent pin of these toggle switches without sorting and no positioning arrangement. Our proposed method consists of five main steps: The first step, the HSV color segmentation is used for background extraction. Next step, the morphological opening, and closing operation are applied for handling noise and holes that conspicuously affect the system's ability to identify the extracted object accurately. Next step, the minimal enclosing rectangle and angle of rotation are calculated for identifying the positions of the disorder toggle switch. Next step, the CNN is used for locating pins in order to extract only the pins out from the binary switch image. In the final step, the average summation of the white pixel is calculated for classifying normal and abnormal bent pins. The experimental results obtained by our proposed method are statistically described as accurate compared to many different methods based on the single pole-double throw toggle switch bent pin inspection. Results show that our proposed method provides high accuracy than other comparative methods with a mean accuracy of 0.9940 from 6,270 images and uses mean time-consuming 0.3385 seconds.**

***Index Terms*—SPDT Toggle Switch, Pin Inspection, Image Processing, CNN**

I. Introduction

The toggle switch is an electrical component actuated by moving a lever mechanism back and forth to connect or disconnect the conducting path in an electrical circuit, diverting the electric current or interrupting it from one conductor to another. Toggle switches are available in many different configurations, styles, sizes, and various ratings for voltage. Generally, the toggle switch can be categorized by the term used into four types: Single Pole-Single Throw (SPST), Single Pole-Double Throw (SPDT), Double Pole-Single Throw (DPST), and Double Pole Double Throw (DPDT). The Pole refers to the number of circuits are controlled by the switch: The Single Pole (SP) switches control only one electrical circuit, and The Double Pole (DP) switches control two independent circuits. The Throw refers to the number of close a circuit position: Single Throw (ST) switches close a circuit at only one position. Double Throw (DT) switches close a circuit in the left position as well as the right position.

The SPDT toggle switch has a single input that controls only an electrical circuit, and it can connect to two outputs circuits in both left and right positions. This switch has a three-pin and only one lever mechanism. The SPDT toggle switch manufacturing process is diverse and complex consists of many processes. The appearance inspection process is one of the main important processes in order to find

foreign particles, stains, flaws, and chipping to prevent an outflow of defective workpieces with an activity such as checking, measuring, examining, testing, and comparing the results with specified requirements. In this process, the checkpoints of the SPDT toggle switch are differentiated into three inspection parts: pin, body, and lever, as shown in Fig. 1 with the red rectangle from left to right, respectively.

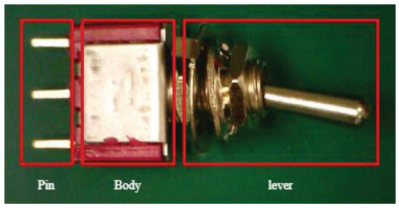

Fig. 1. SPDT Toggle switch inspection parts

The pins inspection for SPDT toggle switches will be measured the dimensions and checked the abnormal that happens to its toggle switch by human visual inspection and automated sensing. Moreover, the examination of a ton of product sample size, many operators are assigned to support the production for a long period of time, and this may result in misinterpretation and reduce the manufacturing efficiency due to exhausted human [1], [2].

Nowadays, machine vision technology has been widely used in electrical components, mainly including the inspection crack, bent, corrosion, texture, degree, straightness, deflection, and other defects [3]. This technology has a more obvious advantage than human manual checking and provides high efficiency and reliability [4]. However, there are little researches on electronic component base on pin inspection by using machine vision. Yewei Xiao's research of Xiangtan University proposed pin detection in the transmission line using pyramid multi-level to scaling image. The cascade detection and no-maximum suppression are used to identify the candidate boundary of the pin in the transmission line, and a convolutional neural network is applied to classify the status of the fastener, whether missed or unmissed pin. His proposed method provides higher accuracy and runs faster than other comparative machine learning methods. However, this method does not cover all of the fastener pin styles [5]. Wu Weihao research of the China Jiliang University proposed defective electrical connector inspection based on machine learning method by using Yolo v3 efficiently algorithm with Darknet-53 as a Convolutional Neural Network (CNN) that acts as a backbone. The mainly defective characteristics include solder point surface, ground wire wrong welding, and inner and outer ring. The defective locations are around the surface and pin of the connector. The qualitative and quantitative experimental results show that his improved Yolo v3 has better performance and runs faster for detection than other competitive machine learning methods. However, the accuracy and speed of his method do not meet the needs of modern automated production lines [6]. Lu Jiayu's research of the Harbin Institute of Technology proposed electrical connector types classification based on the pin position by using a gray-scale centroid algorithm for pin positioning and a template matching algorithm based on gray features for pin recognition in order to classify the type of connector. His main research area is only classified the type of connector; however, the primary defective pin detection has not been performed [7]. Pallabi Ghosh's research of the Institute of Technology Kharagpur proposed automated defective pin identification based on recycled counterfeit integrated circuits using supervised and unsupervised machine learning methods. A convolutional neural network is applied to classify the pin status, whether normal, bent, and corroded pins, from RGB and depth map images. Furthermore, two unsupervised learning methods are used to identify bent pins with 3d construction from depth map images. K-means is used to detect corroded pins with Laws Texture energy measures method for extracting the feature vectors. His proposed approach has been highly accurate in identifying both corroded and bent in counterfeit integrated circuits. However, the speed of this proposed method has not been improved [8]. Du Fuzhou research of Beijing University of Aeronautics and Astronautics proposed the multi-type electrical connector classification based on a binocular vision by using a contour fitting algorithm to locate the pins in the connector and uses Support Vector Machine (SVM) to classify various types of pins. His proposed method has been computed with high accuracy and more efficiency than other methods. However, the speed of his proposed method has not been calculated and it has not been applied to the real production line [9]. Someyot Kaitwanidvilai of King Mongkut Institute of Technology Ladkrabang proposed the integrated circuit pins inspection using the wavelet transform and discrete Fourier's transform to extract the interesting features for classifying the integrated circuit pins pattern. His proposed technique gains a higher average maximum cross-correlation than other methods. However, the defective type has not been classified and has not been applied to the real production inspection process [10].

In summary, there are few researches on inspection of the defective pin of electrical components. The traditional image processing and machine learning techniques are often used for electronic components inspection, which solves problems such as crack, bent, corrosion, and other defective characteristics. However, most of the researches based on the defective pin of electronic component identification are facing problems in poor real-time performance,

limit position identification, unable to work on unsorting images, and does not match the modern automated production lines. Our research proposes a new combination of methods by using image processing and CNN techniques to identify abnormal bent pins of SPDT Toggle switches in a different position and disordering and. Our proposed method will be applied into the real production process.

The remainder of this paper is organized as follows: The first part is aimed at introducing the defective types of SPDT toggle switches and their existing problems. The second part describes the experimental setup for pin inspection with image processing and CNN techniques. Next, the results of the experiment were carried out by comparison with other competitive methods. The fourth part summarizes the paper.

II. Methodology

In the quality inspection process at the defective inspection station, the SPDT toggle switches are conveyed through a belt at a constant speed, and there are placed in different positions, non-stick together, disorder, and unsorting. When the toggle switches pass through a proximity sensor, then a sensor will be activated and sent a signal to a control unit to capture an image of these toggle switches with an installed camera. Fig. 2 shows example RGB images of SPDT toggle switches. These images consist of two types of checked pins are the abnormal bent pin and the normal pin. In the experimental setting, the abnormal bent pins are simulated by different patterns due to extreme testing and validation of the proposed method.

Our proposed method is applied both image processing and deep learning techniques. Fig. 3. gives an overview of our method consists of five main steps: The background image extraction based on HSV Color segmentation, Noises and holes removal using morphological opening and closing, the toggle switches region identification using minimal enclosing rectangle and angle of rotation calculation, pin identification by applying the deep learning-based convolutional neural network architecture and pin inspection by considering the average of summation of the white pixel.

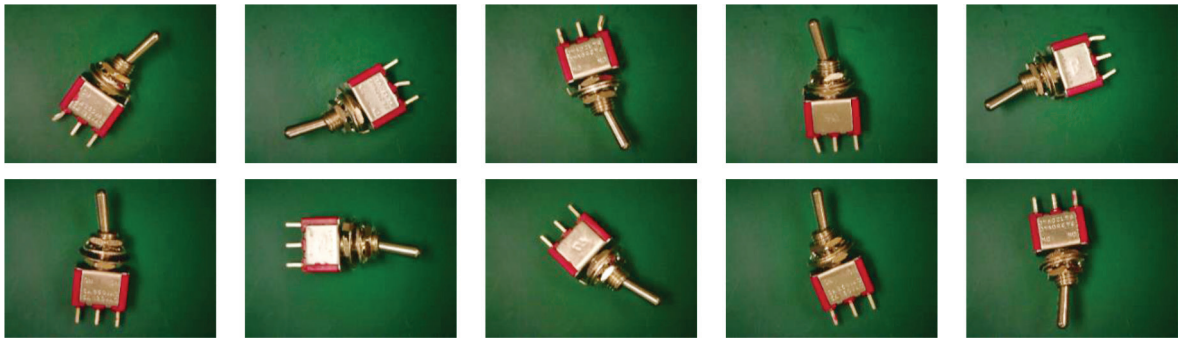

Fig. 2. SPDT toggle switch images with the top row represents abnormal bent pint toggle switches and bottom row represents normal toggle switches.

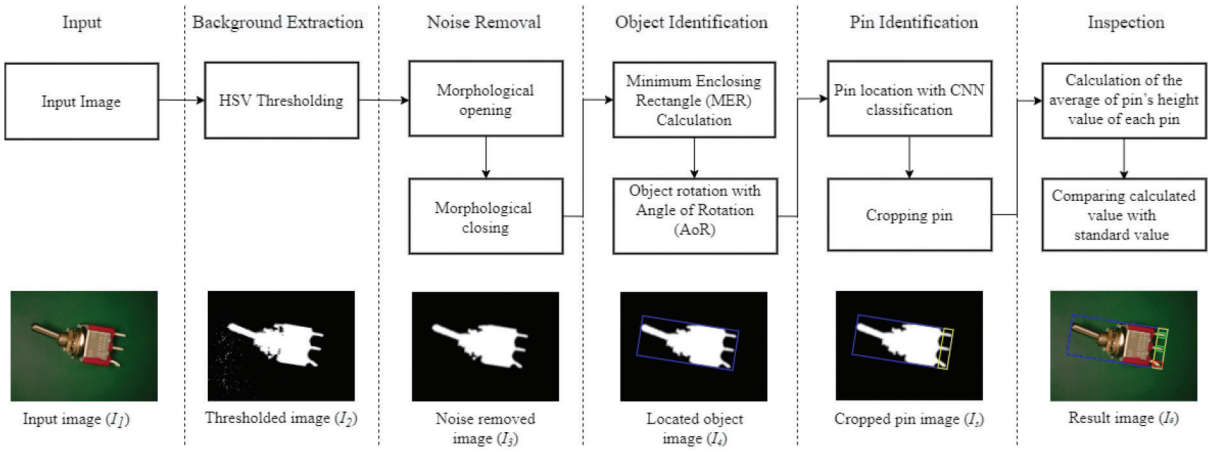

Fig. 3. Proposed method

A. Background Extraction

The first step of object identification using image processing techniques is background extraction [11]. Considering the SPDT toggle switch images color, the belt screen or background is green and it differentiates from the switch color ostensibly. The HSV color segmentation method can be achieved to extract it apart from each other by converting I_0 from the RGB color space where R, G, B represent red, green, and blue components respectively with a value between 0-255 into the HSV color space using the following equations1-3 [12]. The HSV color space is very useful in image processing tasks that need to segment objects based on color according to the H (Hue) channel models the color, the S (Saturation) dimension models the dominance of that color, and the V(Value) dimension models the brightness. Then the background will be separated from the object by thresholding H and V values using equations 4 thus, the result is displayed in the binary image (I1).

$$H=\cos^{-1}\left\{\frac{\frac{1}{2}(2R-G-B)}{\sqrt{(R-G)^2-(R-B)(G-B)}}\right\} \quad (1)$$

$$S=\frac{\max(R,G,B)-\min(R,G,B)}{\max(R,G,B)} \quad (2)$$

$$V=\max(R,G,B) \quad (3)$$

$$I_1(x,y)=\begin{cases}1, & \text{if } 42<H(x,y)<160 \text{ and } V(x,y)<102\\ 0, & otherwise\end{cases} \quad (4)$$

Where $H(x,y)$ represents a Hue value of the coordinate (x,y). $V(x,y)$ represents a Value value of the coordinate (x,y).

B. Noise Removal

The most common problems after segmentation objects are noise and holes. The type of noise is a small white area spreads all over the image, and the hole is a background region surrounded by border-connected foreground pixels. The noise and holes can conspicuously affect the system's ability to rotate and identify the extracted object precisely, to overcome these problems, a series of post-processing methods are applied by using the morphological opening following a closing operation. The morphological opening operation erodes an image and then dilates the eroded image as the equation 5, and the morphological closing operation dilates an image and then erodes as the equation 6, both operations using the same size, shape, and structure element as the equation 7. The morphological opening operation is great for removing small noises. The closing morphological operation is useful for filling small holes while preserving the shape and size of the larger interested region in the image. The result is presented in the binary image (I_2).

$$I'=I_1\circ B=(I_1 \ominus B)\oplus B \quad (5)$$

$$I_2=I'\bullet B=(I'\oplus B)\ominus B \quad (6)$$

Where $\oplus$ and $\ominus$ denote the dilation and erosion, respectively.

$$B=\begin{pmatrix}1 & 1 & \cdots & 1\\ \vdots & \vdots & & \vdots\\ 1 & 1 & \cdots & 1\end{pmatrix} \quad (7)$$

Let B is a structure element with size 10x10

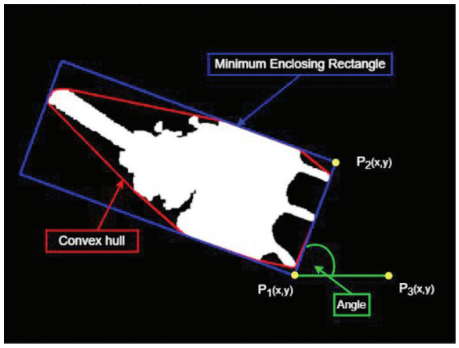

Fig. 4. The blue bounding rectangle is the MER applied result, the red area is the convex hull region and green angle is the angle calculated by AoR.

C. Object Identification

Since noise and hold were eliminated and only interested region is presented then the Minimum Enclosing Rectangle (MER) will be calculated. The MER is the method to compute the smallest bounding rectangle that contains the whole interested region by not required to be axis-aligned and constructed by a convex hull of the region [13]. The implementation of MER involves iterating over the edges of a convex polygon. For each edge, compute the smallest bounding rectangle with an edge coincident of all rectangles, shorting, and choose the one with the minimum area. The maximum distance between the projected vertices is the width of the rectangle, and the maximum distance between the projected vertices is the height of the rectangle [14]. The result of MER is shown in Fig. 4 as the blue bounding rectangle.

Determining the position of the pin in the MER is difficult and requires high accuracy. CNN is presented to determine the location of the pin in MER by learning from the dataset. However, the dataset is obtained from a cropped images with MER is not available, it is necessary to rotate these images into axis-aligned by finding the Angle of Rotation (AoR). Fig. 4 shows the AoR as the green angle, it is the angle

formed by using two vectors u and v performed by the three points P_1, P_2, and P_3. P_1 is the lowest point in the vertical axis of the MER, P_2 is the ending point ordered clockwise staring from P_1, and P_3 is the point to the right of P_1 on the horizontal axis. The u and v can be calculated with equation 8. Therefrom, the AoR is calculated by using the invert of the law of cosines with equation 9. Finally, the toggle switch object will be cropped with MER and rotated with AoR, and the results are possibly arranged into four patterns by pin location: Bottom, Top, Right, and Left. The example results are shown in Table I.

$$u=(p1_x - p2_x, p1_y - p2_y)$$
$$v=(p1_x - p3_x, p1_y - p3_y) \quad (8)$$

$$\theta=\arccos\left(\frac{a\cdot b}{|a||b|}\right) \quad (9)$$

D. Pin Identification

The pin location of the SPDT toggle switch in the image is unpredictable because the toggle switches are pressed in different positions. Once the MER and AoR were applied, the pin location has four possible alignment positions: top, bottom, left, and right inside bounding-box, as shown in Table I. Since this study is part of a larger project that intends to investigate all types of SPDT toggle switch abnormalities, such as bent pins, broken pins, broken levers, and damaged bodies. The inspection of SPDT switches necessitates the alignment of objects into similar patterns. The solution adopted should be adaptable and capable of dealing with all kinds of SPDT toggle switch abnormalities. Thus, the Convolutional neural network is proposed to classify the location of the pin in order to align the objects into similar patterns and it can be applied to use in difference of kinds of SPDT toggle switch abnormalities. The CNN is a class of deep neural networks commonly used to image classification jobs. The use of CNN requires a sufficient dataset and more complex processing to build a model for classifying multi-class of problems [15].

TABLE I
SAMPLE DATASET OF BINARY IMAGE OF SPDT TOGGLE SWITCH

Label	Class	Example	Sample
0	Bottom	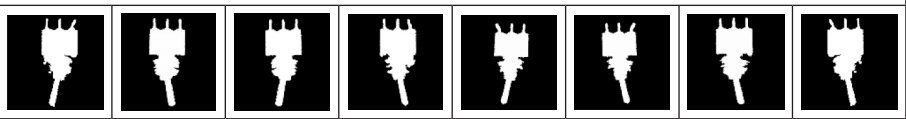	250
1	Top	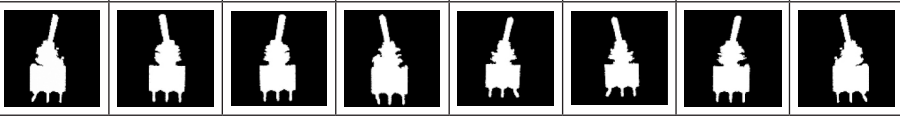	250
2	Right	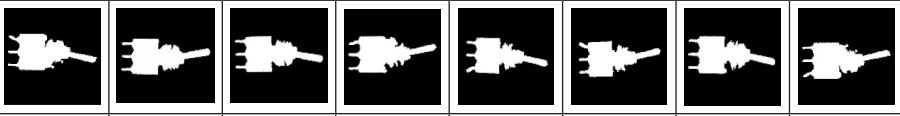	250
3	Left	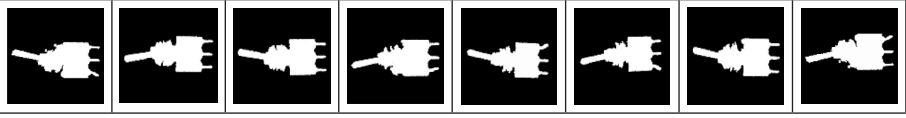	250

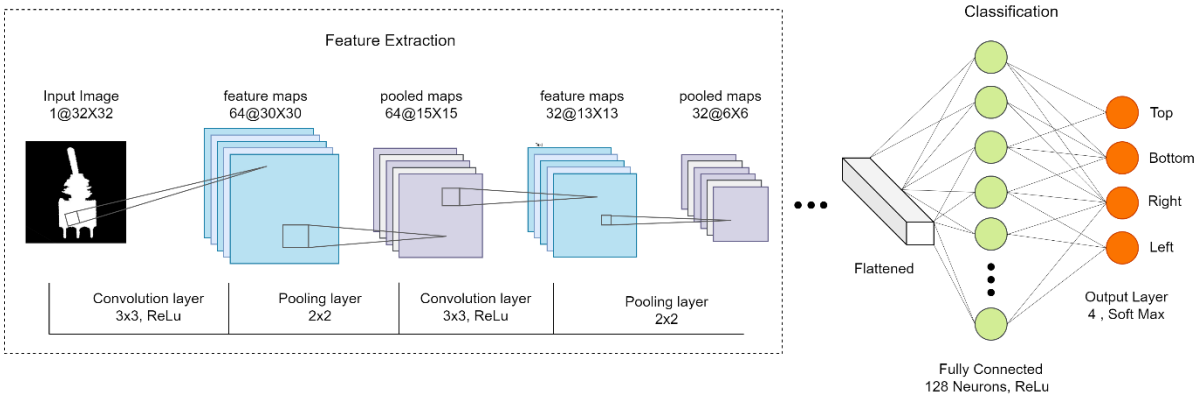

Fig. 5. Architecture of proposed CNN for pin location classification

The dataset consists of 1000 of the SPDT Toggle images and it is a collection of 4 distinct classes: Top, Bottom, Left, and Right. Each class is equally provided 250 images. All images are resized into 32x32 pixels and normalized all pixel values into the range 0-1. The used dataset is split into two parts for training and validating. The first spitted dataset is used to fit the model consists of 80% of all datasets, and the remaining 20% is used for validating.

Once the dataset was ready, the CNN model for pin location classification will be created. Typically CNN is a sequence of multi-layer that transforms one volume of activations to another through a differentiable function and commonly uses three main types of layers. They are a convolutional layer, pooling layer, and fully connected layer. The proposed model uses these layers stacked into five layers of network architecture, as shown in Fig. 5.

Layer-1 is the convolutional layer response to extracts the high-level features from the input image as a convolutional activity [15], [16]. Since the input image has been normalized, the image will be 32x32 (nxn) of the size. This layer is constructed by using 64 of the dimensionality of the output space (d), 3x3 of kernel size (f), 1 of strides (s), and 0 of padding (p). Since ReLu (Rectified Linear Unit) as an activation function was done. The feature maps will be presented with size 64@30x30 where 64 is the number of feature maps which is equal to the number of dimensionality of the output space, and 30 calculate from equation 10.

$$((n+2p-d)/s)+1 \tag{10}$$

Layer-2 is the max-pooling layer. This layer receives the input of size 64@30x30 from the previous layer to calculate the maximum value for each patch of the feature map [15], [16]. Thus, this layer consists of 2x2 of pooling size, 2 of strides (s), and 0 paddings (p). the After max-pooling operation, the feature maps will be presented with size 64@15x15 where 64 is the number of feature maps which is equal to the number of dimensionality of the output space, and 15 is calculate from equation 10.

Layer-3 is second the convolutional layer acts as Layer 1 to reduce feature maps dimensionality output [15], [16]. This layer works with the ReLu activation function and receives the input size 64@15x15 from the previous layer. This layer is created by using 32 of the dimensionality of the output space (d), 3x3 of kernel size (f), 1 of strides(s), and 0 of paddings (p). After this convolution operation, the feature maps will be presented with size 32@13x13 where 32 is the number of feature maps, and 13 is calculate from equation 10.

Layer-4 is the average pooling layer. This layer receives the input of size 32@13x13 from the previous layer to calculate the average value for each patch of the feature map [15], [16]. This layer consists of 2x2 of pooling size, 2 of strides (s), and 0 paddings (p). After the average operation, the feature maps will be presented with size 32@6x6 where 32 is the number of feature maps which is equal to the number of dimensionalities of the output space, and 6 is calculate from equation 10.

Layer-5 is a fully connected layer. Since the flattening has operated using the input from Layer-4, the flattened feature map will be 32x6x6=1152 dimensional vectors. These output vectors will be connected to every input perceptron by learnable weight. This layer computes the class score by using the soft-max activation function [15], [16]. The result presents an array size of four, where each of the four numbers corresponding to a class score representing the Left, Right, Top, and Bottom sides of SPDT toggle switches pin location.

The proposed model is trained by using the best parameter that is conducted in the experimental process, including the Adam as optimization algorithm, 100 epoch for training, 64 of batch size, and learning rate with 0.001. The proposed CNN model highly achieves 100% for training accuracy, whereas validation accuracy is 100%. Fig. 6 shows the confusion matrix of the impact of false class

rate, it clearly shows that the proposed CNN model provides zero false in every class rate. Therefore, it is observed that the proposed model trains effectively, keeping no losses and owing to testing accuracies. Thus, the proposed model is least affected by the over-fitting problem and can be efficiently utilized to classify the pin location to crop pin with 100% accuracy.

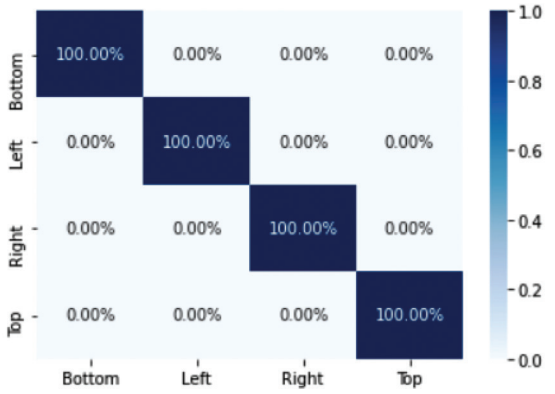

Fig. 6. A confusion matrix analyses of the proposed CNN model

Since the pin of SPDT toggle switch in binary image location was identified by predicting with the proposed CNN model then these pin will be cropped according to the prediction result as shown in Fig. 7 (a). The cropped pin will be rotated according to its class as following: Bottom, Left, Top and Right are rotated with 0°, 90°, 180° and 270° respectively. The rotated pin images are always arranged at the bottom as shown in Fig. 7 (b).

E. Inspection

The abnormal bent pin is very similar to the normal pin of SPDT toggle switch in case of slight bent pin and these pins are very difficult to differentiate whether normal or bent pin. However, differentiating these pins requires a thresholding with specific parameters obtained from the various properties of its pins. The width and height of the pin are the significant considered parameters since the bent directly affects to the width and height of the pin.

Once the pins were located and each pin was cropped from the binary image of the SPDT toggle switch as shown in Fig. 7 (b) The width of pins is considered by counting the number of columns of a cropped pin. So, the width of the bent pin is greater than the normal pin as shown in Fig. 7 (c) that this parameter may be used as a thresholding parameter. However, Fig. 8 (a) shows the distribution of the width of normal and abnormal bent pins are overlapping between the maximum values distribution of normal pins and the minimum values distribution of abnormal bent pins, thus the width of the pin is out of use.

The height is an important parameter for considering to differentiate normal and abnormal bent pins. This height parameter can be calculated in two ways: maximum height and average height. The maximum height is calculated by finding the highest columns of a cropped pin. So the maximum height of the normal pin looks different from the bent pin, as shown in Fig. 7 (c) that this parameter should be used for thresholding. However, the distribution of the maximum height of normal and abnormal bent pins shows that there is overlapping between the minimum value distribution of normal pins and the maximum value distribution of abnormal bent pins, as shown in Fig. 8 (b). Hence, the maximum height of the pin is not good for thresholding.

The average height is calculated by averaging the summation of the white pixel in each column (vertical axis) of a cropped pin. So the average height of the normal pin should be greater than the abnormal bent pin as the maximum height parameter. So the distribution of the average height of normal and abnormal bent pins is significantly different from each other, as shown in Fig. 8 (c) that this parameter can differentiate between the normal pin and abnormal bent pin.

The average height is used to differentiate between the normal and abnormal bent pins of the SPDT toggle switch. Each pin is calculated for this average height value and it is compared with the standard value obtained from non-overlapping range of the distribution of average height. Fig. 8 (c) shows a range of non overlapping range between the maximum distribution of average height of abnormal bent pin and the minimum distribution of average height of normal pin. If the calculated value is lower than the standard value, the pin is bent; on the other hand, if the calculated value is higher than the standard value, the pin is normal.

(a) (b) (c)

Fig. 7. (a) The cropped pin in binary image of SPDT toggle switch, (b) the extracted each pin, (c) Graph of summation of with pixel in column of each pin

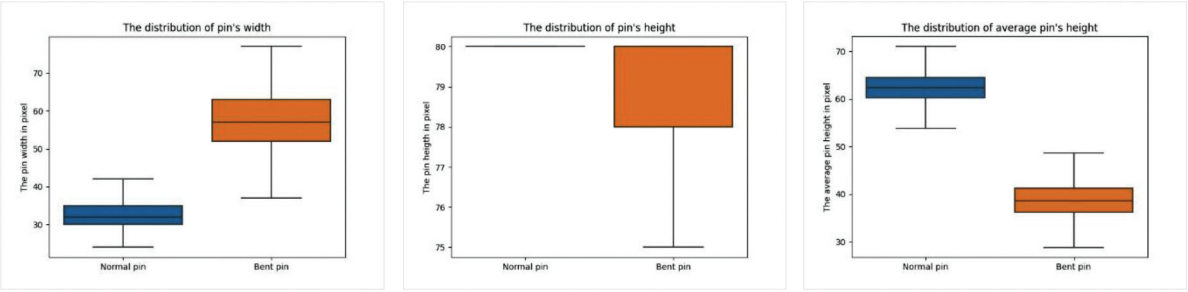

(a) (b) (c)

Fig. 8. The distribution of parameter of SPDT toggle switch. (a) The distribution of pin's width parameter, (b) The distribution of pin's height parameter, (c) The distribution of average pin's height parameter

III. Result and Discussion

In this section, the results of our proposed method for SPDT toggle switch pin inspection are presented. In order to test the effectiveness of our proposed method, many approaches including of supervised learning, transfer learning, feature matching, template matching, and other images processing designed for SPDT toggle switch pin inspection were conducted to compare the inspection results that were obtained from several testing images. All methods in this experiment were programmed in Python and all experiments were implemented on an NVIDIA DGX1 AI cloud server, CPU Dual 20-core Intel Xeon E5-2698 v4 2.2 GHz, GPUs 8X NVIDIA Tesla V100, and 512 GB 2,133 MHz DDR4 of system memory. The total of testing image contains 4,008 images by using 2,261 images for normal pin and 1,747 for abnormal bent pin of SPDT toggle switches. All testing images are the color image with the same size of 1,280x960 pixels and each image taken with a same focal length in a same environment.

Fig. 9 shows the example result images obtained from our proposed method. The region of the SPDT toggle switch in image was drawn with the blue rectangle and its pin location was drown with the yellow rectangle. The red rectangle indicates the abnormal bent pin, on the other hand the green rectangle indicates the normal pin. In order to evaluate the quality level of the results obtained form our proposed method and the other methods, the various matrix-based performances metrics are used as performance measurements, these metrics consist of five main indicators: accuracy, precision, recall, F-measure and time-consuming [17], [18]. Table II shows the results of our proposed method in six runs, the mean accuracy of our proposed is 0.9940 and the mean of time-consuming is 0.0230 second, the standard deviation of all indicators are very small since our proposed method provides the result clustered around the mean. Table III shows the comparative results in every methods and Table IV shows the comparative results by group of methods.

Since supervised learning can differentiate data through learning process with labeled dataset. Therefore, KNN, SVM and CNN are used to classify normal and abnormal bent pin from gray scale images of SPDT toggle switch [19]. The mean accuracy of these methods is 0.9392 and mean time-consuming is 0.2483 where CNN obtains the highest accuracy with 0.9475 and uses least time-consuming with 0.2206 second while KNN obtains the lowest accuracy with 0.9275 and uses the most time consuming with 0.2725 second. Comparison results between all supervised leaning methods and our proposed method, it was found that our proposed method was more accurate but took more processing time than supervised learning methods. However, all supervised learning approaches can tell the difference between a switch with a normal pin and one with a bent pin, but it can't

tell the difference between a switch with a little bent pin and it fail to locate the bent pin in a switch but the proposed method succeeds.

Transfer learning is the subset of supervised learning uses to classify color images as the same as supervised learning. However, this method uses smaller dataset than supervised learning methods [20]. In this research, seven candidate methods of transfer learning are used: Dense-Net, Inception, Mobile-Net, Res-Net, VGG16, VGG19 and Xception. These methods provide mean accuracy with 0.9014 and mean time-consuming with 0.2886 second where Dense-Net obtains the highest accuracy with 0.9725 but it takes the most consuming-time with 0.4636 seconds while Mobile-Net obtains lowest accuracy with 0.7825 but it takes the least consuming-time with 0.1870. Moreover, this Dense-Net transfer learning provides higher accuracy than all supervised learning methods. However, all transfer learning methods provide poorer accuracy than our suggested method for the same reasons as supervised learning approaches.

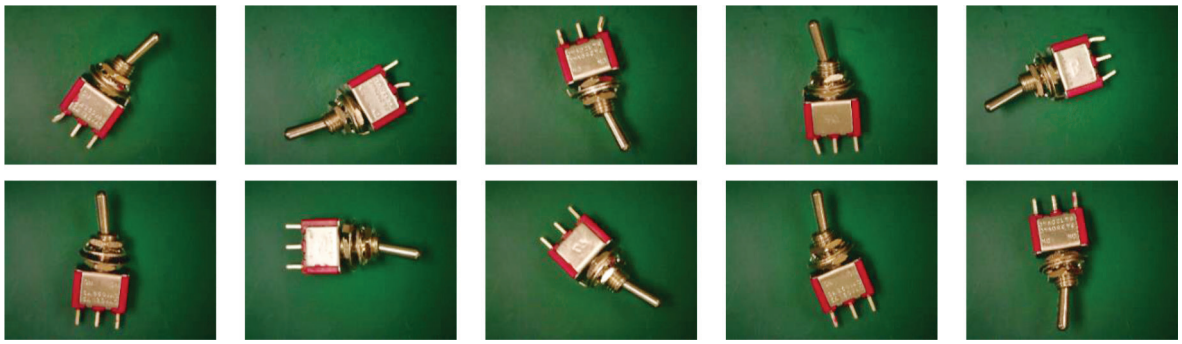

Fig. 9. The example results obtained from our proposed method

TABLE II
THE RESULTS OF OUR PROPOSED METHOD IN SIX RUNS

No	Accuracy (%)	Precision (%)	Recall (%)	F-measure (%)	Time (sec)
1	0.9941	0.9967	0.9914	0.9941	0.3222
2	0.9940	0.9971	0.9909	0.9940	0.3630
3	0.9940	0.9971	0.9909	0.9940	0.3530
4	0.9940	0.9971	0.9909	0.9940	0.2971
5	0.9940	0.9971	0.9909	0.9940	0.3584
6	0.9940	0.9971	0.9909	0.9940	0.3374
Mean	0.9940	0.9970	0.9909	0.9940	0.3385
Std.	0.00003	0.0001	0.0001	0.00003	0.0230

TABLE III
COMPARISON RESULTS OF OUT PROPOSED METHOD AND OTHER METHODS BASED SPDT TOGGLE SWITCH BENT PIN INSPECTION

Methods		Accuracy (%)	Precision (%)	Recall (%)	F-measure (%)	Time (sec)
Supervised Learning	KNN	0.9275	0.9314	0.9275	0.9273	0.2725
	SVM	0.9427	0.9038	0.9533	0.9247	0.2518
	CNN	0.9475	0.9555	0.9475	0.9490	0.2206
Transfer Learning	Dense Net	0.9725	0.8901	0.8625	0.8644	0.4636
	Inception	0.8125	0.8128	0.8125	0.8125	0.2783
	Mobile Net	0.7825	0.7825	0.7825	0.7825	0.1870
	Res Net	0.9725	0.9735	0.9725	0.9725	0.2397
	VGG16	0.9250	0.9300	0.9250	0.9252	0.2324
	VGG19	0.9525	0.9540	0.9525	0.9525	0.3021
	Xception	0.8925	0.9016	0.8925	0.8930	0.3176

TABLE III
COMPARISON RESULTS OF OUT PROPOSED METHOD AND OTHER METHODS BASED SPDT TOGGLE SWITCH BENT PIN INSPECTION (CON.)

Methods		Accuracy (%)	Precision (%)	Recall (%)	F-measure (%)	Time (sec)
Feature matching	SURF	0.4809	0.2068	0.4577	0.2849	0.6378
	MSER	0.5128	0.2169	0.5315	0.3080	0.6418
	BRISK	0.5208	0.2229	0.5514	0.3174	0.6396
Template matching	Square Difference	0.5300	0.2200	0.5789	0.3188	16.257
	Correlation Coefficient	0.5446	0.2772	0.5957	0.2654	7.8490
	Cross Correlation	0.5300	0.2200	0.5789	0.3188	7.6981
Other	PCA	0.5156	0.2286	0.5365	0.3206	0.2279
	MER+AOR	0.5254	0.2655	0.5530	0.3588	0.2205
Proposed Method		**0.9940**	**0.9970**	**0.9909**	**0.9940**	**0.3385**

TABLE IV
MEAN OF EACH PERFORMANCE MEASUREMENT OF DIFFERENT METHODS

Method	Accuracy (%)		Precision (%)		Recall (%)		F-measure (%)		Time (sec)	
	Mean	Std.	Mean	Std.	Mean	Std.	Mean	Std.	Mean	Std.
Supervised Learning	0.9392	0.0085	0.9302	0.0211	0.9427	0.0110	0.9336	0.0108	0.2483	0.0213
Transfer Learning	0.9014	0.0711	0.8920	0.0657	0.8857	0.0656	0.8860	0.0655	0.2886	0.0824
Template matching	0.5348	0.0068	0.2390	0.0269	0.5845	0.0079	0.3010	0.0251	10.601	3.9996
Feature matching	0.5048	0.0172	0.2155	0.0066	0.5135	0.0403	0.3034	0.0136	0.6397	0.0016
Other	0.5205	0.0049	0.2470	0.0184	0.5447	0.0082	0.3397	0.0191	0.2242	0.0037
Proposed Method	**0.9940**	**0.00003**	**0.9970**	**0.0001**	**0.9909**	**0.0001**	**0.9940**	**0.00003**	**0.3385**	**0.0230**

Template matching and feature matching are a technique in digital image processing for finding small parts of an image which match a template image and feature of the object respectively [21], [22]. Our experiment uses these methods to address the SPDT toggle switch and its pin in an image and uses our inspection method for determining normal and abnormal bent pins of the toggle switch. However, the mean accuracy of both methods is lower than our mean accuracy of the proposed method and it's mean time-consuming is higher than the mean time-consuming of our proposed method. Moreover, F-measure and precision of template matching and feature matching method are very low because the weighted harmonic mean is the imbalanced distribution of classes with accuracy. Once the object has less rotation, template matching and feature matching perform effectively. However, if the object has a lot of rotation, it won't be able to locate it. Since the switches in this study are arranged without ordering and wide range of rotation, Template matching and feature matching are unable to locate the position of this switch as effectively as they should resulting in lower accuracy than the proposed method.

Principle component analysis is a statistical procedure that extracts two important parameters are eigenvectors and eigenvalues from a binary objects in the image [23]. These two parameters are used to calculate the angle between an object and the horizontal axis. This research uses the calculated angle to rotate the SPDT toggle switch object in the image and its pin is always on the bottom of the object. Our inspection method will be applied for pin inspection. However, the results of this method are not different from the previous method for the same reason, the overall efficiency is lower than the proposed method.

In summary, even though all of the methods presented have a similar task to inspect the pin of SPDT toggle switches, our proposed method able to produce better accuracy results than other competitive methods. Moreover, our proposed method can distinguish between the normal pin and abnormal bent pin, and it can locate only specific abnormal bent pin of SPDT toggle switch while the other cannot be performed. However, our proposed method takes more the time-consuming than the supervised learning and transfer learning method because the abnormal bent pin identification process is quite time-consuming but it is worth it because it can clearly identify abnormal bent pin address which leads to further improvements in production quality.

IV. Conclusion

In this paper, combining image processing and machine learning techniques to inspect the bent pin of the SPDT toggle switch is proposed. The major contribution of this work is the successful development of an effective methodology, in which the image processing is implemented to extract the background out from the image using HSV color segmentation, remove noise and hole based morphological operation, locate toggle switch using MER and AoR, pin identification-based CNN classification and pin inspection by considering the average of summation of white pixels in the vertical. Furthermore, a detailed comparison between the proposed method and other methods including supervised learning, transfer learning, template and feature matching, and other image processing methods are presented in our experiments.

The results obtained from our proposed method provide high accuracy for pin inspection than other competitive methods and our proposed can differentiate between normal and abnormal bent pins. In addition, the proposed method is reliable and highly effective from the perspective of solution quality. The proposed method will be applied in the actual industry to improve the accuracy of the pin inspection for toggle switch products.

However, there is still conducted in a controlled environment for improvement in the capability of the proposed method. Applying in real industry processes should guarantee the parameters suit the industry environment to avoid noise and error in order to provide the highest accuracy. The future work is developing the inspection method for handling every defective type of the toggle switch and improving the speed of the method.

Acknowlegment

We would like to thank Digital Academy Thailand and Faculty of Engineering at Sriracha, Kasetsart University, Sriracha Campus for support of time and facilities for this study.

References

[1] F. Zhong, X. Shao, and C. Quan, "3D Digital Image Correlation Using a Single 3CCD Colour Camera and Dichroic Filter," *International Journal of Measurement Science and Technology*, vol. 29, no. 4, pp. 1-9, Apr. 2018.

[2] F. Zhong, R. Kumar, and C. Quan, "A Cost-Effective Single-Shot Structured Light System for 3D Shape Measurement," *IEEE Sensors Journal*, vol. 19, no. 17, pp. 7335-7346, May. 2019.

[3] Y. Shu, B. Li, and H. Lin, "Quality Safety Monitoring of LED Chips Using Deep Learning-Based Vision Inspection Methods," *Journal of the International Measurement Confederation*, vol. 168, pp. 1-10, Jan. 2020.

[4] O. Celik, C. ZhiDong, and F. N. Catbas, "A Computer Vision Approach for the Load Time History Estimation of Lively Individuals and Crowds," *An International Journal of Computers & Structures*, vol. 200, pp. 32-52, Apr. 2018.

[5] Y. Xiao, Z. Li, D. Zhang et al., "Detection of Pin Defects in Aerial Images Based on Cascaded Convolutional Neural Network," *IEEE Access*, vol. 9, pp. 73071-73082, May. 2021.

[6] W. Wu and Q. Li, "Machine Vision Inspection of Electrical Connectors Based on Improved Yolo v3," *IEEE Access*, vol. 8, pp. 166184-166196, Sep. 2020.

[7] L. Jiayu, "Research on Technologies of Pin's Detection for Avionics Electronic Connector Based on Machine Vision," Ph.D. dissertation, Harbin Institute of Technology, Harbin, China, 2017.

[8] G. Pallabi, B. Aritra, F. Domenic et al., "Automated Defective Pin Detection for Recycled Microelectronics Identification," *Journal of Hardware and Systems Security*, vol. 3, pp. 250-260, May. 2019.

[9] D. Fu-Zhou and Z. De-long, "Research on Multi-Type Electrical Connectors Detection Based on Binocular Vision," *Aviation Precision Manufacturing Technology*, vol. 52, no. 5, pp. 23-28, May. 2016.

[10] S. Kaitwanidvilai, A. Saenthon, and A. Kunakorn, "Pattern Recognition Technique for Integrated Circuit (IC) Pins Inspection Using Wavelet Transform with Chain Code-Discrete Fourier Transform and Signal Correlation," *International Journal of Physical Sciences*, vol. 7, no. 9, pp. 1326-1332, Feb. 2012.

[11] F. G. Lamont, J. Cervantes, A. López et al., "Segmentation of Images by Color Features: A Survey," *Neurocomputing*, vol. 292, pp. 1-27, Mar. 2018.

[12] R. C. Gonzalez and R. E. Woods, "Digital Image Processing," London: Person Prentice, 2009, pp. 1-976.

[13] F. P. Preparata and M. I. Shamos, *Computational Geometry: An Introduction.* New York, USA: Springer Verlag, 1985, pp. 1-390.

[14] J. O'Rourke, "Finding Minimal Enclosing Boxes," *International Journal of Computer & Information Sciences*, vol. 14, pp. 183-199, Jul. 1985.

[15] S. Albawi, T. A. Mohammed, and S. Al-Zawi, "Understanding of a Convolutional Neural Network," *International Conference on Engineering and Technology*, pp. 21-23, Aug. 2017.

[16] R. Yamashita, M. Nishio, R. K. G. Do et al., "Convolutional Neural Networks: An Overview and Application in Radiology," *Journal of Insights into Imaging*, vol. 9, pp. 611-629, Jul. 2018.

[17] M. Sokolova, N. Japkowicz, and S. Szpakowicz, "Beyond Accuracy, F-Score and ROC: A Family of Discriminant Measures for Performance Evaluation," *Advances in Artificial Intelligence*, vol. 4304, pp. 1015-1021, Jan. 2006.

[18] C. Liu, M. White, and G. Newell, "Measuring and Comparing the Accuracy of Species Distribution Models with Presence-absence data," *Ecography*, vol. 34, no. 2, pp. 232-243, Mar. 2010.

[19] J. Qiu, Q. Wu, G. Ding et al., "Survey of Machine Learning for Big Data Processing," *EURASIP Journal on Advances in Signal Processing*, vol. 67, pp. 1-16, May. 2016.

[20] K. Weiss, T. M. Khoshgoftaar, and D. D. Wang, "A Survey of Transfer Learning," *Journal of Big Data*, vol. 3, no. 9, pp. 1-40, May. 2016.

[21] T. Mahalakshmi, R. Muthaiah, and P. Swaminathan, "An Overview of Template Matching Technique in Image Processing," *Journal of Applied Sciences, Engineering and Technology*, vol. 4, no. 24, pp. 5469-5473, Jan. 2012.

[22] C. Leng, H. Zhang, B. Li et al., "Local Feature Descriptor for Image Matching: A Survey," *IEEE Access*, vol. 7, pp. 6424-6434, Dec. 2018.

[23] S. Sehgal, H. Singh, M. Agarwal et al., "Data Analysis Using Principal Component Analysis," in *Proc. International Conference on Medical Imaging, m-Health and Emerging Communication Systems (MedCom),* pp. 45-48, Nov. 2014.

Tamnuwat Valeeprakhon is a lecturer of the Department of Computer Engineering, Faculty of Engineering, Kasetsart University, Sriracha campus. He graduated M. Eng in Computer Engineering from Khon Kaen University. He was granted a scholarship from the National Science and Technology Development Agency (NSTDA) for studying at the Kochi University of Technology. His research interests include compute vision, image processing and artificial Intelligence.

Penpun Chaihuadjaroen is an Assistant Professor at Department of Computer Engineering, Faculty of Engineering, Kasetsart University, Sriracha campus. She graduated M.S in Computer Science from King Mongkut's Institute of Technology Ladkrabang. Hir research field including of Computer vision and Image processing.

Chakapan Chanpilom is lecturer of the Department of Industrial Engineering, Faculty of Engineering, Kasetsart University, Sriracha campus. He graduated M.Sc. in Operations Management from Birmingham University. He was granted a scholarship from the National Science and Technology Development Agency (NSTDA) for studying at Pennsylvania State University. His research interests include Parameter Design and Material Science.

Pairat Sroytong is a lecturer of Department of Computer Engineering, Faculty of Engineering, Kasetsart University, Sriracha campus. He graduated M. Eng. in Computer Applied Technology from Harbin Engineering University, P.R. Harbin, China. His research field including of computer vision and image processing.

Development of Business Intelligence System and Prediction with Data Mining of Lam Sam Kaeo Town Municipality, Thailand

Watchawee Wongart[1] and Somchai Lekcharoen[2]

[1,2] College of Digital Innovation Technology, Rangsit University, Pathum thani, Thailand
E-mail: watchawee.w63@rsu.ac.th, somchai@rsu.ac.th

Received: June 13, 2021 / Revised: July 12, 2021 / Accepted: July 27, 2021

***Abstract*—The purpose of this research was to develop a business intelligence system and make predictions with data mining of Lam Sam Kaeo Town Municipality. The process of development used Microsoft Visual Studio (SSDT) with SQL Server Integration Services (SSIS) to create a data warehouse, then using SQL Server Analysis Services (SSAS) to create cube and using SQL Server Reporting Services (SSRS) to create reports then publish to web browsers for local administration officers to make decisions.**

The sample data used in this project covered local government taxpayers living in Lam Sam Kaeo Town Municipality in 2020: altogether about 200 taxpayers. The analysis was based on the new land and building tax act 2019. RapidMiner Studio was used to create the analysis model to determine the factors that cause tax delays in Lam Sam Kaeo Town Municipality. A comparison of three classification algorithms showed similar accuracy: J48 Decision Tree has accuracy = 96%, Naïve Bayes has accuracy = 92%, Neural Network has accuracy = 96.50%, ANOVA test found no significant difference at 0.05 level is not different so the researcher chooses the Decision Tree method for this research.

The results are that the most influential factors causing overdue tax payments are 'forget to pay', 'lack of advertising', and 'lack of e-payment method.

***Index Terms*—Business Intelligence System, Data Warehouse, Decision Tree, Naïve Bayes, Neural Network**

I. Introduction

The Thai government has recently approved a new tax on land and buildings, as described in the Land and Buildings Tax Act 2019 [1], and the Land and Buildings Tax Reduction Act 2020 [2].

There are three parts to this new law: a land and buildings tax, a signboard tax, and a corporate building tax [1].

Lam Sam Kaeo Town Municipality is looking for a business intelligence system to handle the administration of this tax, and this paper describes the system that was developed for them. Currently, the data about the land size, its ownership, and use are stored in a spreadsheet, which has to be manually sorted and updated with each change to the land title deed holder, change of address of the landowner, newly-surveyed land that has no appraisal value, etc., This system is inefficient and error-prone, resulting in much manual checking and delay [3].

Having studied the problem, the following solution approach was adopted: firstly, use SQL Server technology to store data, then use the SQL Server Integration Services (SSIS) to create, extract, transform and load information into the data warehouse [4]. This will combine the relevant information and automatically make the various tax calculations for the people covered by the new land tax. Next, the results will be extracted as a dimensional model data structure and separated into a dimension table and fact table to import into SQL Server Management Studio to become a data warehouse. Finally, the SQL Server Analysis Services (SSAS) will be used to create a model for analyzing the data of the dimension table and fact table, allowing the user to view details of multidimensional data [5].

In addition, a cube was developed to support forecasting and decision-making. With this, SQL Server Reporting Services (SSRS) can be used to create a dashboard for summarizing information and to automatically generate customizable reports for executives which can be viewed with a Web Browser [6].

The first step in the process was to create a data gathering spreadsheet about village land, including land data, land address, landowner, landowner

address, land utilization, date and time tax was paid, and the formula for calculating tax. All the data was sorted by village and was checked by government officers [7].

The second step was to use a dimensional model to structure the data, then to use the SQL Server Integration Services (SSIS) to create, extract, transform, and load information into the data warehouse. Dimension tables were created for land data, land address, landowner, landowner address, land utilization, and the date and time taxes were paid. A fact table was created for the formula to calculate tax [8].

It is important that the extract, transform and load (ETL) process be evaluated by the intended users until they are satisfied with the structure and knowledgeable enough to analyze the data and customize reports and create tables and charts for their management. A typical report might show which village pays the most tax, and how the land in a particular village is segmented by usage: residential, agricultural, commercial, or wasteland [9].

This information is essential to support local administration officers with operational insights and decision-making for overdue tax payments because the main income of local government is a local tax. And with this process, the information can be analyzed much more quickly and efficiently than the manual method [10].

At each stage, the government officers are required to verify that the information is accurate and can be used to make decisions.

Now the Lam Sam Kaeo Town Municipality didn't create a data warehouse. The researcher has developed an organized, accurate, and complete business intelligence system to help collect land and building taxes [5]-[7]. It can be used to check who paid taxes on time, who paid late, and who is overdue with their payment. Analyzing historical data by data mining also allows the user to predict the factors that cause tax delays [15]-[17]. This was done by importing the data into RapidMiner Studio to create three types of forecasts, namely Decision Tree [11], Naïve Bayes [12], and Neural Network [13].

II. Objective

1. To develop a business intelligence system to collect data of taxpayers with Visual Studio (SSDT) to build SQL Server Integration Services (SSIS) and then use SQL Server Analysis Services (SSAS) to create a cube. Additionally, use SQL Server Reporting Services (SSRS) to create reports [4]-[10].

2. To predict the factors of delayed tax payment in Lam Sam Kaeo Town Municipality using data mining techniques [17]-[25].

III. Related Work

Develop business intelligence with SQL Server, which consists of a business intelligence process that can be described as follows:

- The data warehouse must be designed carefully by dividing it into dimension tables and fact tables with primary keys and foreign keys. In this case, the design consists of dimension tables (dates, land, land address, owner address, and utilization) and one fact table (land tax) with relevant constraints defined by primary keys and foreign keys. Then the raw spreadsheet data can be extracted in Table I and II. [4], [5], [7].

TABLE I
Dimension Table (Dim Date)

Date_Key	Full_Date_Land_Tax	Year_Land_Tax	Month_Land_Tax	Day_Land_Tax	Quarter	EnglishMonthName	EnglishDayName	ThaiMonthName	ThaiDayName
1	2020-04-01	2020	4	1	3	April	Monday	มิถุนายน	วันจันทร์
2	2020-04-02	2020	4	2	3	April	Tuesday	มิถุนายน	วันอังคาร
3	2020-04-03	2020	4	3	3	April	Wednesday	มิถุนายน	วันพุธ
4	2020-04-04	2020	4	4	3	April	Thursday	มิถุนายน	วันพฤหัสบดี
5	2020-04-05	2020	4	5	3	April	Friday	มิถุนายน	วันศุกร์
6	2020-04-06	2020	4	6	3	April	Monday	มิถุนายน	วันจันทร์
7	2020-04-07	2020	4	7	3	April	Tuesday	มิถุนายน	วันอังคาร
8	2020-04-08	2020	4	8	3	April	Wednesday	มิถุนายน	วันพุธ
9	2020-04-09	2020	4	9	3	April	Thursday	มิถุนายน	วันพฤหัสบดี
10	2020-04-10	2020	4	10	3	April	Friday	มิถุนายน	วันศุกร์
11	2020-04-11	2020	4	11	3	April	Monday	มิถุนายน	วันจันทร์
12	2020-04-12	2020	4	12	3	April	Tuesday	มิถุนายน	วันอังคาร
13	2020-04-13	2020	4	13	3	April	Wednesday	มิถุนายน	วันพุธ
14	2020-04-14	2020	4	14	3	April	Thursday	มิถุนายน	วันพฤหัสบดี
15	2020-04-15	2020	4	15	3	April	Friday	มิถุนายน	วันศุกร์
16	2020-04-16	2020	4	16	3	April	Monday	มิถุนายน	วันจันทร์

TABLE II
FACT TABLE (FACT_LAND_TAX) WITH LAND_NUM , ORDER_NUM, UTILIZATION_CODE, DATE_KEY AS FOREIGN K.EY

SSN	Parcel_ Num	Survey	Utilization _Code	Value_of_land	Utilization_rate	After_Tax_Rate	Discount_90	Payment_10	House_Tax_2019	Tax Relief	Tax Relief_Incr ease_50	Real_Tax_Pay	Full_Date_Land_Tax
3 3107 00719 08 5	60373	38217	4	1,750,000.00	0.3	5,250.00	4,725.00	525.00	150.00	375	187.5	337.50	2020-08-16
3 1013 00445 03 7	56321	16428	4	3,024,000.00	0.3	9,072.00	8,164.80	907.20	151.00	756.2	378.1	529.10	2020-08-17
3 1005 01723 45 9	20165	6739	4	550,000.00	0.3	1,650.00	1,485.00	165.00	152.00	13	6.5	158.50	2020-08-18
3 1006 00549 85 6	32470	9576	4	1,750,000.00	0.3	5,250.00	4,725.00	525.00	153.00	372	186	339.00	2020-08-19
3 2406 00286 57 9	29550	8291	4	1,400,000.00	0.3	4,200.00	3,780.00	420.00	154.00	266	133	287.00	2020-08-20
3 1001 00787 37 5	11317	3573	4	1,800,000.00	0.3	5,400.00	4,860.00	540.00	155.00	385	192.5	347.50	2020-08-21
3 1001 00787 39 1	11318	3574	4	1,800,000.00	0.3	5,400.00	4,860.00	540.00	156.00	384	192	348.00	2020-08-22
3 1009 05776 05 8	29499	8240	4	1,470,000.00	0.3	4,410.00	3,969.00	441.00	157.00	284	142	299.00	2020-08-23
3 1020 02465 07 3	47093	14612	4	875,000.00	0.3	2,625.00	2,362.50	262.50	158.00	104.5	52.25	210.25	2020-08-24
3 1010 00641 47 7	11314	3570	4	1,800,000.00	0.3	5,400.00	4,860.00	540.00	159.00	381	190.5	349.50	2020-08-25
3 1704 00100 57 0	47288	14902	4	550,000.00	0.3	1,650.00	1,485.00	165.00	160.00	5	2.5	162.50	2020-08-26
3 1005 01307 08 1	29672	8413	4	1,400,000.00	0.3	4,200.00	3,780.00	420.00	161.00	259	129.5	290.50	2020-08-27
3 1202 00070 87 1	29553	8294	4	700,000.00	0.3	2,100.00	1,890.00	210.00	162.00	48	24	186.00	2020-08-28
3 1009 03818 42 0	9018	2515	4	992,000.00	0.3	2,976.00	2,678.40	297.60	163.00	134.6	67.3	230.30	2020-08-29
3 1005 03934 06 6	32469	9575	4	1,312,500.00	0.3	3,937.50	3,543.75	393.75	164.00	229.75	114.875	278.88	2020-08-30
3 1017 00739 63 1	19908	6493	4	1,512,000.00	0.3	4,536.00	4,082.40	453.60	165.00	288.6	144.3	309.30	2020-08-31
3 1306 00004 80 9	21771	7420	4	1,000,000.00	0.3	3,000.00	2,700.00	300.00	166.00	134	67	233.00	2020-09-01
3 1002 00194 57 1	20008	6582	4	750,000.00	0.3	2,250.00	2,025.00	225.00	167.00	58	29	196.00	2020-09-02
3 1019 00120 44 9	2214	497	4	23,192,000.00	0.3	69,576.00	62,618.40	6,957.60	168.00	6789.6	3394.8	3,562.80	2020-09-03
3 7699 00228 02 1	19982	6556	4	1,050,000.00	0.3	3,150.00	2,835.00	315.00	169.00	146	73	242.00	2020-09-04
3 5208 00008 68 5	20031	6605	4	750,000.00	0.3	2,250.00	2,025.00	225.00	170.00	55	27.5	197.50	2020-09-05

● The next process is one of extracting, transforming, and loading (ETL) the spreadsheet data into the data warehouse using Microsoft Visual Studio (SSDT) and SQL Server Integration Services (SSIS). The dimension table will be imported first. The primary key and data type will be set appropriately before importing. The fact table will be imported last. To assure data integrity, we create foreign keys to associate with the primary key in each dimension table, then create an Entity Relationship Diagram (ER diagram) to check the database relationship. Each dimension table must have a primary key to point to the fact table, and the data that has been through this process is considered correct. It is stored in a data warehouse in Microsoft SQL Server Management Studio in Fig. 1 [4], [6], [7].

● Using Microsoft Visual Studio (SSDT) to create SQL Server Analysis Services (SSAS), then create data source to retrieve data that we need from the data warehouse in Microsoft SQL Server Management Studio by selecting the database name and selecting all the required tables. This must include a dimension table and a fact table. Then create a data source view and select all the tables that we want to display in the ER diagram, then create a cube by assigning a table of quantitative numerical values that can be calculated as a fact table and the rest will be a dimension table by selecting the fields that need to be analyzed. When finished, test the deployed data to see if it passes. If not passed, the error must be found and corrected. If passed, it is considered to be set up correctly in Fig. 2 [5], [6].

● Display, after the deployment is successful, go to tab browser to select the output as a spreadsheet, which is a symbol of the program Microsoft Excel. The display can select data in the columns of the dimension table and fact table as needed in order to be able to create a dashboard to summarize the selected information. Then the size, color, font, various graph styles, tables, and dashboard designs can be customized for the executive report Fig. 3 [6].

● Report display, use Microsoft Visual Studio (SSDT) to create SQL Server Report Services (SSRS) as a more complex report format. You can import data from the data warehouse to select only the attributes that you want to display. When deployed, the data will be imported into a web browser, which can be browsed using a web browser Fig. 4 [6]-[10].

IV. DEVELOPMENT OF BUSINESS INTELLIGENCE SYSTEM TECHNIQUE

A. Data Warehouse Design (Snow Flake Schema Dimension Model)

B. SQL Server Integration Services (SSIS)

Data imported into SQL Server Management Studio becomes a data warehouse with a snowflake schema dimension model. There is a processing list from spreadsheet to database in Fig. 1.

- Dim_Date import to be OLE DB Dim_date
- Dim_Land import to be OLE DB Dim_Land
- Dim_Land_Address import to be OLE DB Dim_Land_Address

- Dim_Owner import to be OLE DB Dim_Owner
- Dim_Owner_Address import to be OLE DB Dim_Owner_Address
- Dim_Utilizations import to be OLE DB Dim_Utilizations
- Fact_Land_Tax import to be OLE DB Fact_Land_Tax

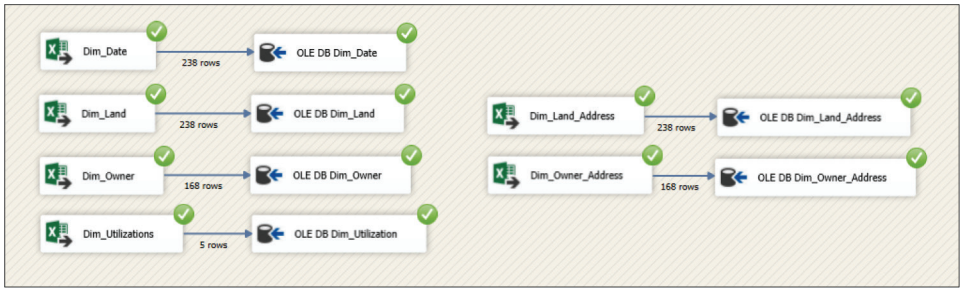

Fig. 1. Use SQL Server Integration Services (SSIS) to extract, transform, and load (ETL) process by using Visual Studio (SSDT) create SSIS using spreadsheet import into SQL Server Management Studio.

C. SQL Server Analysis Services (SSAS)

SSAS will bring Dimensional Table and Fact Table after verifying ETL process from SSIS into a data warehouse. Data were analyzed by using Cube. Tables were analyzed as follows: Dim_Date, Dim_Land, Dim_Land_Address, Dim_Owner, Dim_Owner_Address, Dim_Utilization, Fact_Land_Tax in Fig. 2.

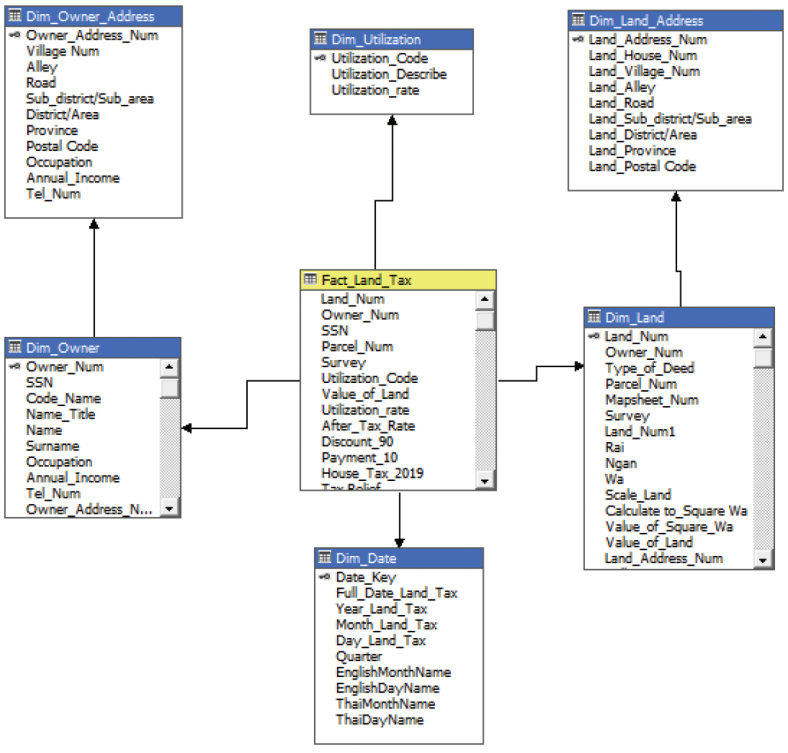

Fig. 2. Relation model Snow flake schema.

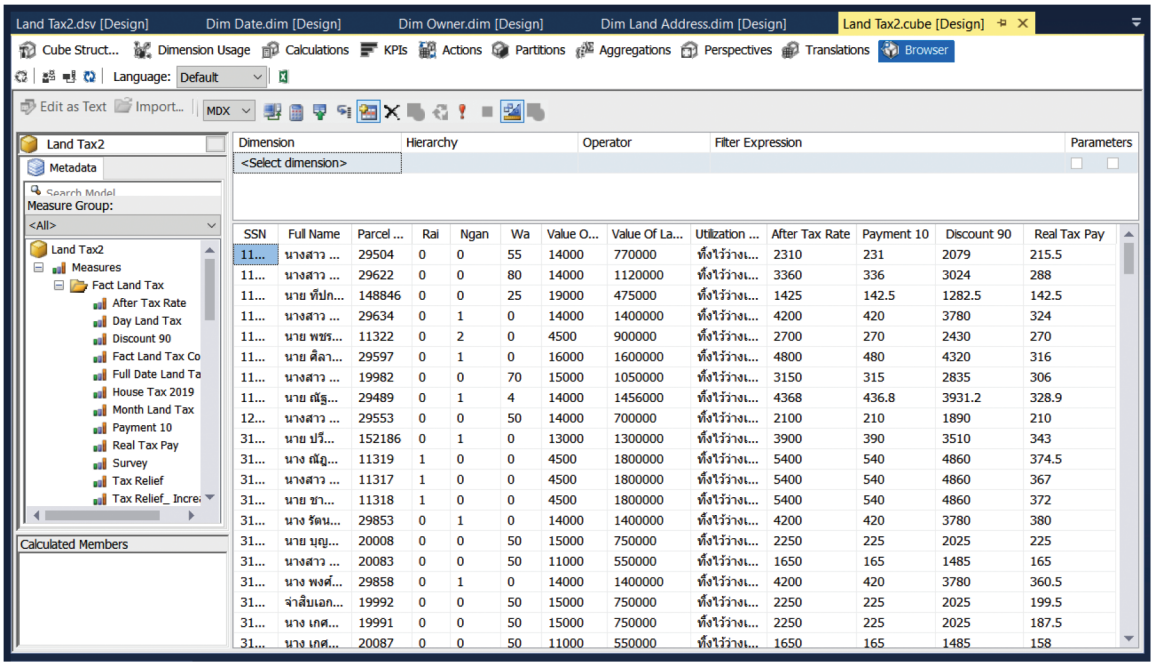

Fig. 3. Cube browser has the following data attributes: SSN, Full_Name, Parcel_Num, Rai, Ngan, Wa, Value of Square Wa, Utilization describe, House tax 2019, Discount 90, Payment 90, Real_Tax_Pay.

D. SQL Server Report Services (SSRS)

SSRS report issuing report is to bring data from the data warehouse to produce a more complex table report by selecting the attribute to be exported and able to deploy to display on a web browser.

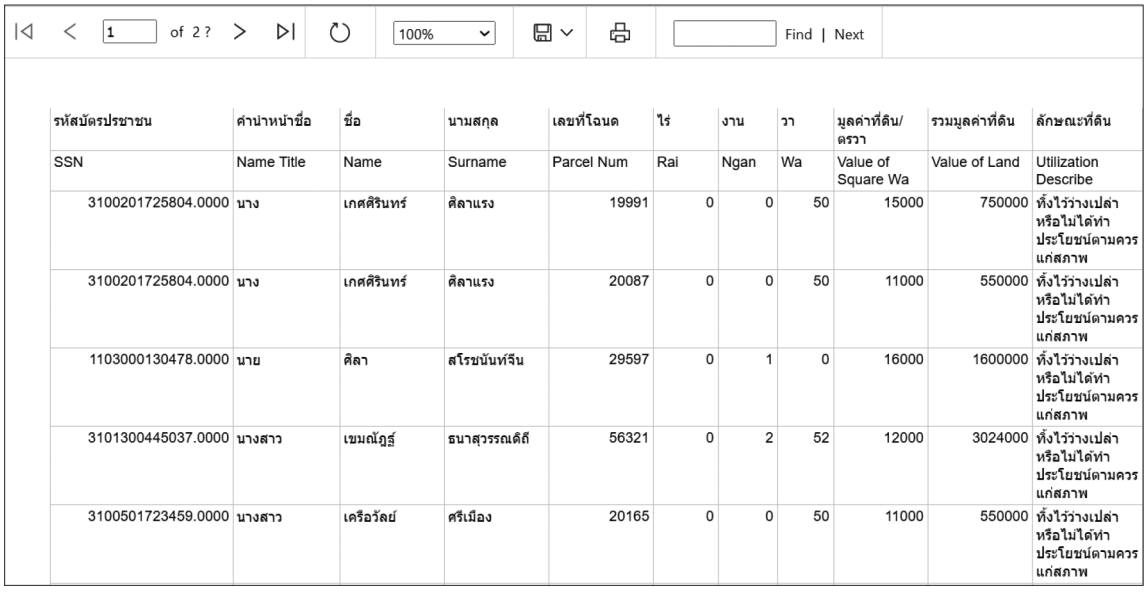

รหัสบัตรประชาชน	คำนำหน้าชื่อ	ชื่อ	นามสกุล	เลขที่โฉนด	ไร่	งาน	วา	มูลค่าที่ดิน/ตรวา	รวมมูลค่าที่ดิน	ลักษณะที่ดิน
SSN	Name Title	Name	Surname	Parcel Num	Rai	Ngan	Wa	Value of Square Wa	Value of Land	Utilization Describe
3100201725804.0000	นาง	เกศศิรินทร์	ศิลาแรง	19991	0	0	50	15000	750000	ทิ้งไว้ว่างเปล่าหรือไม่ได้ทำประโยชน์ตามควรแก่สภาพ
3100201725804.0000	นาง	เกศศิรินทร์	ศิลาแรง	20087	0	0	50	11000	550000	ทิ้งไว้ว่างเปล่าหรือไม่ได้ทำประโยชน์ตามควรแก่สภาพ
1103000130478.0000	นาย	ศิลา	สโรชบันทร์จีน	29597	0	1	0	16000	1600000	ทิ้งไว้ว่างเปล่าหรือไม่ได้ทำประโยชน์ตามควรแก่สภาพ
3101300445037.0000	นางสาว	เขมณัฏฐ์	ธนาสุวรรณเดิถี	56321	0	2	52	12000	3024000	ทิ้งไว้ว่างเปล่าหรือไม่ได้ทำประโยชน์ตามควรแก่สภาพ
3100501723459.0000	นางสาว	เครือวัลย์	ศรีเมือง	20165	0	0	50	11000	550000	ทิ้งไว้ว่างเปล่าหรือไม่ได้ทำประโยชน์ตามควรแก่สภาพ

Fig. 4. Create a report on web browser.

V. Prediction Data with Data Mining Technique

Analyze the factors of delayed tax payment with RapidMiner Studio consisting of the following techniques:

1) Decision tree (J48*)* is a tool to help make strategic or operational decisions in a business, government agency, or other organization by using a decision tree. It resembles an upside-down tree. Where the very first note at the top will be the root of the tree called the Root Node, where each node will display attributes as a Branch, each branch will show the results in the test, and the Leaf Node will show the results of classification data in Fig. 5 [11].

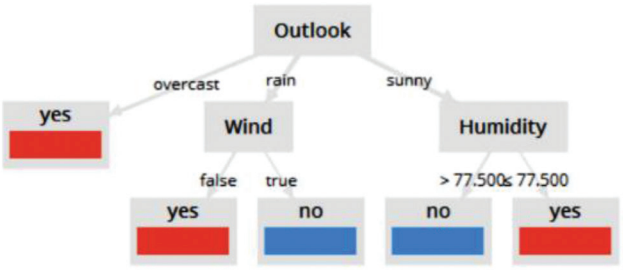

Fig. 5. Decision Tree

2) Naïve Bayes classification is a technique that uses probability theory according to Bayes' Theorem as an algorithm for classifying data. It works by learning the problems that arise to create new classification conditions. There is a principle for calculating the probability of predicting results. It is a technique for solving a classification problem that can predict the outcome. By analyzing the relationship between two or more variables to create a probabilistic condition for each relationship. Suitable for the case of a large number of samples and each attribute is independent of the other. The probability of the data in Eq. (1) [12].

$$P(h/D) = \frac{P(D|h)P(h)}{P(D)} \tag{1}$$

Naive Bay's equation

Where P(h/D) is the probability distribution of the hypothesis, h using the data D. According to the theory,

- P(h) is the previous probability of the hypothesis, h.
- P(D) is the previous probability of the sample data set, D.
- P(h|D) is the probability of h when known D.
- P(D|h) is the probability of D when known h.

3) A Neural network is a structure for processing information that is similar to the neurons in the human brain. It consists of a basic processor called neural processing and occurs in a sub-processor called a node, which simulates the behavior of a cell-signaling between nodes connected in three layers: the input layer, the hidden layer, and the output layer in Fig. 6 [13], [14].

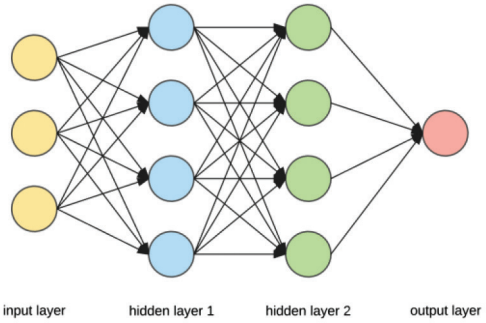

Fig. 6. Neural network

- The input layer is numeric data. If it is qualitative data, the data must be converted to a quantitative format acceptable to the neural network.
- The hidden layer is an intermediate step. They function like deep learning. Each layer can have as many neural nodes as possible, and the increase affects the performance.
- The output layer model is the actual result of the learning process of the neural network [13].

TABLE III
ORGANIZE THE DATA IN A TABULAR FORM FOR EASY CALCULATIONS.

Data No.	Process 1	2	3	...	k	
1	X_{11}	X_{12}	X_{13}	…	X_{1k}	
2	X_{21}	X_{22}	X_{23}	…	X_{2k}	
3	X_{31}	X_{32}	X_{33}	…	X_{3k}	
	.	.	.	.	.	
	.	.	.	.	.	
N	X_{n1}	X_{n2}	X_{n3}	…	X_{nk}	
Total	T_1	T_2	T_3	…	T_j	$T_.$
Mean	$\bar{X}_1$	$\bar{X}_1$	$\bar{X}_1$	…	$\bar{X}_1$	$\bar{X}_.$

Symbols used in the calculations

X_{ij} is the observation I in the procedure j when i = 1, 2, 3, …, n; j = 1, 2, 3, …, k

T_j is the sum of the observations in the procedure J.

$T_.$ is the sum of all observations.

$T_.$ is the number of data in the group J.

N is the total number of data.

4) The variance between the groups (Sum of Square Between the Groups (SSB)) is the variance between the mean of the data of each group. It is calculated in Eq. (2) [13], [14].

$$SSB = \sum_{i=1}^{k} (x_i - \overline{x})^2 \quad (2)$$

(4.1) Sum of Square Within the Groups (SSE) is the variance between data within the same group. It is calculated in Eq. (3) [12].

$$SSE = \sum_{i=1}^{k} \sum_{j=1}^{n_i} (x_{ij} - \overline{x}_i)^2 \quad (3)$$

(4.2) The total variance (Sum of Square Total: SST) is the total variance of all data from all populations in Eq. (4) [13], [14].

$$SST = \sum_{i=1}^{k} \sum_{j=1}^{n_i} (x_{ij} - \overline{x}_i)^2 \ , SST = SSB + SSE \quad (4)$$

In this research, the researcher used Analysis of Variance (ANOVA) to compare the performance of the three forecasting models because ANOVA was able to compare two or more forecasting models. This makes it appropriate to compare the performance of the forecast model. The data to be analyzed for a variance must comply with the following prerequisites [13], [14].

- The samples were randomly drawn from the normal distribution.
- The Population must independent of each other .
- The number of population variances must have the same amount.

(4.3) Accuracy is a measure of accuracy to compare forecast models to find a suitable model. Determination of work efficiency in Eq. (5) [13].

$$Accuracy = \frac{TP + TN}{TN + TP + FN + FP} x\ 100\% \quad (5)$$

TP is positive correct prediction value.
TN is negative correct prediction value.
FN is a positive error prediction value.
FP is negative faulty value.

(4.4) Precision is a measure of whether the forecast is true. The accuracy of the forecasting model can find the precision in Eq. (6) [13].

$$Precision = \frac{TP}{TP + FP} \quad (6)$$

TP is a positive prediction value.
FP is a negative prediction error value.

(4.5) Recall is a measure of the forecast that is true. What is the ratio of all true values of the forecast model? Remembrance can be found in Eq. (7) [13].

$$Recall = \frac{TP}{TP + FN} \quad (7)$$

TP is a positive prediction value.
FP is a positive prediction error value.

(4.6) Tool

In this research, the researcher used spreadsheet data to collect a survey for forecasting factors causing a delay in local tax payment. By extracting data from spreadsheet and using RapidMiner Studio as a tool to experiment with forecasting models each model could be compared [17]-[20].

VI. Results

The results of the research can be summarized into three parts:

Part 1 Comparison of Decision Tree, Naïve Bayes, and Neural Network Analysis.

Selecting three forecast models to find Accuracy, Precision and Recall in each forecast model, which will consist of the following operations. Import Data is to retrieve data in spreadsheet format, prepared for use in forecasting with various forecasting models. Select attributes is the selection of attributes to be used as a class in forecasting, and Cross Validation is to test the performance of each forecast model which uses RapidMiner Studio as a forecasting tool.

The process of creating a forecast model using a decision tree (J48) consists of operators as follows: first, forecasting with a Decision Tree forecast model, then the application of the created forecast model to make predictions. Finally, measure the performance of the forecasting model, for attributes such as Accuracy, Class Recall Accuracy, Class Precision accuracy, etc.

The forecasting process with the Decision Tree Forecasting Model is shown in the figure in Fig. 7.

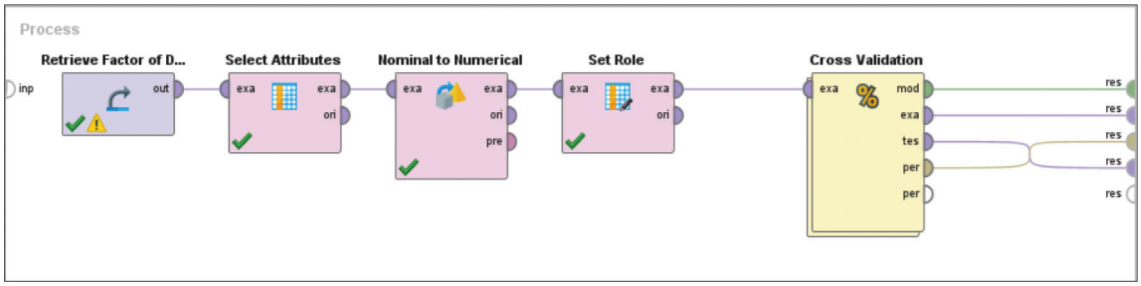

Fig. 7. The core process of forecasting with various forecasting models.

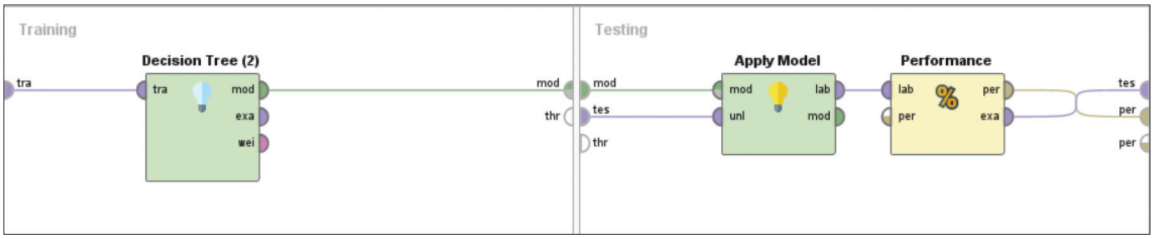

Fig. 8. Forecasting process with decision tree forecasting model

After forecasting with the Decision Tree Forecasting Model, the results are as shown in Table IV.

TABLE IV
FORECAST RESULTS WITH DECISION TREE FORECASTING MODEL

Model	Accuracy	Class Recall (True Yes)	Class Recall (True No)	Class Precision (Pred. Yes)	Class Precision (Pred. No)
Decision Tree	96.00%	96.00%	96.00%	97.56%	93.51%

Decision Tree Forecasting Model Accuracy = 96.00% Accuracy of Tax Factor Forecasting True Variable Yes = 96.00% Accuracy of Tax Factor Forecast False Variable No = 96.00%

Forecasting modeling process using Naïve Bayes consists of the following operators: first is forecasting with the Naïve Bayes forecasting model, then the application of forecasting models. Finally, measure of the performance of the forecast model, such as the Accuracy, Class Recall accuracy, and the accuracy of the Class Precision class, etc.

Forecasting process with the Naïve Bayes forecasting model as shown in the figure in Fig. 9.

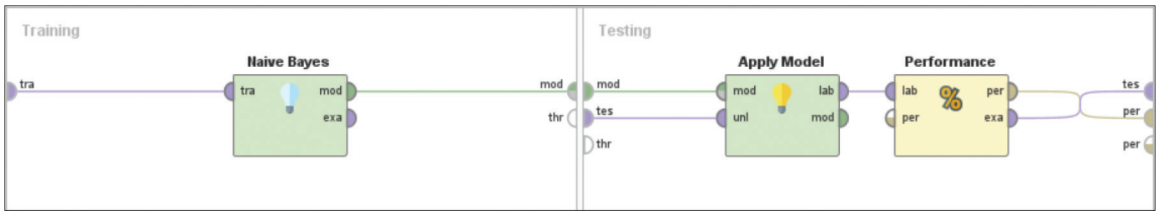

Fig. 9. Forecasting process with the Naïve Bayes forecasting model

After forecasting with the Naïve Bayes forecasting model, the results were as shown in Table V

TABLE V
FORECAST RESULTS WITH THE NAÏVE BAYES FORECASTING MODEL

Model	Accuracy	Class Recall (True Yes)	Class Recall (True No)	Class Precision (Pred. Yes)	Class Precision (Pred. No)
Naïve bayes	92.00%	100.00%	78.67%	88.65%	100.00%

Naïve Bayes Forecast Model Accuracy = 92.00 % Tax Factor Forecast Accuracy True Variable Yes = 100.00 % Tax Factor Forecast Accuracy False Variable No = 78.67%

The process of building a forecast model using a neural network consists of the following operators: forecast with a neural network forecast model, apply the forecasting model that has been created, then use measure the performance of the forecast model, in terms of Accuracy, Class Recall class accuracy, the accuracy of the Class Precision class, etc.

Forecasting Process with Neural Network Forecasting Model in Fig. 10.

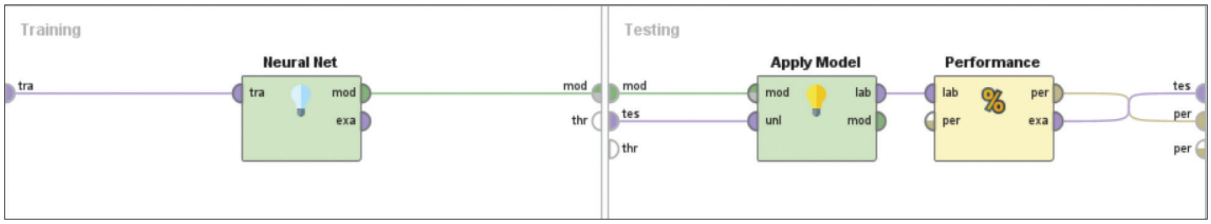

Fig. 10. The forecasting process with the Neural Network forecasting model.

After forecasting with the Neural Network forecasting model, the results are shown in Table VI.

TABLE VI
FORECAST RESULTS WITH NEURAL NETWORK FORECAST MODEL

Model	Accuracy	Class Recall (True Yes)	Class Recall (True No)	Class Precision (Pred. Yes)	Class Precision (Pred. No)
Neural Network	96.50%	96.00%	97.33%	98.36%	93.59%

Neural Network Forecasting Model Accuracy = 96.50% Accuracy of Tax Factor Forecast True Variable Yes = 96.00% Accuracy of Tax Factor Forecast False Variable No = 97.33%

Part 2 Compares the performance of Decision Tree, Naïve Bayes, and Neural Network forecasting models using ANOVA statistics in Fig. 11.

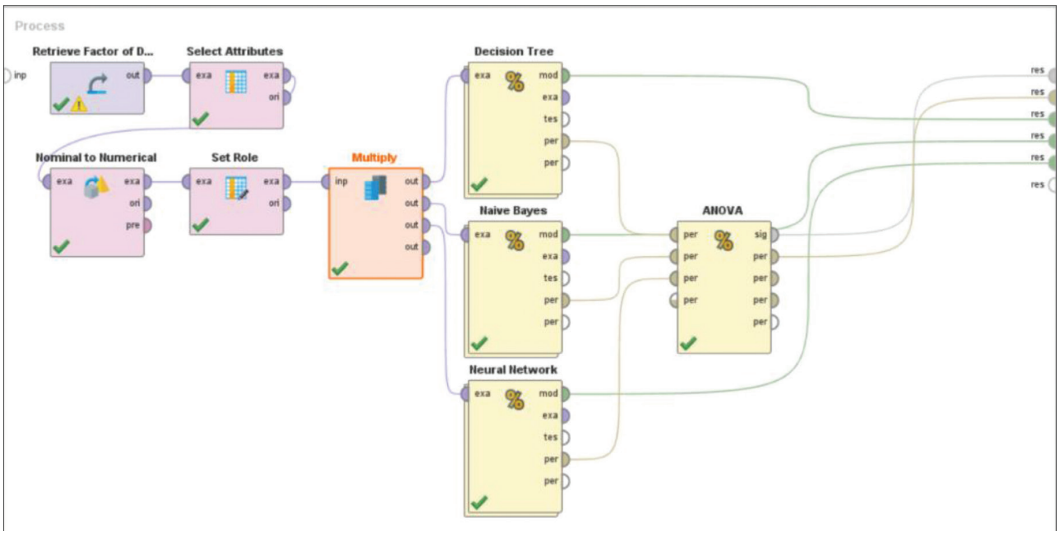

Fig. 11. Comparison of forecasting models with Rapid Miner Studio

Comparison of all 3 forecast models by using ANOVA statistics. Comparison of forecast models results as shown in Table VII.

TABLE VII
ANOVA FORECAST MODEL COMPARISON RESULTS

Source	Square Sums	DF	Mean Square	F	Prob
Between	0.007	2	0.004	1.817	0.182
Residuals	0.053	27	0.002		
Total	0.060	29			

The comparison of forecast models with ANOVA statistics revealed that the Decision Tree, Naïve Bayes and Neural Network forecast models had F = 1.817 and Prob = 0.182, which were not significantly different at the 0.05 level. The three forecasting methods were not significantly different. Therefore, any type of forecasting model can be used in research.

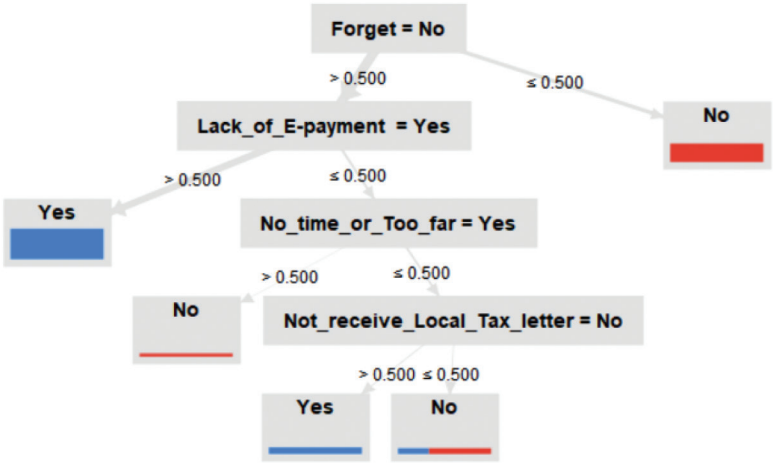

Fig. 12. Forecast results factors of delay payment with Decision Tree

From the forecasting of delayed local tax factors to Lam Sam Kaeo Town Municipality in 2020 with the Decision Tree forecasting model in Fig. 12.

1) IF Forget = "≤ 0.500" = "No"
#No means: Forget to pay tax".

2) IF Forget = "> 0.500" AND
Lack_of_E-payment = "> 0.500" = "Yes"
#Yes means: lack of E-payment method.

3) IF Forget = "> 0.500" AND
Lack_of_E-payment = "≤ 0.500" AND No_Time_or_Too_far = "> 0.500" = "No"
#No means: not worth the time and cost to travel to the local government organization.

4) IF Forget = "> 0.500" AND
Lack_of_E-payment = "≤ 0.500" AND No_Time_or_Too_far = "≤ 0.500" AND Not_receive_Local_Tax_Letter = "≤ 0.500" = "No"
#No means: not receive tax letter to inform tax from local government organization.

5) IF Forget = "> 0.500" AND
Lack_of_E-payment = "≤ 0.500" AND No_Time_or_Too_far = "≤ 0.500" AND Not_receive_Local_Tax_Letter = "≤ 0.500" = "Yes"
#Yes means: receive tax letter to inform tax from local government organization.

VII. Conclusion

The business intelligence system is a convenient way to collect data, calculate taxes, check tax payments, and make decisions about Land and Building taxes for Local Administration officers. The prototype developed in this project was given to five Local Administration officers to test. They found the program satisfied their needs and they could easily customize the reports to make them convenient.

A technique was used to predict the factors resulting in delayed tax payment: comparing the three forecasting models of Decision Tree, Naïve Bayes, and Neural Network, found no significant difference at 0.05 level (the ANOVA test found that F = 1.817 and Prob = 0.182.) The researcher chose the Decision Tree forecasting model to use in forecasting factors of late local tax payments in 2020.

The ANOVA test identifies whether there is a significant difference between groups. It allows you to decide whether you can reject the null hypothesis that there is no difference between the groups, and accept the alternate hypothesis that the groups are different.

It was found that the lack of electronic tax payment options (Lack of E-Payment) has the greatest impact, followed by forgetting to pay taxes (Forget) in second place. A solution approach is to add the payment status along with the payment due date and compare them. If the payment status is "NO" after the due date, that means the villager forgot. The delinquent villager can then be sent a reminder letter containing a QR code payment instruction to Lam Sam Kaeo Town Municipality bank account and ID Line to make payment easy and convenient.

Business intelligence (BI) can help companies make better decisions by showing present and historical data within their taxpayer context. Analysts can leverage BI to provide performance and competitor benchmarks (another local government organization) to make the organization run smoother and more efficiently. Analysts can also more easily identify the problems to increase tax. With this knowledge, the local administrators will be able to solve the problem in the following year.

VIII. Discussion

The research found the main factors that delayed local taxation to Lam Sam Kaeo Town Municipality in 2020. Three different forecasting models were compared using a sample of 200 local taxpayers in Lam Sam Kaeo Town municipality. The factors for delaying tax payment to Lam Sam Kaeo Town Municipality are discussed as follows:

From the forecast of factors causing the delay in local taxation to Lam Sam Kaeo Town Municipality it was found that

- Decision Tree analysis found that if the sample group forgot to pay the tax it would result in the most delay in tax payment.
- If the sample group has a problem with tax payment via electronic transaction system, i.e., Prompt Pay, it will result in the second most late tax payment.
- If the sample group has to pay the tax in person, and considers it not worth the time and cost to travel to the local government organization because the distance is far, this would result in delayed tax payment as well.
- If the sample does not receive a letter to inform them of the land and building tax, this will have the effect of delaying the payment of taxes.
- If the sample received a letter to inform them of the land and building tax, then there will be no effect on the late tax payment.

From the analysis, the factors affecting the late payment of local taxes to Lam Sam Kaeo Town Municipality were found. The two major reasons resulting in late payment of local taxes to the municipality are a) that people forgot and b) people found it difficult or inconvenient to make the payments.

Furthermore, according to the research comparing the efficiency and accuracy of the three forecast models, the Neural Network analysis model has an accuracy of 96.50%; the Decision Tree at 96.00%; and the Naïve Bayes model with an accuracy of 92.00% were not significantly different at level 0.05 therefore, any forecasting model can be used in forecasting. In this research, the researcher chose the Decision Tree forecasting Model to determine the factors affecting the late payment of local taxes to Lam Sam Kaeo Town Municipality because the decision tree model is a top-down tree-like structure that explains the decision-making rules for prediction.

At each step, a decision is made based on the attribute in question, and the result generates a branch of the tree. Using this divide and conquer approach, classification rules are generated. The rule is a path from the root node to an end node. An advantage of the Decision Tree is that the information gained can be used in feature selection as well [14]. That is why it is a widely popular and easy-to-understand algorithm.

XI. Suggestions

1) In the future this research should be a group analysis by village numbers. Adding a method for collecting data on surveys of the remaining uncompleted land areas to gain insights into the decisions of local administration officers.

2) Since it is the first year that the Land and Buildings Tax Act 2019 has been applied, there is still a lack of payment systems through the transaction

system. Electronic is Prompt Pay and the address of the taxpayer changes as well. As a result, the tax is delayed. Therefore, Lam Sam Kaeo Town Municipality can apply the research results to solve the problem in the coming years.

3) The results of the analysis can be used as a guideline for solving the problem of late tax payments to Lam Sam Kaeo Town municipality. For example, the development of a business intelligence system to collect complete and current data about land ownership and taxation, and generate reports about who pays taxes on time, late or forgets to pay taxes. This will save a lot of administration time, as well as reduce the need to create and store a lot of paper forms. This will result in more tax collection covering the entire municipality and reduce delays in tax payments.

REFERENCES

[1] Department of Local Administration, Ministry of Interior. (2021, June 10). *Land and Buildings Tax Act 2019*. [Online]. Available: http://www.dla.go.th/work/mixlaw2.pdf

[2] Department of Local Administration, Ministry of Interior. (2021, Jan. 10). *Royal Decree on reduces land and building taxes by 90%.* (2nd ed.) [Online]. Available: http://www.dla.go.th/upload/document/type2/2021/2/24981_1_1613034073130.pdf

[3] Department of Finance, Lam Sam Kaeo. (2021, May 10). *Data of Land and Building Taxpayers*. [Online]. Available lamsamkaeo.go.th/public/list/datal/index/Manu/1149

[4] Craig Stedman, Ed Burns. (2020, Sep.). *Business Intelligence (BI)*. [Online]. Available: https://searchbusiness.analyticstechtarget.com/definition/business-intelligence-BI

[5] O. Medovoi. (2019, Apr. 20). *Complete Guide to Business Intelligence and Analytics: Strategy, Steps, Processes, and Tools.* [Online]. Available: https://www.altexsoft.com/blog/business/complete-guide-to-business-intelligence-and-analytics-strategy-steps-processes-and-tools/

[6] P. Tiangsombun, (2018, Sep.). Business Intelligence Systems To Support Executive Forecasting And Decisions Making Case Study: Healthcare. *Veridian E-Journal, Science and Technology Silpakorn University.* [Online]. *5(4),* pp. 16-30. Available: https://ph01.tci-thaijo.org/index.php/VESTSU/article/view/148906

[7] S. Leelataweewud. (2020, May.) The Studying of Cloud Business Intelligence System Architecture for Asean Economic Community. *Suthiparitthat Journal DPU.* [Online]. *30(93)*, pp. 177-192. Available: https://so05.tci-thaijo.org/index.php/DPUSuthiparithatJournal/article/view/242764

[8] E. Sangiamkul and T. Panrungsri (2019, Jun.). Development of Decision Support System in Impact and Severity from Flood in Phuket. *Information Technology Journal.* [Online]. *15(1)*, pp. 60-70. Available: https://ph01.tci-thaijo.org/index.php/IT_Journal/article/view/199901

[9] P. Pipatjessadakul and O. Pinngern (2019, Dec.). Development of Business Intelligence System to Support Electrical Distribution. *Journal of project in Computer Science and Information Technology.* [Online]. *5(2)*, pp. 49-56. Available: https://ph02.tci-thaijo.org/index.php/project-journal/article/view/204706

[10] E. Naowanich and N. Jeerungsuwan (2017 Jun.). The Development of Business Intelligence System for Supporting the Administrations' Decision Making to Access Occupation Internationally for Students of Rajamangala University of Technology. *Academic Journal Bangkokthonburi University.* [Online]. *6(1)*, pp. 184-198. Available: https://so01.tci-thaijo.org/index.php/bkkthon/article/view/210782

[11] S. Hai-Jew. (2021, Jun. 10). *Using Decision Trees to Analyze Online Learning Data*. [Online]. Available: https://newprairiepress.org/cgi/viewcontent.cgi?article=1005&context=isitl

[12] S. Ray. (2021, Jun. 10). *6 Easy Steps to Learn Naive Bayes Algorithm with Codes in Python and R. India.* [Online]. Available: https://www.analyticsvidhya.com/blog/2017/09/naive-bayes-explained/

[13] A. Dertat. (2021, Jun. 10). *Applied Deep Learning - Part 1: Artificial Neural Networks*. [Online]. Available: https://towardsdatascience.com/applied-deep-learning-part-1-artificial-neural-networks-d7834f67a4f6

[14] H. Deng, G. Runger, and E. Tuv. "Artificial Neural Networks and Machine Learning," Presented at ICANN 2011. Conf. Artificial Neural Networks, Jun. 14-17, 2011.

[15] B. Hembree. (2006, Feb.). *One way ANOVA (Analysis of Variance)*. [Online]. Available: https://www.itl.nist.gov/div898/handbook/ppc/section2/ppc231.htm

[16] P. Siriattakul. (2012, Sep.). One-Way ANOVA: Social Science Research. *Journal of Interdisciplinary Research: Graduate Studies,* vol. 1, no. 1, pp. 1-11, Sep. 2012.

[17] N. Hongboonmee and P. Trepanichkul (2019, Jun.). Comparison of Data Classification Efficiency to Analyze Risk Factors that Affect the Occurrence of Hyperthyroidusing Data Mining Techniques. *Journal of Information Science and Technology (JIST).* [Online] *9(1)*, pp. 41-51. Available: https://ph02.tcithaijo.org/index.php/JIST/articleview/179188

[18] R. Caruana and A. Niculescu-Mizil. (2006, Jun.). *An Empirical Comparison of Supervised Learning Algorithms. Present at Proceedings of the 23rd International Conference on Machine Learning, Pittsburgh, PA.* [Online]. Available: https://www.researchgate.net/publication/215990477_An_Empirical_Comparison_of_Supervised_Learning_Algorithms

[19] A. Chutipascharoen (2018, Nov.). A Comparison of the Efficiency of Algorithms and Feature Selection Methods for Predicting the Success of Personal Overseas Money Transfer. *KKU Research Journal of Humanities and Social Sciences*. [Online]. *6(3),* pp. 105-113. Available: https://so04.tci-thaijo.org/index.php/gskkuhs/article/view/156370

[20] N. Hongboonmee and P. Trepanichkul. (2019, Jun.). Comparison of Data Classification Efficiency to Analyze Risk Factors that Affect the Occurrence of Hyperthyroid using Data Mining Techniques. *Journal of Information Science and Technology*. [Online]. *9(1)*. pp. 41-51. Available: https://ph02.tci-thaijo.org/

[21] R. Caruana and A. Niculescu-Mizil. (2006, Jun.). *An Empirical Comparison of Supervised Learning Algorithms. Present at Proceedings of the 23rd International Conference on Machine Learning, Pittsburgh, PA*. [Online]. Available: https://www.researchgate.net/publication/215990477_An_Empirical_Comparison_of_Supervised_Learning_Algorithms

Watchawee Wongart is a student at Master of Science (Information Technology), College of Digital Innovation Technology. He graduates B. in Business Computer Information System form Rangsit University in 2013 and graduates M. in Business Logistic Management in 2016.

Somchai Lekcharoen was born in Bangkok, Thailand in 1965. He received the M.Sc. degree in Information Technology from King Mongkut's University of Technology in 1998, Thonburi Campus, Thailand. He received his Ph.D. in Computer Science at Assumption University of Thailand in 2008. He is an assistant professor of faculty of digital innovation technology, Rangsit University, Thailand. He has published more than 90 scientific papers. He is scientific research and for leadership in the area of science in Telecommunication engineering and his research interest is today focused on congestion control, network of queue and data mining.

Materials on Wheels: Batteries for Electric Vehicles

Paritud Bhandhubanyong[1] and John T. H. Pearce[2]

[1]Faculty of Logistics and Transportation Management, Panyapiwat Institute of Management, Nonthaburi, Thailand
[2]Faculty of Engineering and Technology, Panyapiwat Institute of Management, Nonthaburi, Thailand
E-mail: paritubha@pim.ac.th, johnthomasharrypea@pim.ac.th

Received: August 26, 2021 / Revised: September 24, 2021 / Accepted: September 28, 2021

***Abstract*—The Thai government is placing the advanced automotive industry sector among the 12-targeted industries as the key drivers for economic and social development. So, all kinds of Electric Vehicles (EV), namely, Battery Electric Vehicles (BEV), Hybrid Electric Vehicles (HEV), Plug-in Hybrid Electric Vehicles (PHEV), and Fuel Cell Electric Vehicles (FCEV) will be the focus for Thai automotive sector promotion by the government. Two key components of EVs are the motor and battery pack. Present battery types and major characteristics are elaborated and discussed with emphasis on materials development, obstacles, and appropriate solutions for the future sustainability of EV manufacturing and application.**

***Index Terms*—Materials on Wheels, Batteries for Electric Vehicles, Future Aspect of Batteries**

I. Introduction

Electric vehicles are typically classified into four general types [1], [2]:

- All-electric vehicles where the battery pack is the sole power source, hence these are termed Battery Electric Vehicles (BEVs). The battery is charged by the plug-in to an external source of electrical power. These vehicles reduce the consumption of oil and gas-based fuels and during driving they do not produce exhaust emissions.
- Hybrid Electric Vehicles (HEVs) are powered by a conventional Internal Combustion Engine (ICE) but are also fitted with an electric motor supplied via a relatively small battery pack. This battery is recharged while driving under ICE power and by regenerative braking during which the motor can act as a generator. The electric motor power enables the use of a smaller capacity ICE giving improved fuel consumption and reduced emissions without loss in performance.
- Plug-in Hybrid Electric Vehicles (PHEVs) are also powered by a conventional ICE and by an electric motor. The battery pack fitted is larger than in HEVs and is charged by plugging into an outside electrical power source, and as in HEVs via the ICE and during regenerative braking. When fully charged it is possible to drive under electric power only for up to about 50 km.
- Fuel Cell Electric Vehicles (FCEVs) are driven by an electric motor powered by electricity generated onboard from hydrogen-based fuel cells. A FCEV does not need a heavy energy storage battery but is normally equipped with a smaller battery to provide extra power for acceleration and to increase efficiency by regaining of energy via regenerative braking.

The need for and the increasing awareness of reducing carbon emissions combined with government incentives in many countries have resulted in greater public interest in and ever-increasing worldwide use of EVs [3]. As well as being free from exhaust emissions BEVs offer lower running and maintenance costs compared to ICE and hybrid vehicles. Forecasts estimate that, by the year 2040, EVs will account for around 55% of all new passenger cars [3], [4] and this figure may be as high as 66% if major car groups cease production of ICEVs by 2035. Projections for conservative and accelerated growth in zero and low emission vehicle (ZLEV) sales in the European market are illustrated in Fig. 1 [5]. The accelerated uptake prediction assumed that major car producers will cease ICEV manufacture from 2035 onwards.

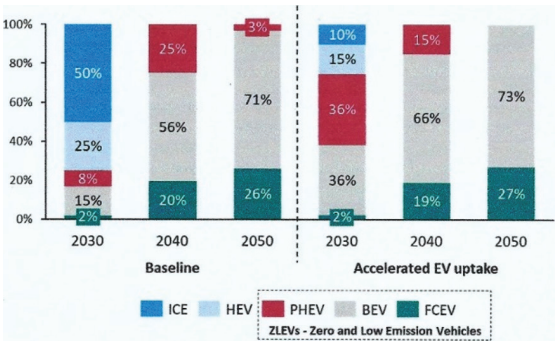

Fig. 1. Forecasts for vehicle sales in Europe under conservative baseline and accelerated EV uptake conditions [5].

One definite target is that of the EV30@30 Initiative which was launched in 2017 with current participation by Canada, China, Finland, France, India, Japan, Mexico, Netherlands, Norway, Sweden, and the United Kingdom [6]. The aim of this initiative is for all types of electric vehicles, apart from 2-wheeled, to collectively achieve a market share of 30% by 2030. A recent survey [7] suggests that continuing reductions in the price of battery packs will soon make EVs as affordable as comparable ICE models. In 2020 the average cost of a Lithium-ion battery pack was $137 per kWh approaching the $100 per kWh at which EVs cost roughly the same to manufacture as ICEVs.

In general, the continued developments in EV batteries and the materials used for their construction are aimed at:

- Increasing the driving range
- Reducing the time needed for recharge
- Improving safety by prevention of overheating
- Reducing cost of battery packs
- Solving environmental and ethical problems in the supply of raw materials
- Improving the working life and the potential for reuse and recycling.

Focusing on BEVs, this overview of materials for EVs considers the property requirements and availability of materials for the manufacture of anodes and cathodes for battery packs and comments briefly on the extra importance for light-weighting of body sections and other parts in order to compensate for the additional weight of the batteries. Material aspects of fuel cells are not included in this review and are covered elsewhere [8]-[10].

II. Battery Types and Characteristics

Electric vehicles need batteries that can supply high energy storage and high power. The energy storage capacity of a battery controls the potential charge-to-charge driving range and can be characterized by the specific energy in Wh./kg or by the energy density as Wh./l. Acceleration depends on battery power which can be described as specific power in W/kg or as power density in W/l. Hence, the relative performance of EV batteries is often compared on a Ragone type diagram [11] in which the specific energy or energy density is plotted versus the specific power or power density. An example of such representation (Fig. 2) from 2007 [12] illustrates the then required trade-off ranges between energy and power for HEV, PHEV, and BEV and indicates why more recent EV battery developments and usage have been focused on Li-Ion technology.

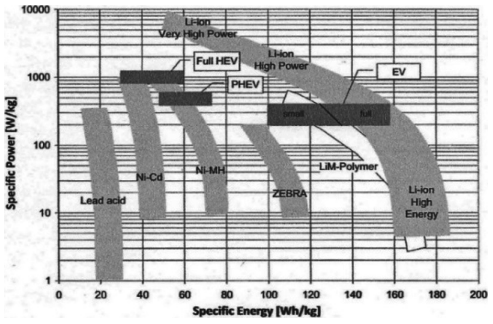

Fig. 2. Specific Power-Specific Energy relationships for various battery types in 2007 [12].

The characteristics of established and developing battery technologies are compared in Fig. 3, which plots energy density as Wh./l against specific energy [13]. The higher the value of power density, for a given acceleration, the smaller is the volume requirement for the battery while higher values for energy density reduce the mass of the battery enabling weight-saving and/or possible increased range.

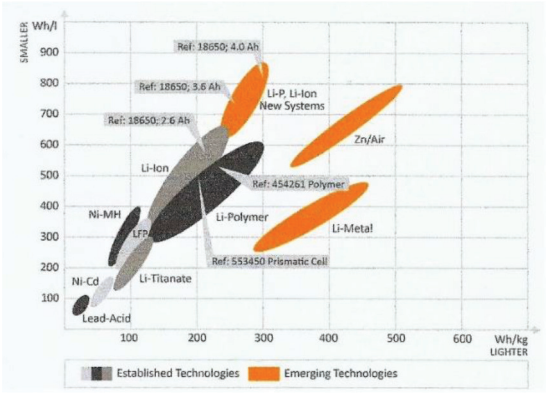

Fig. 3. Plot of energy density as (Wh./l) against specific energy (Wh./kg) for established and some emerging battery technologies [13].

The reference number indicated relate to battery cell size: 18650 is a cylindrical cell 18 mm in diameter with height of 65 mm; 454261 is rectangular with dimensions 45x42x61mm and 553450 is also rectangular 55x34x50 mm.

In addition to batteries, capacitors and fuel cells also have potential to provide power for EVs. Like batteries, capacitors store energy. They can supply this energy rapidly but unfortunately only in small amounts since they have lower specific energy than batteries [14].

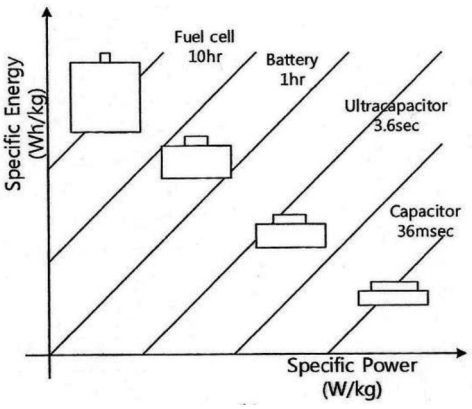

Fig. 4. The barrel model of Lee & Jung used to compare energy sources [15]. A capacitor has a small volume but a large opening area whereas a fuel cell has a large volume but only a small opening area.

Capacitors can be used in hybrid battery-capacitor systems where the capacitor can boost acceleration and store energy from regenerative braking. Fuel cells, like ICEs, generate energy and they offer high specific energy but this is offset by low specific power. Comparison between batteries, capacitors, and fuel cells can be conveniently made by reference to the barrel model proposed to supplement Rag one plots [15] as shown in Fig. 4.

III. Lead – Acid Batteries

The history, present status and future of EV batteries can be considered with reference to Fig. 2 and 3. In the early days of the "horseless carriage" some 120-150 years ago, BEVs fitted with the first rechargeable lead-acid batteries provided strong competition for steam powered and ICE vehicles [16]. However, lead-acid batteries (LABs) have very limited levels of 20-35 Wh./kg for specific energy and hence are not suitable for use in traction applications, other than for golf and indoor carts and forklift trucks. To meet noise regulations and prevent exhaust fumes, electric forklifts and other off-road vehicles are increasingly replacing those powered by diesel or LPG, and as such are essential for indoor applications [17]. The weight of LABs is not a problem since the weight of the forklift must be sufficient to provide counterbalance during lifting operations. This is a complete contrast to automotive applications, where the weight of the battery is required to be as light as possible. However, even in forklifts, LABs can be replaced by hybrid Li-Ion/supercapacitor systems which offer improved power performance, energy efficiency, and cycle life plus reduced charging time and less maintenance [18]. It is recognized that, in addition to the larger traction battery, all electrified powertrains, HEVs and BEVs, retain a 12V start-up, board-net, and electronic component supply which continues to be provided by an auxiliary 12V LAB. This auxiliary is also used to maintain the safety management of the larger traction battery and, in start-stop systems store energy recovered via regenerative braking [19].

Ongoing LABs research is aimed at improving their capability in regenerative brake charging and motor assistance in hybrid vehicles [20], [22], applications in which they must be able to perform at high discharge and recharge rates. Unfortunately, at high rates of discharge, LABs suffer from irreversible growth of large, insulating lead sulfate crystals on the negative electrode, which subsequently reduces fast recharge ability. This problem can be reduced by adding carbon to the electrode to improve conductivity, to reduce sulfate crystal growth, and to provide capacitive behavior to buffer high charge and discharge rates [20], [21]. Although the negative electrode is improved in this lead-carbon battery, the positive electrode still suffers from softening and shedding. Further work is needed to provide additives to the positive electrode material to reduce this deterioration to further improve cycle life [22].

IV. Nickel – Metal Hydride (Ni-MH) Batteries

A number of Ni-based alkaline battery systems have been developed including Ni-Cd, Ni-Fe, Ni-Zn, and Ni- metal hydride (Ni-MH). Of these, only the Ni-MH type became suitable for use in EVs. Ni-Cd batteries were originally considered as an alternative to lead-acid but their use in on the road automotive application is restricted due to toxicity issues. However, Ni-Cd batteries continue to be used in off the road industrial vehicles due to their insensitivity to external factors such as low temperatures, their wide operational temperature range of -40°C to +60°C, plus their lack of requirement for complex management systems [17]. Collection and recycling of used industrial alkaline batteries is close to 100% in Europe where the battery industry has set up a well-controlled closed-loop recycling system in which the battery manufacturer takes back used batteries which are then recycled at certificated companies [17]. Ni-Fe battery cells suffer from high self-discharge rate and hydrogen gassing, while Ni-Zn batteries are limited by the instability of the Zn electrodes under cycling conditions and dendritic growth causing short circuits [2], [23], [24].

Nickel-Metal Hydroxide (Ni-MH) battery cells consist of a metal hydroxide anode (negative electrode) plus a Ni hydroxide cathode (positive electrode) with a microporous polymer film separator and a potassium hydroxide-based electrolyte to provide ionic conductivity between the anode and cathode in the cell. The separator, which must be permeable to ions and be inert in the battery environment, acts as a physical barrier between the positive and negative electrodes to prevent electrical shorting. MH alloys are inter-metallics used for H storage, such as AB_5,

A_2B_7, and AB_2, where A is a combination of rare and alkaline earth elements, and B is mainly Ni with other transition metals. They are used as the active component in the anode since they are able to reversibly store hydrogen in an electrochemical environment [25]. The electrochemical reactions in Ni-MH, LAB, Li-Ion and other battery cells are compared in a number of reviews [25]-[28].

Reactions during the charging and discharging stages of a Ni-MH battery [28] are summarized as equations (1)-(3). In each case, the forward reaction occurs during charging and the reverse on discharge. On charging bivalent Ni is oxidized to become trivalent and M is reduced on absorbing H.

$$\text{At the cathode: } Ni(OH)_2 + OH^- \rightleftharpoons NiOOH + H_2O + e^- \quad (1)$$

$$\text{At the anode: } M + H_2O + e^- \rightleftharpoons MH + OH \quad (2)$$

$$\text{Overall cell: } Ni(OH)_2 + M \rightleftharpoons NiOOH + MH \quad (3)$$

Ni-MH batteries have twice the specific energy combined with much higher energy density than lead-acid types, and have been used in EVs since the late 1990's [29], [30]. For example, the original Ford Ranger Electric pick-ups, made available in California to meet local environmental requirements, were fitted with a lead-acid battery pack which had mass of 870 kg. This was soon replaced by a Ni-MH pack weighing much less at 485 kg to give increases in payload and range [29]. Also, to be sold in California, the first electric version of the Toyota RAV4 SUV was powered by Ni-MH battery packs. Problems with patents and limitations to supply caused the brakes to be applied to the further development of Ni-MH large format battery packs for BEVs [30]. However, Ni-MH batteries continued to be fitted to hybrid vehicles having become the preferred power source in the hybrid Toyota Prius introduced in 1997 as the first mass-produced hybrid vehicle. Over the last 20 years, Ni-MH batteries have been used in many hybrid vehicles but in most current models they have been replaced by Li-Ion batteries which provide higher specific energy and energy density (Fig. 3).

Ni-MH batteries have proven durability and can be safely and profitably recycled to reclaim their high Ni content. Consequently, they continue to be subject to further development in China [31], Japan [32], Europe [33], and the US [27]. Continued developments [28], [34]-[39] are aimed at increasing energy density, improving charging efficiency, increasing cycle life and reducing self-discharge rates with materials research focused on the composition and structure of the anode and cathode materials. The most commonly used anodes have the general formula of AB_5 where B represent Ni and other elements such as Co, Al, Mn, and Cr while A represents Ce, Nd, La, Pr, Y, Hf, Zr, Ti, Nb, and Pd, etc. For example, one variant of AB_5 is $MmNi_{3.55}Co_{0.75}Mn_{0.4}Al_{0.3}$ where Mm refers to mischmetal containing a suitable combination of rare earth elements [25]. AB_2 Laves phase anodes have also been used in EV batteries, notably for the General Motors EV1 model, while A_2B_7 type are used in stationary applications [36]. Development to increase energy density is mainly focused on optimizing composition for the C14 hexagonal crystal structure of the AB_2 type. As for Li-ion packs, other work has examined ways of improving high-rate capability [38] and battery thermal management/cooling systems [39]. Although R&D on Ni-MH batteries continues, a survey by automotive battery manufacturers [19] has suggested that the potential for further market penetration by Ni-MH batteries has been reduced due to the increased performance and reduced cost of Li-Ion batteries coupled with concerns over Ni prices. Because Ni-MH batteries have already reached a relatively high degree of technological maturity, this survey expects that there will be only limited improvements in their performance by 2025.

V. Lithium – Ion (Li-ion) Batteries

Li-ion batteries have become preferred for EV applications since they have 2 times the energy density of the Ni-NH type, have a low self-discharge rate, can operate over a range of temperatures and have long cycle life [40]-[45]. Li-ion batteries are also the least affected by the memory effect by which some types of batteries gradually offer reduced maximum energy capacity with repeated charging. Li is the third lightest element, has a very small ionic radius and has the lowest reduction potential of all the elements enabling the highest possible cell potential, hence Li-based batteries have been developed for traction applications. A schematic view [40] of the electrochemical processes that take place in a basic Li-ion cell is given in Fig. 5 in which the cathode is represented as a layered lattice structure and the anode as a 2D graphite structure. Examples of basic cell arrangements in batteries are given as pouch, cylindrical and prismatic in Fig. 6. The main differences between these arrangements center on the dissipation of heat during charging and the relationship between packing arrangement of the cells in a battery module and cooling efficiency via thermal management, the pouch type cell enabling better heat dissipation [46]. Conventional cylindrical cells have a so called "swiss roll" construction and are encased in Al or steel, prismatic cells are encased in Al or polymer, and pouch cells in Al-polymer composite material which needs to be supported within a frame.

In a basic cell the anode consists of Li retained in graphite while the cathode has a layered structure of $LiMO_2$ where M is Co, Ni or Mn. The standard electrolyte is made up of Li salts such as $LiPF_6$ in a mixture of organic carbonate solvents such as

ethylene carbonate and dimethyl carbonate. Because Li reacts with water, an aqueous electrolyte cannot be used. Both the anode and the cathode materials permit Li^+ ions to become intercalated or extracted from within their lattice structures during charging or discharge. During charging, the cathode provides Li^+ ions which move to the anode and are stored therein. As indicated in Fig. 5, during discharge electrons move from the anode to the cathode while Li^+ ions exit the anode to move simultaneously in the same direction through the electrolyte and back into the cathode lattice.

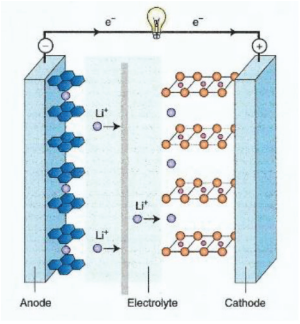

Fig. 5. Electrochemical processes in a Li-ion cell. After Goodenough [40].

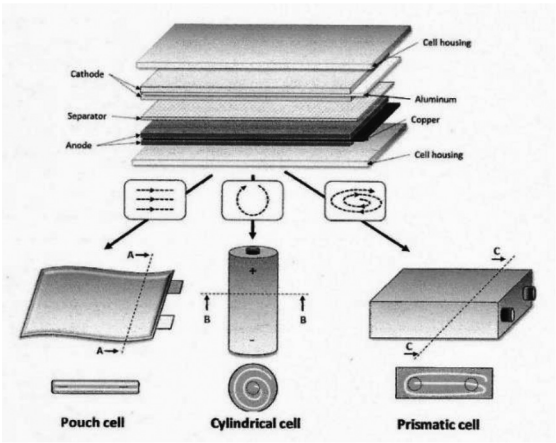

Fig. 6. Examples of lithium-ion cell arrangements: pouch, cylindrical and prismatic [46].

Reactions during the charging and discharging stages of the cell shown in Fig. 5 are summarized in equations (4)-(6). In each case, the forward reaction occurs during charging and the reverse on discharge.

At the cathode: $LiCoO_2\ CoO_2 + Li^+ + e^-$ (4)

At the anode: $C_6 + Li^+ + e^-\ LiC_6$ (5)

Overall cell: $C_6 + LiCoO_2\ LiC_6 + CoO_2$ (6)

The electrolyte contains a porous membrane, made of polyethylene and polypropylene, called a separator which allows passage of the Li^+ ions and is used to prevent any direct contact between the anode and the cathode [47]. As seen in Fig. 6, to allow electron transport, the anode is in contact with a Cu current collector and the cathode with one made of Al. Al cannot be used at the anode since it is reactive with Li. To produce the electrodes the active materials are mixed with binders and additives in a solvent to form a slurry that is coated onto the respective current collectors. A water-based solvent is used for the anodes and an organic solvent such as N-methyl pyrrolidone for the cathode. After drying the coated electrodes are roll-pressed and cut to size for final processing and cell assembly [48], [49].

VI. Anode Materials in Li-Ion Cells

A. Graphite Anodes

Li metal cannot be safely used as an anode in conventional liquid electrolyte systems since during cycling it tends to form dendritic growths which can penetrate the separator material causing internal short circuits, thermal runaway on the cathode, and a risk of combustion [41], [42], [50]. Dendritic Li can also be detached to form "dead Li," gradually reducing performance. The large volume changes of the electrode during repeated dissolution and deposition of Li can also deteriorate the cell. Metallic Li is highly reactive such that surface corrosion in organic electrolytes can occur increasing interfacial resistance and reducing both efficiency and life of the cell [42]. Hence, graphite has become widely used as the anode material because Li ions can be intercalated into its layered structure between graphene plates and by this means Li dendrite growth can be prevented [51]. Graphite is an abundant relatively low-cost material with high electrical conductivity, high Li diffusivity and only undergoes small volume changes during loss and gain of Li atoms. Up to 1 Li atom per 6 C atoms can be stored. For EV batteries synthetic graphite is used due to its low impurity level which ensures less variation in production quality and greater stability when operating over a wide temperature range [41].

During the first few charging cycles, it is fortunate that a solid electrolyte interphase (SEI) layer is spontaneously generated on the graphite anode of lithium-ion batteries via the breakdown of the electrolyte. Although it reduces efficiency, the SEI layer allows through transport of Li ions while passivating the surface of the anode thus inhibiting any further decomposition of the electrolyte and increasing cycle life [52]-[54]. The SEI also controls the efficiency and safety of lithium batteries. The SEI is multiphase containing LiF, Li_2O, inorganic carbonates such as Li_2CO_3 and lithium ethylene di-carbonate (LiEDC). To improve the stability of the SEI, electrolyte additives such as vinylene carbonate and fluoroethylene carbonate can be used [55]. Volume changes in the anode can damage the SEI. The formation, nature and breakdown of the SEI layer is reported as complex and continues to be researched to determine the effects of electrolyte additives and formulation on Li ion conductivity and on potential improvement in SEI stability on conventional

graphite anodes during long-term cycling [54], [56] and on other potential anode materials [57]. To develop an understanding of SEI formation and other electrode reactions requires the application of cryogenic high resolution electron microscopy [58], [59].

Graphite anodes tend to be intercalated with electrolyte as well as Li ions causing a reduction in capacity and strains in the graphite lattice and hence in the SEI layer. The intercalation with electrolyte is not reversible and causes volume expansion over charging and discharging cycles leading to exfoliation. Also, if battery cells become overheated C anodes can catch fire [44], [60]. Hence, there is continued development in the use of alternative anode materials such as lithium titanium oxide (LTO), conversion compounds, Li metal, and silicon.

B. Lithium Titanium Oxide Anodes

Lithium titanium oxide (LTO) with a formula $Li_4Ti_5O_{12}$ and a spinel structure has been used for anodes for some 30 years [61]. Like graphite, LTO is an intercalation anode since lithium ions can be inserted and removed from its lattice structure. Compared to graphite LTO has a lower specific capacity, a higher lithiation/de-lithiation plateau and lower conductivity of electrons, and diffusion rate of Li ions [60]-[63]. Graphite gives a specific capacity of 372 $mAhg^{-1}$ but LTO only 175 $mAhg^{-1}$. Graphite has a low working potential of about 0.2V couple whereas LTO operates at an excessively high potential of 1.55V vs Li^+/Li which limits output energy density. When paired with conventional cathodes LTO only provides a nominal cell voltage of 2.4 V compared to that of 3.7 V for graphite [42]. Nevertheless, LTO is reported to offer increases in power density, efficient charging at low temperatures, and improved cycling stability as a zero-strain material [41], [42], [44], [61]-[64]. Due to its higher Li insertion potential LTO is also less likely to form Li dendrites and whiskers than graphite [42], [62]. However, LTO can generate high gas volumes due to reaction between the organic electrolyte, and active material especially at higher temperatures of 40-60◦C [45], [65].

To improve the electrochemical properties and performance of LTO other elements such as Ru, W, Ce and La have been used to modify the lattice structure. For example, the inclusion of La can give rise to a perovskite lattice with a higher specific capacity of 225 $mAhg^{-1}$ and a lower potential of 1.0V vs Li^+/Li [64]. To improve conductivity, the forming of composites with better electronic conductors such as C has also been considered [45]. Another approach is to produce nano-structured material. In batteries, power output and minimum charging time both depend on movements of ions as well as electrons with ionic diffusion being the main factor that limits the rate of charge and discharge. Hence, to increase these rates, nanotechnology is being used to produce nano-sized crystal structures in active materials in order to reduce the Li+ diffusion distances [66], [67]. Nanotechnology is also being used in preparing LTO from $TiOSO_4$ which is said to be an inexpensive Ti-source produced during the mining process of ilmenite ($FeTiO_3$). The LTO is prepared as microspheres which are nucleated on small clusters of TiO_2 nanoparticles [68]. To improve the energy density of graphite anode cells carbon nano-structures have also been investigated but the production and handling of carbon nanotubes and graphene gives rise to environmental concerns such that nanostructured LTO is considered to a be a safer alternative [69].

For both graphite and LTO, anode materials surface coating can be applied to improve charge transfer between the anode and the electrolyte. Coating materials include Ag, C, Cu, Sn oxide, alumina and conductive polymers [45], [67], [70]-[72]. LTO can be coated with C to suppress the gas evolution that stems from reactions between the LTO and organic electrolyte although such coating can enhance electrolyte decomposition and cause SEI formation [70]. To reduce gassing, the use of electrolyte additives to form passivating surface films on LTO has also been investigated [73]. Nano-coatings of amorphous C, metal, metal oxides and polymers are used to protect graphite anodes from reactions with the electrolyte with application via wet chemical methods or vacuum deposition [67].

C. Conversion and Alloying Type Anodes

As potential alternatives to intercalation anodes there is continued development of conversion anodes and alloy type anodes [42], [44], [45], [57], [74]-[76]. Conversion reaction type anodes consist of M_aX_b where M represents transition metals such as Co, Cu, Fe, Mn and Ni, and X represents H, N, F, O, P, and S. Examples are Fe_2O_3, Co_2O_3, SnO_2, and CuO. Instead of intercalation a chemical reaction occurs such that all the M in the transition metal compound MaXb is fully replaced by Li forming metal nanoparticles M. Conversion anodes can offer high theoretical specific capacities of 500-1500 $mAhg^{-1}$ but suffer from low Li diffusion rates and large volume changes during cycling. Towards improvement, research is focused on optimizing their chemical composition and nanostructure [77]-[80]. Oxide nano-particles with hollow structures offer the ability to withstand stress from high volume changes and their high surface to volume ratio can increase Li mobility [80].

Other possible anode materials are the alloying-type which include Si, Sn, Pb, Sb, Zn, Al, Ag, Ge, and In and metal oxides, sulphides and phosphides [45], [57], [75], [76], [79]. This type can alloy with Li^+ to form Li-alloy compounds after lithiation and can exhibit discharge capacity of up to 4x higher than that of graphite since these anodes can store more Li^+ per unit (volume or mass) than intercalation anodes [75],

[76]. However, their practical application is restricted by slow Li^+ reaction rate and very large volume changes (>300%) during Li alloying and dealloying causing degradation and limited cycle life.

Si has a theoretical specific capacity of 3578 $mAhg^{-1}$, almost 10 x of that of graphite. Si is also non-toxic and has ready availability hence it is one of the most promising materials for anodes [46], [75]. Replacing the use of graphite with silicon could increase energy density and reduce costs. The large volume changes involved in repeated expansion and contraction of Si during battery cycling result in loss in capacity due to pulverization and electronic isolation of Si, and the instability in the SEI layer. To improve cycle life, attempts to minimize the effects of these large volume changes in Si when gaining or losing Li ions have led to the development of Si nanoparticle anodes [67], [79]. These employ nanostructured Si materials such as nanowires, hollow spheres, porous particles, and composite Si/C yolk–shell structures combined with polymer binders. The binders prevent disintegration of the anode and delamination from the current collector, and also improve the stability of the SEI layer thus preventing continuous exposure of fresh surfaces that could react consuming Li ions and electrolyte [81]-[84]. Recent binder research has examined the replacement of synthetic polymer binders, such as polyvinylidene fluoride and carboxymethyl cellulose, by natural biopolymers which have structural arrangements such as long chains that can better withstand strains from volume changes [83], [84].

In Si nanoparticle/C composites hollow or porous structures provide spaces for volume expansion with the inclusion of C improving electron conductivity. The combination of intercalation C material with a low content of alloy-type anode material such as silicon in mixed systems can increase theoretical capacity, for example, about 1000 $mAhg^{-1}$ can be achieved using mixed anode of 20% Si and 80% carbon [46]. To increase SEI stability also requires the development of improved interfacial polymer inorganic composite surface films which could be produced via decomposition of electrolyte additives or from preformed interfaces. In assessing the performance characteristics of anodes, it is expected that the silicon content in graphite or carbon-based anodes will gradually increase from the current 5-10% levels. Although Si–C and SiO_x–Si–C composite anode materials have been the subject of considerable R&D, there is little information on their commercial production [85], [86]. There is interest in silicon oxides (SiO_x) - based anode material since, although when compared to Si it has a lower initial theoretical capacity of 2615 $mAhg^{-1}$, it undergoes a significantly smaller volume change of 160% than the 300% for Si during lithiation/de-lithiation. Hence, SiO_x is more likely to provide better cycling performance since it should be less prone to pulverization and SEL instability [87], [88].

At the company's 2020 Battery Day to introduce a new tabless design for 46 dia.x80mm sized cylindrical cells, Tesla announced a move away from C-based materials such as graphitic carbon and graphene to Si-based material for anodes [89], [90]. To avoid Si expansion problems the COBRA battery consortium in Europe is focused on developing Si-C composite materials for anodes to be ready for commercialization by 2025 [91]. These nano-structured Si/C composites as for use with LNMO Co free cathodes as the EU funded COBRA protect is entitled "Cobalt-free Batteries for Future Automotive Applications". Other battery producers are also reported to be introducing Si-based anodes including NEO Battery Materials in Canada [92], Israel-based StoreDot, Gotion High-Tech in China and Enovix and Sila Nanotechnologies in the USA [93].

D. Li Metal Anodes

Li metal is an ideal candidate anode material for high energy density Li-Ion batteries since it exhibits a high theoretical capacity of 3860 $mAhg^{-1}$ and a low potential of -3.04 V vs SHE [50]. However, despite considerable R&D efforts practical application remains difficult due to a number of problems [94], [95]. These include high volume changes, dendrite formation, high reactivity, instability of the SEI, and the associated loss of active Li and degradation of the electrolyte [94]-[97]. The net effect is high internal resistance, low efficiency, shortened life, and not least concerns over safety if dendritic Li penetrates the cell separator. These problems are very difficult to overcome when using conventional liquid electrolytes [50], hence most research efforts have focused on replacement by solid-state electrolyte systems.

VII. Cathode Materisls in Li-Ion Cells

Cathode materials need high capacity for Li ions with minimum structural change during the removal and gain of Li ions and should offer a high potential vs Li^+/Li. Li-ion batteries can be conveniently classified according to their cathode chemistry with, in most cases, graphite serving as the anode material. Since the introduction of the original $LiCoO_2$ lithium cobalt oxide (LCO) cathode [40] a number of commercialized cathode materials have been developed. Most of these are based on layered or spinel transition metal oxides having a general formula of $LiMO_2$ where M signifies transition metals of which some examples are listed in Table I. As for anode materials, Li ions can be intercalated into the lattice structures of these cathode materials with Li stored between parallel MO_2 layers. NMC type cathodes have now become the most widely

used for both PHEV and BEV electric vehicles. From a 2017-18 survey of 30 models from 17 major car manufacturers, it was reported [98] that 24 models used NMC batteries, 5 used NCA and only 1 used LFP. However, since then the manufacturing capability and use of LFP cathodes has significantly increased such that their estimated global market share was up to near 20% in 2020 and is forecast to increase to 25% in 2021 [99].

TABLE I
EXAMPLES OF CATHODE MATERIALS USED IN LI-ION BATTERIES. DATA FORM [41], [44], [106], [146].

Cathode Type	Formula	Structure	Practical specific capacity (Ah/kg)	Discharge Potential v Li (V)
LCO	$LiCoO_2$	Layered oxide	140-150	3.9
LNO	$LiNiO_2$	Layered oxide	220-240	3.75
NMC 111	$LiN_{0.33}Mn_{0.33}Co_{0.33}O_2$	Layered oxide	160	3.7
NMC 532	$LiN_{0.5}Mn_{0.3}Co_{0.2}O_2$	Layered oxide	165-170	3.7
NMC 622	$LiN_{0.6}Mn_{0.2}Co_{0.2}O_2$	Layered oxide	170-180	3.7
NMC 811	$LiN_{0.8}Mn_{0.1}Co_{0.1}O_2$	Layered oxide	190-200	3.7
NMC 955	$LiN_{0.9}Mn_{0.05}Co_{0.05}O_2$	Layered oxide	200-205	3.7
NCA	$LiN_{0.8}Co_{0.15}Al_{0.05}O_2$	Layered oxide	200	3.7
LMO	$LiMn_2O_4$	Spinel	110	4.1
LMNO	$LiMn_{1.5}Ni_{0.5}O_4$	Spinel	140	4.7
LFP	$LiFePO_4$	Olivine	165-170	3.45
LFMP	$LiMn_{0.7}Fe_{0.3}O_4$	Olivine	155	3.9

A. Lithium Cobalt Oxide (LCO) and Lithium Nickel Oxide (LNO) Materials

The original LCO type cathode material is no longer considered suitable for automotive applications due to safety concerns and the high and volatile cost of its high cobalt content. LCO has a high theoretical specific capacity of 274 Ah/kg but its reversible capacity is limited to 140 Ah/kg since irreversible structural collapse occurs if too much Li is removed when operated at potentials over 4.35 V vs Li/Li^+ [41], [44], [100]. LCO cathodes have high reactivity and suffer from low thermal stability such that thermal runaway can occur causing batteries to catch fire [41], [42]. However, small-sized LCO batteries continue to be used and developed for portable electronic equipment applications. Additions of Al, Cr, Fe, and Mn as dopants or as Co substitutes and oxide coatings such as Al_2O_3, TiO_2, and ZrO_2 have been made towards improving not only thermal stability but also structural stability especially at charging potentials of over 4.35V, the latter providing possible increases in useable capacity [100]-[103]. Since it has the same type of lattice structure and a similar theoretical specific capacity of 275 Ah/kg, $LiNiO_2$ (LNO) has also been investigated as a potential alternative to LCO. However, LNO is more thermally unstable than LCO and tends to form a self-passivating layer blocking Li ion diffusion [104], [105]. $LiNiO_2$ is difficult to produce with the correct stoichiometry and it also undergoes damaging irreversible structural changes during gain and loss of Li ions from its lattice [105]

It was found [106] that partial substitution of Co by Ni in LCO combined with small additions of Al could improve both electrochemical behaviour and thermal stability. This led to the development of the commercially used NCA cathodes which have a general formula of Li $(Ni_xCo_yAl_{1-x-y})$ O_2 [107], [108]. Recent work [109] has found that the stability and cycling behavior of NCA became gradually improved with increasing Al content from 0 to 5.6%. However, Al contents above 5.6% gave deleterious effects, including increased residual lithium on the cathode surface and the formation of impurity phases ($LiAlO_2$ and Li_5AlO_4) which reduced cell capacity.

B. Lithium Manganese Oxide (LMO)

Lithium manganese oxide $LiMn_2O_4$ (LMO) has a spinel type lattice structure which allows improved ionic movement compared to a layered structure. LMO has better thermal stability and safety than LCO but has lower capacity and shorter life. Due to its low cost, non-toxicity and high rate of discharge capability, LMO was used in the first-generation Nissan Leaf but in later models has been replaced by NMC [110]. Wider use of LMO has been limited by its fast rate of fading in capacity during cycling which is associated with solution of Mn ions, distortion of its lattice, and side reactions between LMO, and the electrolyte [67], [111]-[114].

During discharge at high current, the diffusion rate of Li^+ ions in the electrolyte is higher than that in the bulk of cathode such that Li^+ ions accumulate

on the surface of the cathode leading to the formation of a Mn^{3+} rich region and to the dissolution of Mn^{2+} into the electrolyte. The formation of Mn^{3+} results in the Jahn-Teller (J-T) distortion whereby distorted Mn^{3+} ions destabilize the lattice causing an irreversible cubic to tetragonal structural transformation which causes anisotropic volume changes [111]-[113]. This restricts the three-dimensional Li^{+} diffusion pathways reducing capacity retention after repeated charge/discharge cycles and promotes cracking in the cathode particles. Performance is also reduced by the Mn^{2+} going into solution and then plating out in the SEI on the graphitic anode [112], [113]. The reduction in performance is much worse at temperatures over 50°C.

The JT distortion can be reduced by doping with Fe, Co, Al or Ni, while Mn^{2+} dissolution and other side reactions can be reduced by surface treatment of the cathode with nano-coatings of oxides such as ZrO_2 and TiO_2 [112]-[116]. Fluoride and phosphate coatings have also been used to prevent reaction with and decomposition of the $LiPF_6$-based carbonate electrolyte [117]. Doping with Ni can be used to form a core-shell type structure in which $LiMn_2O_4$ is protected by a shell of $LiNi_xMn_{2-x}O_4$ (LNMO) [118], [119]. Cathodes prepared from Ni doped LMO coated with $NiCo_2O_4$ have also been studied [120]. $LiMnPO_4$ (LMP) coating is also being examined as a potentially more effective alternative to coating with LNMO [121]. There is also interest in using carbon coating to protect LMO cathodes. A solvent-free mechanofusion method, which uses repeated strong centrifugal force combined with high shear and compression forces, has been shown to produce a uniformly dense, stable C coating [122]. This coating ensured no direct exposure of the core material to the electrolyte, ensuring minimal active metal dissolution with improved conductivity via interparticle contact and improved electrochemical and cycling performance.

It is also reported that the J-T distortion and Mn^{2+} dissolution can be suppressed by using composite cathodes in which there is a fine mixture of spinel and layered domains [113], [123]-[126], for example, nano-domains of layered Li_2MnO_3 can be embedded into micro-sized $LiMn_{1.5}Ni_{0.5}O_4$ to stabilize the structure [119]. Li_2MnO_3 has also been used to form experimental layered composite cathode material with $LiCoO_2$ [127]. For such layered structures, this work suggested that control of fine-scale microstructure, notably the domain size of the Li_2MnO_3-component, is the most important parameter to achieve improved electrochemical behavior.

C. Nickel-rich Cathode Materials, NCA and NCM.

To overcome problems associated with the thermal instability and limited life cycle of LCO and LNO materials layered ternary metal oxides with high Ni contents have been progressively developed as the NCA and NMC series of cathodes [128]-[133]. As commented earlier, controlled additions of Ni and Al to LCO to give NCA, normally with the ratio Ni:Co:Al as 0.8:0.15:0.05, are used to improve performance [107]-[109]. It was also found that including Co in LNO and $LiNi_xMn_{2-x}O_4$ (LNMO) material can help to maintain reversible capacity by preventing cation mixing in which Ni ions and Li ions can exchange their positions in the Ni-Mn mixed oxide lattice [130], [132].

Raising the Ni content increases the energy density and hence vehicle range [129], [130]. The Ni:Mn:Co ratio used in NMC cathodes was originally 1/3:1/3:1/3 but has gradually changed to become increasingly Ni rich to 5:3:2 then 6:2:2 and now 8:1:1 [133] and in the near future it is changing to 9:0.5:0.5 [108], [134]. The NMC cathodes are most frequently classified in terms of these compositional ratios as NMC111, NMC532, NMC622, and NMC81, but are sometimes referred to as NCM cathodes [132], [135]. High Ni contents also became necessary to replace Co due to increasing concerns over the cost and security of Co supplies and not least due to reported unethical and environmentally damaging mining practices used in the Democratic Republic of Congo (DRC) in central Africa, a region that supplies some 65% of the world's Co [133], [136]-[138]. The geographic distribution of Co is uneven with the other 35% coming mainly from China and Canada, each with 6%, and Russia, Cuba, and Australia. The supply of Co is dependent on Cu and Ni mining since 90% of Co is obtained as by-product [137]-[139]. With the expected rapid growth in EV production, it has been estimated that by 2030 the annual demand for Co just to be used in Li based batteries will be around 285,000 tons which is nearly twice the total world Co output of 145,000 during the year 2019 [139]. Naturally, there are additional concerns and predictive models for other critical elements such as Li, Ni, and Mn that are needed for EV batteries, and over suitable developments for efficient and safe recycling of end-of life batteries and recovery of all component elements [135], [139]-[142].

Increasing the Ni content improves capacity in NMC cathodes but it also has some adverse effects. It reduces thermal stability and resistance to cycling damage, and gives higher surface reactivity which can cause unwanted side-reactions, electrolyte decomposition and oxygen evolution [112], [143]-148]. With higher N contents in NMC the layered structure tends to become unstable during delithiation such that a surface layer of NiO can be produced together with outer layers of Li-P-O compounds and polycarbonates giving rise to a cathode electrolyte interface (CEI) [146]. Considerable research efforts have focused on degradation studies [112], [144], [147] towards improving NMC stability via the use of:

- doping agents such as Mg and Zr [149]
- coating materials such as C [150], phosphate [151], and polymers [152]-[154]
- tailored concentration gradients and core-shell structures [155], [156]
- grain boundary and particle size control [157]-[159].

Although doping of NMC622 with Mg and Zr, performed during the NMC622 synthesizing co-precipitation process reduced capacity, it improved stability by inhibiting structural changes and prevented collapse of the layered structure. The effects of such doping were said to be complex and difficult to predict [149].

Uncoated cathodes are prone to degradation of active materials and hence capacity fade due to their reaction with hydrofluoric acid containing electrolytes. Coating of the cathode may reduce or prevent such reactions with the thickness, uniformity and ionic and electronic conductivity of the coating being the main factors in coating selection [130], [143], [150]-[153]. Ultrathin thin rough surface coatings have been the subject of considerable development [130] with atomic layer deposition (ALD) being of most interest to provide effective thin layer coatings consisting of Al_2O_3 [143]. Phosphate coatings based on Li_3PO_4 may be used to provide not only protection of the active material but also to themselves act as active layers to improve electrochemical properties [143], [151]. Cathode particles can be encapsulated with a S-containing polymer called PERDOT which unlike conventional coatings can penetrate the interior of the particle aggregates to give additional protection [153], [154]. The coating allows transport of Li ions and electrons and is also said to prevent both structural conversion to spinel phase and oxygen release thus enabling the battery to operate at higher voltage to increase energy output or promote longer life [154].

Concentration gradient structures have been produced in LMNO type cathode particles in which the surface of each particle is Mn rich while the core is Ni rich with each particle containing tailored near linear concentration gradients for both Mn and Ni [155]. The higher Ni level at the surfaces is designed to reduce capacity fade, Mn ion solution and side reactions [111]-[114] outlined earlier. In contrast to LMO and LNMO, for improved stability and cycle life in the Ni rich NMC materials the surface of each particle needs to be Mn rich with the high-capacity core being Ni rich. This is achieved by producing particles having core-shell structures [156]. Using the core-shell approach, which is said to be easier to achieve than controlled concentration gradients, cathode particles with overall composition equivalent to NMC811 but with Ni rich core compositions near to NMC9.5.5 and Mn rich surfaces equivalent to NMC111 have been reported to provide significantly improved capacity retention when compared to homogeneous NMC811 material [156].

In conventional polycrystalline NMC the cathode particles consist of near-spherical aggregates of small sub-micron crystals. During cycling, volume changes occur causing cracking of these particles leading to isolation of the active material and capacity loss. The cracking may be reduced by infiltration along grain boundaries of low melting point oxides or Li_3PO_4 solid electrolyte [157] or by producing the cathode particles as single crystals of 2-10 micron in size. The use of single crystals not only suppresses cracking but also significantly increase Li ion diffusivity raising power density [158]-[160].

D. Lithium Iron Phosphate (LFP) Cathodes.

Unlike the layered cathode materials, LFP, with a formula $LiFePO_4$, has an olivine type lattice structure. It is one of a group of polyanion compounds based on $(XO_4)^{3-}$ where X=P, S, Si, As. Mo or W [41]. The main advantages of LFP as a cathode include good thermal stability, high safety, Co free, environmentally friendly, non-toxic, long cycle and shelf life, and relative low cost since it contains abundant elements [41], [131]-[133], [146]. LFP has higher resistance to heating effects than other cathode materials and is much less likely to suffer thermal runaway. However, LFP has limited electronic and ionic conductivity and hence is difficult to charge at high rates, has low nominal voltage of 3.4V versus Li/Li^+, and limited practical specific capacity of 120-160 mAh/g, the latter giving a shorter range per charge compared to NMC types [131], [132], [136], [161], [162]. The performance of LFP can be improved by reducing particle size to nano-scale, by C coating, by doping and by producing composites with various forms of C [146], [161]-[164]

The advantages offered by LFP, especially regarding safety aspects, have outweighed its disadvantages for applications in hybrids such as BMW 3 and 5 Series, motor-homes, forklifts, tourist boats, and especially for public transport buses in China [132], [133], [146]. Over the last 2 years, the increased need for reduction in the use of Co and Ni in order to lower costs has renewed interest in batteries fitted with LFP cathodes. In China, it is reported that LFP batteries now have 47% of the market and that Tesla is now using LFP in its China-made Model 3 saloon while Volkswagen is also planning for its use in entry level models [165], [166]. Although Ni based cathode batteries can offer ranges of 450 km, for economic reasons, in spite of its limited range of only about 160 km, the current best-selling car in China is the Hong Guang Mini, produced by a GM joint venture [165]. In a recent techno-economic report it has been predicted that, in the light of increasing

safety standards, LFP could become increasingly used after 2022 when patent restrictions that currently limit its production to China are due to expire [167].

LFP batteries suffer from lower performance and reduced range in cold climatic conditions, however the recent reported development in thermally modulated (TM) LFP batteries is claimed to be a solution to this problem [168]. The TM-LFP battery which operates safely at 60^{o}C in all types of ambient conditions is said to offer equivalent performance to NMC622 and additionally can be fast-charged in 10 minutes to provide suitable cruising range.

For future alternatives to LFP there are some other olivine type structures that could be developed as cathode materials include $LiMnPO_4$ (LMP), $LiFeSPO_4$ (LFSP) and $Li_3V_2(PO4)_3$ (LVP) [41], [146], [169].

VIII. A Note on Future Development

A 2021 battery technology roadmap has highlighted some potential future developments [170]. Examples of such developments include improvements in solid state batteries, Li-O and Li-S batteries, Al- and Zn-air batteries, and Na, K, Mg and Ca based batteries. It is estimated that during the last 20 years around 170,000 scientific/technical papers have been published on battery developments [170]. Although about 45% of this work has focused on Li-Ion batteries there is increasing R&D interest in Na-ion, Li-S, and other metal-ion types [170], [171], and for safety reasons in batteries that can use aqueous electrolytes [172].

At present and over the next few years the move to use solid state electrolytes in Li-ion batteries will improve safety since these electrolytes, when compared to flammable organic liquid or gel media-based electrolytes, can inhibit the growth of Li dendrites, do not pose leakage problems and reduce fire risk [42], [89], [173]-[176]. They can operate at higher voltage, be charged at high rates and require less space in the vehicle. The solid electrolyte also acts as a separator. Solid electrolytes may allow the use of thin Li films as the anode decreasing the weight and volume of the battery in comparison with conventional anodes [95], [96]. Developments in solid-state electrolytes are focused on a variety of inorganic materials such as complex Li metal oxides, sulphides, halides and phosphates, garnets, perovskites [177]-[179], and also on polymer composites [180]-[182]. Of particular importance is the study of the behaviour of solid electrolytes at their interfaces with the electrodes and effects on performance and life [183], [184]. In composite solid electrolytes, the polymer provides flexibility and effective interfacial contact with the electrodes while the inorganic gives higher ionic conductivity [182]. On an industrial scale the handling and processing of such materials and the manufacture of solid-state cells presents a number of practical difficulties, for example, during sintering after conventional slurry-based processing [179]. In laboratory and pilot scale development of batteries a number of different processing routes, such as tape casting, wet powder spraying, roller coating, hot pressing and physical/chemical deposition, are used. However, the choice of both materials and processing methods can become much narrower when a particular development needs to be scaled up for manufacturing [185], [186]. Problems related to scaling up of processing for mass production are nevertheless being solved such that Toyota and Volkswagen expect to have solid state batteries in some of their EVs before 2025, with other manufacturers to follow. The Toyota battery is reported to provide 500 km range per charge and a full recharge capability within 10 minutes [187]. Since Na is an abundant low-cost resource, it is an attractive substitute for Li in the development and commercialization of Na-ion type batteries [170], [188]-[191]. Na is chemically similar to Li but has a larger ionic diameter such that diffusion rates of Na ions are relatively slow, even when cathodes with sufficiently large enough space to accommodate within their lattice can be found [170]. The larger Na ion also results in larger volume changes during cycling. With further development it is predicted that Na-ion batteries with hard C anodes and Co-free cathodes will be suitable for applications in short range EVs and in large-scale stationary energy storage applications [188], [189].

As other alternatives to conventional Li-ion batteries, there is growing research interest in the use of metal anodes such as Li, Na, Al, and Zn in combination with cathodes such as S, Se, and O_2. [170]. Of these Li-S batteries are believed to offer the greatest potential since not only can they offer a theoretical energy density of 2600Whkg^{-1} (about 5x higher than for conventional Li-ion) but also S can be readily sourced at low cost. At present Li-S batteries remain limited by low ionic conductivity, the short life of Li anodes and precipitation and transformational changes within electrolytes [192], [193].

Al metal anodes have also shown promise to deliver high-capacity cells but their development continues to be restricted by difficulties in finding suitable cathode materials and in formulating electrolytes which are not corrosive to current collector and battery container materials [170], [194]. For metal-air batteries which use oxygen-permeable cathodes, and safe, aqueous electrolytes, Zn may prove to be the most suitable anode material. However, the main problems to be overcome include the formation of Zn dendrites and passivation by Zn

oxide [170], [195]. There is also interest in developing organic electrode materials [196] and in anionic batteries [197]. For all types of battery developments, the characterization, production, and control of consistent nano-structured materials continues to be of increasing significance in seeking to improve performance and safety [67], [69], [198]-[200].

Sustainability is the rationale for the change from internal combustion engines to electric vehicles. Battery developments must continue to focus on sustainability with the need to conserve, recover, reclaim and re-use critical materials [135], [136], [140], [142], [201]-[209] and, linked to the re-use of materials, on the need to further develop efficient and environmentally safe manufacturing processes [210], [211]. Data from a 2020 Greenpeace report on EV batteries reinforces the need for sustainability research and action. Greenpeace estimate that between 2021 and 2030 there will be 12.85 million tons of "spent" EV lithium-ion batteries while during the same period some 10.35 million tons of lithium, cobalt, nickel, and manganese will be mined for new batteries [212]. By 2030, lithium use for global battery production is projected to be 29.7 times higher than in 2018. In addition, from 2021 to 2030, EV battery production will use up 30% of the world's current proven cobalt reserves.

EV battery packs are heavy, hence for efficiency and environmental reasons, the light-weighting of body and other parts in EVs is essential to offset this extra weight. Light-weighting allows the use of smaller battery packs thus reducing materials usage and costs. Alternatively, it may enable an increase in vehicle range per charge by allowing an increase in battery pack size. Over the last 50 or so years, the auto-industry has gained considerable experience in weight saving from their efforts in reducing body-in white (BIW) mass of ICE and hybrid vehicles [213]. These advances in light-weighting together with improvements in IC engine efficiency and more effective use of catalytic converters have reduced the amount and toxicity of harmful exhaust emissions. Vehicle weight reduction and emission controls will continue to be key drivers in ICE and hybrid vehicle development as the gradual transition to BEV and FCEV usage takes place over the next 2 or 3 decades. BIW weight savings have been achieved via the use of advanced high-strength steels and by replacement of steels by Al alloys in sheet and extruded form and as die-castings. First generation EVs made use of steels but the trend for BIW is now to completely replace steels by Al alloys [214]. For lightness and impact resistance, Al alloys are also used for the enclosures or housings needed to contain and protect the battery modules. Al alloys also provide sufficiently high thermal conductivity required for thermal management of battery temperature and by providing an electromagnetic shield avoid interference effects with other electrical and electronic vehicle systems [215]. Battery enclosures are normally constructed from hollow extruded sections and/or sheet material and are integrated into the body structure of the vehicle. In a novel recent development by Tesla, very large high-pressure die cast Al alloy parts are used for single-piece front and rear underbody. These 2 sections are joined with a honeycomb type Al alloy battery enclosure such that the enclosure actually contributes to the strength of the vehicle structure rather than just containing the battery cells [89], [216].

IX. Outlook of EV Battery Industry in Thailand

According to the ERIA (Economic Research Institute for ASEAN and East Asia) research project report [217], Thailand has a strong position in conventional starter battery production and exports. In terms of trade value, NiMH batteries are not a significant item with 0.1 million US dollars in exports value and 21 million dollars imports value in 2019. A significantly higher import level of 122.5 million US dollars than exports of 8.4 million US dollars for Li-ion batteries suggests that Thailand does not play a significant role in the global supply chain for this type of battery.

On the other hand, the numbers for import and export values for battery modules, cells, and components are significant (110.0 vs 112.2 million US dollars) which could be interpreted as Thailand being a source of EV batteries assembly.

According to the Kasikorn Research Center (K-Research), Thailand's assembly and output of EV batteries are predicted to reach 430,000 units by 2023 which would account for three percent of global EV battery production, placing Thailand in the top four in Asia. Sales of the three types of EVs; HEV, PHEV, and BEV in the country will account for 25% of the total car market. In addition, Thailand will be the hub for EV battery export in ASEAN with 40% of the production or 170,000 units intended for export in 2023. Battery EVs will be mainly delivered to Japan, Oceania, Singapore, and Malaysia due to the rising income growth and government's support for EV facilities [218]. Battery manufacturers in Thailand consist of both multinational companies from Europe and Japan and domestic companies stimulated by the strong investment promotion incentives by the government [219].

X. Conclusion

This general review has covered the battery materials that have and are being used in electric and hybrid vehicles, and has outlined some possible

future developments. It is believed that Li-ion battery technology will continue to dominate the EV market for at least the next decade. Several new promising battery technologies continue to be increasingly researched. In 2015 the number of academic papers on battery developments was 15,000 but by 2020 this number had increased to 23,000 [170]. Potential new battery technologies such as Li-S, Zn-Air, Al-Ion and capacitors and fuel cells require long times to commercialize since the transition from laboratory scale studies to production viable battery cells is a very arduous process.

Li-ion batteries will continue to be improved, in particular by developments in nano-materials for anodes and cathodes and by improvements in solid state electrolytes. There needs to be further studies into degradation mechanisms especially in countries like Thailand where ambient temperatures can be well above 25^{o}C. However, it is equally if not more important for the industry R&D to pay more attention to the recycling and next-life reuse of EV spent batteries in order to conserve critical materials and avoid further damage to the environment. In terms of raw material supply, in the future production of Ni-rich cathodes Thailand has to face possible strong competition from the Philippines and Indonesia, who unlike Thailand have natural reserves of Ni.

With regards to recycling and reuse there is the question of who is to be responsible for these activities. Will the OEM vehicle builder be liable to finance recycling at the end of life of the battery and who will be responsible for the collection and testing, etc., of batteries from vehicles at the end of their lives? In Europe, for example, there is the Extended Producer Responsibility (EPR) scheme which is part of the Waste Framework Directive 2008/98/EC (WFD). This scheme is to ensure that producers of products bear financial responsibility or financial and organizational responsibility for the management of the waste stage of a product's lifecycle [220]. For Thailand, the Ministry of Higher Education, Science, Research and Innovation (MHESI), in collaboration with the Electric Vehicle Association of Thailand (EVAT) and a number of science and academic institutions have recently joined forces to form the Thailand Energy Storage Technology Alliance (TESTA) to create a collaborative platform and network as well as ensuring that R&D, especially on Lithium-ion batteries, is fully commercialized. [221] Meanwhile, the Department of Industrial Works, Ministry of Industry (MOI) is preparing the plan for EV battery end-of-life management and the Pollution Control Department, Ministry of Natural Resources and Environment (MONRE) is enacting the Acts for the EV battery end-of-life management [222].

Rererences

[1] C. E. Thomas, "Fuel Cell and Battery Electric Vehicles Compared," *International Journal of Hydrogen Energy*, vol. 34, no. 15, pp. 6005-6020, Aug. 2009.

[2] F. Un-Noor, S. Padmanaban, L. Mihet-Popa et al., "A Comprehensive Study of Key Electric Vehicle (EV) Components, Technologies, Challenges, Impacts and Future Direction of Development," *Energies,* vol. 10, no. 8, p. 84, Aug. 2017.

[3] International Energy Agency. (2021, Jul. 5). *Global EV Outlook 2020*. [Online]. Available: https://www.iea.org/reports/global-ev-outlook-2020

[4] S. Baltac and S. Slater. (2021, Jul. 10). *Batteries on Wheels: The Role of Battery Electric Cars in the EU Power System and Beyond*. [Online]. Available: https: www.elementenergy.co.uk/wordpress/wpcontent/upload/2019/06/Batteries on wheelsPublicreport 4th-June-2019.pdf

[5] S. Baltac and S. Slater. (2010, Jun. 4). *Batteries on Wheels: The Role of Battery Electric Cars in the EU Power System and Beyond*. [Online]. Available: http://www.elementenergy.co.uk/wordpress/wpcontent/uploads/2019/06/Batteries_on_wheels Public-report_4th-June-2019.pdf

[6] Clean Energy Ministerial. (2021, Jul. 10). *EV30/30 Increasing*. [Online]. Available: https://www.cleanenergyministerial.org/compaign-clean-energy-ministerial/ev3030-campaign

[7] I. Boudway. (2021, Jul. 10). *Batteries for Electric Cars Speed Towards a Tipping Point*. [Online]. Available: https://www.bloomberg.com/news/articles/2020-12-16/electriccars-are-about-to-be-as-gas-powered models

[8] J. Kurtz, S. Sprik, G. Saur et al., "On-Road Fuel Cell Electric Vehicles Evaluation: Overview," Technical Report National Renewable Energy Laboratory Golden, Co., USA, Re. NREL/TP-5400-73009. May 2019.

[9] Y. Manoharan, S. E. Hosseini, B. Butler et al., "Hydrogen Fuel Cell Vehicles; Current Status and Future Prospect," *Applied Sciences,* vol. 9, p. 17, Jun. 2019.

[10] Y. Wang, D. F. R. Diaz, K. S. Chen et al., "Materials, Technological Status and Fundamentals of PEM Fuel Cells-a Review," *Materials Today*, vol. 32, pp. 178-203, Feb. 2020.

[11] T. Christen and M.W. Carlen, "Theory of Ragone Plots," *Journal of Power Engineering*, vol. 91, p. 216, Dec. 2000.

[12] F. R. Kalhammer, B. M. Kopf, D. Swan et al. (2007, Apr. 10). *State of California Air Resources Board Sacramento, California, USA*. [Online]. Available. http://w2agz.com/Library/Storage/EV%20Batteries/Kalhammer_2007_zev_panel_report.pdf

[13] E. Rahimzei, K. Sann, and M. Vogel. (2015, May 2). *Kompedium: Li-Ionen Betterien*, *Frankfurt-am-Main, Germany: Verband der Elctrotechnik*. [Online]. Available: https://www.dke.de/resource/blob/933404/3d80f2d93602ef58c6e28ade9be093cf/kompendium-li-ionen-batterien-data.pdf

[14] B. D. McCloskey, "Expanding the Ragone Plot: Pushing the Limits of Energy Storage," *Journal of Phys, Chem, Letters*, vol. 6, pp. 3592-3593, Jun. 2015.

[15] S. C. Lee and W. Y Jung, "Analogical Understanding of the Ragone Plot and a New Categorization of Energy Devices," *Energy Procedia*, vol. 88, pp. 526-530, Jun. 2016.

[16] M. Guarnieri, "Looking Back to Electric Cars," in *Proc. 3rd IEEE Hist. Electro-Technol*, 2012, pp. 1-6.

[17] EUROBAT. (2017, Jun. 20). *Battery Technology for Motive Off-Road Application*. [Online]. Available: https://www.eurobat.org/images/news/publications/final_eurobat_motive_power_report_lores.pdf

[18] T. Paul, T. Mesbahi, S. Durand et al., "Sizing of Lithium-Ion Battery/Sup Ercapacitor Hybrid Energy Storage System for Forklift Vehicle," *Energies,* vol. 13, p. 18, Jul. 2020.

[19] EUROBAT. (2014, May 14). *A Review of Battery Technologies for Automotive Applications*. [Online]. Available: https://www.acea.auto/publication/a-review-of-battery-technologies-for-automotive-applications/

[20] P. T. Moseley, D.A. Rand, and K. Peters. "Enhancing The Performance of Lead-Acid Batteries with Carbon-In Pursuit of Understanding," *Journal of Power Sources,* vol. 295, pp. 268-274, Nov. 2015.
[21] J. Yang, C. Hui, H. Wang et al., "Review on the Research of Failure Modes and Mechanisms for Lead-Acid Batteries," *International Journal of Energy Research*, vol. 41, pp. 336-352, Mar. 2017.
[22] H. Hao, K. Chen, H. Liu et al., "A Review of the Positive Electrode Additives in Lead-Acid Batteries," *International Journal of Electrochemical Science*, vol.13, no. 3, pp. 2329-2340, Mar. 2018.
[23] S. F. Tie and C. W. Tan, "A Review of Energy Sources and Energy Management Systems in Electric Vehicles," *Renewable & Sustainable Energy Reviews*, vol. 20, pp. 82-102, Apr. 2013.
[24] M. A. Hannan, M. M. Hoque, and A. Mohamed "Review of Energy Storage Systems for Electric Vehicle Applications: Issues and Challenges," *Renewable & Sustainable Energy Reviews*, vol. 69, pp. 771-789, Mar. 2017.
[25] C. C. Yang, C. C. Wang, M. M. li et al., "A Start of the Renaissance for Nickel Metal Hydride Batteries: A Hydrogen Storage Alloy Series with an Ultra-Long Cycle Life", *Journal of Materials Chemistry A*, vol. 5, pp. 1145-1152, Dec. 2017.
[26] B. G. Pollet, I. Staffell, and J. L. Shang, "Current Status of Hybrid, Battery and Fuel Cell Electric Vehicles: From Electrochemistry to Market Prospects," *Electrochimica Acta,* vol. 84, pp. 235-249, Dec. 2012.
[27] S. Chang, K. H. Young, and C. Fierro, "Reviews on the US Patents Regarding Nickel/Metal Hydride Batteries," *Batteries*, vol. 2, no. 10, p. 29, Apr. 2016.
[28] K. H. Young and S. Yasuoka, "Capacity Degradation Mechanisms in Nickel/Metal Hydride Batteries," *Batteries*, vol. 2, no. 3, p. 28, Mar. 2016.
[29] B. Sanchez, J. C. Argucha, and J. W. Smith. (2021, Jul. 22). *Performance Characterization of 1998 Ford Ranger Electric with Nickel/Metal Hydride Battery*. [Online]. Available: https://avt.inl.gov/sites/default/files/pdf/fsev/ranger_nimh_report.pdf
[30] S. Boschert, *Plug-in Hybrids: The Cars that Will Recharge America*, New Society Publishers, Gabriola Island, Canada, 2006, p. 213.
[31] K. H. Young, X. Cai, and S. Chang, "Reviews on the Chinese Patents Regarding Nickel/Metal Hydride Batteries", *Batteries,* vol. 3, no. 24, p. 60, Aug. 2017.
[32] T. Ouchi, K. H. Young, and D. Moghe, "Reviews on the Japanese Patent Applications Regarding Nickel/Metal Hydride Batteries," *Batteries,* vol. 2, no. 21, p. 30, Jun. 2016.
[33] S. Chang, K. H. Young, and Y. L. Lien, "Reviews of European Patents on Nickel/Metal Hydride Batteries," *Batteries,* vol. 3, no. 25, p. 16, Aug. 2017.
[34] K. H. Young, "Research in Nickel/Metal Hydride Batteries 2017", *Batteries,* vol. 4, no. 1, p. 5, Feb. 2018.
[35] S. B. Cao and F. Y. Huang, "Analysis of the Status Quo and Development of Ni-MH Batteries for Hybrid Electric Vehicles," *Batteries Bimonthly*, vol. 46, pp. 289-291, Apr. 2016.
[36] K. H. Young, S. Chang, and X. Lin, "C14 Laves Phase Metal Hydride Alloys for NI/MH Batteries Applications," *Batteries*, vol. 3, no. 27, Sep. 2017.
[37] X. Sun, Z. Li, X. Wang, and C. Li, "Technology Development of Electric Vehicles: A Review," *Energies*, vol. 13, no. 90, p. 29, Aug. 2020.
[38] K. Liu, W. Zhou, D. Zhu et al., "Excellent High-Rate Capability of Micron Sized Co-Free A-Ni $(OH)_2$ for High Power Ni-MH Battery," *Journal Alloys & Compounds*, vol. 768, no. 5, pp. 269-276, Nov. 2018.
[39] A. Chu, Y. Yian, J. Zu et al., "The Design and Investigation of a Cooling System for a High-Power Ni-MH Battery Pack in Hybrid Electric Vehicles," *Applied Sciences*, vol. 10, p. 1660, Mar. 2020.
[40] J. B. Goodenough, "How We Made the Li-Ion Rechargeable Battery," *Nature Electronics*, vol. 1, p. 204, Mar. 2018.
[41] N. Nitta, F. Wu, J. T. Lee et al., "Li-ion Battery Materials: Present and Future," *Materials Today*, vol. 18, pp. 252-264. Jun. 2015.
[42] Y. L. Ding, Z. P. Cano, A. Yu et al., "Automotive Li-Ion Batteries: Current Status and Future Perspectives," *Electrochemical Energy Reviews*, vol. 2, no. 1, pp. 1-28, Mar. 2019.
[43] Z. P. Cano, D. Banham, S. Ye et al., "Batteries and Fuels Cells for Emerging Electric Vehicle Markets," *Nature Energy*, vol. 3, pp. 279-289, Apr. 2018.
[44] Y. Miao, P. Hynan, A. von Jouanne et al., "Current Li-Ion Battery Technologies in Electric Vehicles and Opportunities for Advancement," *Energies*, vol. 12, p. 20, Mar. 2019.
[45] X. Zeng, M. Li, D. A. El-Hady et al., "Commercialization of Lithium Battery Technology for Electric Vehicles," *Advanced Energy Materials*, vol. 9. No. 27, Jul. 2019.
[46] P. V. Tichelen, "Preparatory Study on Ecodesign and Energy Labeling of Batteries," *European Commission Report*, Brussels, BE. Rep. FWC ENER/C3/2015-619-Lot 1, Aug. 2019.
[47] A. Li, A. C. Y. Yuen, W. Wang et al., "A Review of Lithium-Ion Battery Separators Towards Enhanced Safety Performance and Modelling Approaches," *Molecules*, vol. 26, pp. 15, Jan. 2021.
[48] H. C. Kim, T. J. Wallington, R. Arsenault et al., "Cradle-to-Gate Emissions from a Commercial Electric Vehicle Li-Ion Battery: A Comparative Analysis," *Environmental Science & Technology*, vol. 50, pp. 7715-7722, Jun. 2016.
[49] M. Schönemann, *Battery Production and Simulation*. Brussels, BE: Springer, Cham, 2017, pp. 11-37.
[50] W. Xu, J. Wang, F. Ding et al., "Lithium metal Anodes for Rechargeable Batteries," *Energy & Environmental Science*, vol. 7, pp. 513-537, Oct. 2014.
[51] Y. Li, Y. Lu, P. Adelhelm et al., "Intercalation Chemistry of Graphite: Alkali Metal Ions and Beyond," *Chemical Society. Review*, vol. 7, p. 34, Jul. 2019.
[52] E. Peled and S. Menken, "Review-SEI: Past, Present and Future," *Journal of the Electrochemical Society*, vol. 164, no. 7, pp. 1703-1719, Jun. 2017.
[53] S. K. Heiskanen, J. Kim, and B. L. Lucht, "Generation and Evolution of the Solid Electrolyte Interphase of Lithium-Ion Batteries," *Joule*, vol. 3, pp. 2322-2333, Oct. 2019.
[54] J. F. Ding, R. Xu, C. Yan et al., "A Review on the Failure and Regulation of Solid Electrolyte Interphase in Lithium Batteries," *Journal of Energy Chemistry,* vol. 59, pp. 306-319, Aug. 2021.
[55] M. J. Lain, I. R. Lopez, and E. Kendrick, "Electrolyte Additions in Lithium-Ion EV Batteries and the Relationship of the SEI Composition to Cell Resistance and Lifetime", *Electrochem*, vol. 1, pp. 200-216, Jun. 2020.
[56] M. A. Gialampouki, J. Hashemi, and A. A. Peterson, "The Electrochemical Mechanisms of Solid–Electrolyte Interphase Formation in Lithium-Based Batteries," *The Journal of Physical Chemistry*, vol. 123, pp. 20084-20092, Aug. 2019
[57] M. Li, J. Lu, and X. Ji, "Design Strategies for Nonaqueous Multivalent-Ion and Monovalent-Ion Battery Anodes," *Nature Reviews Materials*, vol. 5, 276-294, Feb. 2020.
[58] W. Huang, P. M. Attia, H. Wang et al., "Evolution of the Solid–Electrolyte Interphase on Carbonaceous Anodes Visualized by Atomic-Resolution Cryogenic Electron Microscopy," *Nano Lett*ers, vol. 19, pp. 5140-5148, Jul. 2019.
[59] Y. Yuan, K. Amine, J. Lu et al., "Understanding Materials Challenges for Rechargeable Ion Batteries with in Situ Transmission Electron Microscopy," *Nature Communications*, vol. 8, p. 14, Aug. 2017.
[60] J. Duan, X. Tang, H. Dai et al., "Building Safe Lithium-Ion Batteries for Electric Vehicles," *Electrochemical Energy Reviews*, vol. 3, pp. 1-42, Dec. 2020.

[61] T. Ohzuku, A. Ueda, and N. Yamamoto, "Zero-Strain Insertion Material of Li (Li1/3Ti5/3) O4 for Rechargeable Lithium Cells," *Journal of the Electrochemical Society*, vol. 142, pp. 1431-1435, May. 1995.

[62] T. D. H. Nguyen, H. D. Pham, S-Y. Lin et al., "Featured Properties of Li^{+}-Based Battery Anode $Li_4Ti_5O_{12}$," *RSC Advances*, vol. 10, pp. 14071-14079, Apr. 2020.

[63] T. Nemeth, P. Schroer, M. Kuipers et al., "Lithium Titanate Oxide Battery Cells for High-Power Automotive Applications: Electrothermal Properties, Aging Behavior and Cost Considerations," *Journal of Energy Storage*, vol. 31, p. 101656, Oct. 2020.

[64] L. Zhang, X. Zhang, Q. Zhang et al., "Lithium Lanthanum Titanate Perovskite as an Anode for Lithium-Ion Batteries," *Nature Communications*, vol. 11, p. 8, Jul. 2020.

[65] Y. B. He, B. Li, M. Liu et al., "Gassing in $Li_4Ti_5O_{12}$-Based Batteries and Its Remedy," *Scientific Reports*, vol. 2, p. 913, Dec. 2012.

[66] F. Wang, L. Wu, C. Ma et al., "Excess lithium Storage and Charge Compensation in Nanoscale Li_4+xTi_5O_{12}," *Nanotechnology*, vol. 24, no. 24, p. 9, Sep. 2013.

[67] J. Lu, C. Chen, Z. Ma et al., 'The Role of Nanotechnology in the Development of Battery Materials for Electric Vehicles," *Nature Nanotechnology*, vol. 11, pp. 1031-1038, Dec. 2016.

[68] H-J. Hong, G. Ban, S-M. Lee et al., "Synthesis of 3D-structured $Li_4Ti_5O_{12}$ from Titanium (IV) Oxysulfate ($TiOSO_4$) Solution as a Highly Sustainable Anode Material for Lithium-Ion Batteries," *Journal of Alloys & Compounds*, vol. 844, p. 156203, Dec. 2020.

[69] L. A. Ellingsen, C. R. Hung, G. Majeau-Bettez et al., "Nanotechnology for Environmentally Sustainable Electromobility," *Nature Nanotechnology*, vol. 11 no. 12, pp. 1039-1051, Dec. 2016.

[70] X. Li, P. Huanga, W. Yang et al., "In-situ Carbon Coating to Enhance the Rate Capability of the $Li_4Ti_5O_{12}$ Anode Material and Suppress the Electrolyte Reduction Decomposition on the Electrode," *Electrochimica Acta*, vol. 190, pp. 69-75, Feb. 2016.

[71] J. K. Yoon, S. Nam, H. C. Shim et al., "Highly-Stable $Li_4Ti_5O_{12}$ Anodes Obtained by Atomic-Layer-Deposited Al2O3," *Materials*, vol. 11, p. 10, May. 2018.

[72] N. Delaporte, P. Chevallier, and S. Rochon, "A Low-Cost and Li-Rich Organic Coating on a $Li_4Ti_5O_{12}$ Anode Material Enabling Li-Ion Battery Cycling at Subzero Temperatures," *Material Advances*, vol. 1, pp. 854-872, Jun. 2020.

[73] M. S. Milien, J. Hoffmann, M. Payne, "Effect of Electrolyte Additives on Cycling Performance and Gas Evolution," *Journal Electrochemical Society*, vol. 165, no. 16, pp. A3925-A3931, Dec. 2018.

[74] M. R. Palacin, "Recent Advances in Rechargeable Battery Materials: A Chemist's Perspective," *Chemical Society Reviews*, vol. 38, pp. 2565-2575, Jun. 2009.

[75] R. Borah, F. R. Hughson, J. Johnston et al., "On Battery Materials and Methods," *Materials Today Advances*, vol. 6, p. 22, Jun. 2020.

[76] Y. Wu, X. Huang, L. Huang et al., "Strategies for Rational Design of High-power Lithium-Ion Batteries," *Energy & Environmental Materials*, vol. 4, pp. 19-45, May 2021.

[77] S-H. Yu, S. H. Lee, D. J. Lee, et al. "Conversion Reaction-Based Oxide Nanomaterials for Lithium-Ion Battery Anodes," *Small*, vol. 12, pp. 2146-2172, Dec. 2016.

[78] S-H. Yu, X. Feng, N. Zhang et al., "Understanding Conversion-Type Electrodes for Lithium Rechargeable Batteries," *Accounts of Chemical Research*, vol. 51, no. 2, pp. 273-281, Jan. 2018.

[79] Q. Cui, Y. Zhong, L. Pan et al., "Recent Advances in Designing High-Capacity Anode Nanomaterials for Li-Ion Batteries and Their Atomic-Scale Storage Mechanism Studies," *Advanced Science*, vol. 5, p. 22, Apr. 2018.

[80] T. W. Kwon, J. W. Choi, and A. Coskun, "The Emerging Era of Supra-Molecular Polymeric Binders in Silicon Anodes," *Chemical Society Reviews*, vol. 47, pp. 2145-2164, Feb. 2018.

[81] N. Yuca, O. S. Taskin, and E. Arici, "An Overview of Efforts to Enhance the Si Electrode Stability for Lithium-Ion Batteries," *Energy Storage*, vol. 2, no. 94, pp, 15, Oct. 2020.

[82] Y-M. Zhao, F-S. Yue, S-C. Li et al., "Advances of Polymer Binders for Silicon-Based Anodes in High Energy Lithium-Ion Batteries," *InfoMat*, vol. 2, pp. 460-501, Mar. 2021.

[83] S. Li, Z-Gu. Wu, Y-M. Liu et al., "A Compared Investigation of Different Biogum Polymer Binders for Silicon Anode of Lithium-Ion Batteries," *Ionics*, vol. 27, pp.1829-1836, Mar. 2021.

[84] R. Schmuch, Z. G. Wu, Y-M. Liu et al., "Performance and Cost of Materials for Lithium-Based Rechargeable Automotive Batteries," *Nature Energy*, vol. 3, pp. 267-278, Apr. 2018.

[85] J. Asenbaue, T. Eisenmann, M. Kuenzel et al., "The Success Story of Graphite as a Lithium-Ion Anode Material-Fundamentals, Remaining Challenges, and Recent Developments Including Silicon (Oxide) Composites," *Sustainable Energy Fuels*, vol. 4, pp. 5387-5416, May 2020.

[86] T. Chen, J. Wu, Q. Zhang et al., "Recent Advancement of Siox Based Anodes for Lithium-Ion Batteries," *Journal of Power Sources*, vol. 363, pp. 126-144, Sep. 2017.

[87] Z. Liu, Q. Yu, and Y. Zhao, "Silicon Oxides: A Promising Family of Anode Materials for Lithium-Ion Batteries," *Chemical Society Reviews*, vol. 48, pp. 285-309, Dec. 2019.

[88] J. Frazelle, "Battery Day," *ACM Queue*, vol. 8, no. 5, pp. 5-25, Oct. 2020.

[89] E. Fox. (2020, Sep. 28). *Tesla Silicon Anode for 4680 Battery Cell: What's the Secret?* [Online]. Available: https://www.tesmanian.com/blogs/tesmanian-blog/tesla-silicon-the-new-4680-battery-cell-anode

[90] COBRA. (2021, Jul. 10). *Tesla vs COBRA: A look at Tesla's Battery Day*. [Online]. Available: https//projectcoobra.eu/2020/10/10/tesla-vs-cobratesla-vs-cobra-battery-day

[91] MINING.COM. (2021, Mar. 30). *NEO's Silicon Anodes Achieve Long-Term Cycling*. [Online]. Available: https://www.mining.com/neos-silicon-anodes-achieve-long-term-cycling/

[92] N. Willing. (2021, Jan. 29). *Battery Makers Expand Silicon Anode Production*. [Online]. Available: https://www.argusmedia.com/en/news/2182042-battery-makers-expand-silicon-anode-production

[93] Y. Che, Y. Luo, H. Zhang, "The Challenge of Lithium Metal Anodes for Practical Applications," *Small Methods*, vol. 3, no. 7, p. 23, Apr. 2019.

[94] R. Wang, W. Cui, F. Cu et al. "Lithium metal Anodes Present and Future," *Journal of Energy Chemistry*, vol. 48, pp. 145-159, Sep. 2021.

[95] D. Lin, Y. Liu, and Y. Cui, "Reviving the Lithium Metal Anode for High-Energy Batteries," *Nature Nanotechnology*, vol. 2, pp.194-206, Mar. 2017.

[96] Y. Han, B. Liu, Z. Xiao et al., "Interface Issues of Lithium Metal Anode for High-Energy Batteries: Challenges, Strategies, and Perspectives," *InfoMat*, vol. 3, pp. 155-174, Jan. 2021.

[97] G. Zubi, R. Dufo-Lópeza, M. Carvalho et al., "The Lithium-Ion Battery: State of the Art and Future Perspectives," *Renewable & Sustainable Energy Reviews*, vol. 89, pp. 292-308, Jun. 2018.

[99] K. Shang. (2021, Jul. 20). *Lithium-ion Batteries: LFP Cathode Materials Market Share Forecast to Increase in 2021*. [Online]. Available: https://roskill.com/news/lithium-ion-batteries-lfp-cathode-materials-market-share-forecast-to-increase-in-2021/

[100] J. Li, M. Weng, Y. Qiu et al., "Structural Origin of The High-Voltage Instability of Lithium Cobalt Oxide," *Nature Nanotechnology*, vol. 16, pp. 599-605, Feb. 2021.

[101] J-N. Zhang, Q. Li, C. Ouyang et al., "Trace Doping of Multiple Elements Enables Stable Battery Cycling of Licoo2 at 4.6V," *Nature Energy*, vol. 4, pp. 594-603, Jun. 2019.

[102] K. Wang, J. Wang, Y. Xian et al., "Recent Advance and Historical Developments of High Voltage Lithium Cobalt Oxide Materials for Rechargeable Lithium-Ion Batteries," *Journal Power Sources*, vol. 460, p. 228062, Jun. 2020.

[103] Y. Lyu, X. Wu, K. Wang et al., "An Overview of the Advances of $LicoO_2$ Cathodes for Lithium-Ion Batteries," *Advanced Energy Materials*, vol. 11, no. 2, p. 2000982, Jun. 2020.

[104] S. Muto, Y. Sasano, K. Tatsumi et al., "Capacity-Fading Mechanisms of $LiNiO_2$-Based Li-ion Batteries. II. Diagnostic Analysis by Electron Microscopy and Spectroscopy," *Journal of Electrochemical Society*, vol. 156, pp. A371-A377, Mar. 2009.

[105] J. Xu, F. Lin, M. M. Doeff et al., "A Review of Ni-based Layered Oxides for Rechargeable Li-ion Batteries," *Journal of Materials Chemistry A*, vol. 5, pp. 874-901, Nov. 2017.

[106] C. H. Chen, J. Liua, M. E. Stoll et al., "Aluminium-Doped Lithium Nickel Cobalt Electrodes for High-Power Lithium-Ion Batteries," *Journal of Power Sources*, vol. 125, no. 2, pp. 278-285, Apr. 2004.

[107] A. Purwanto, C. S. Yudha, U. Ubaidillah et al., "NCA Cathode Material: Synthesis Methods and Performance Enhancement Efforts," *Materials Research Express*, vol. 5, no. 2, p. 122001, Sep. 2018.

[108] C. M. Julien and A. Mauger, "NCA, NCM 811 and the Route to Ni-Richer Lithium-Ion Batteries," *Energies,* vol. 13, no. 23, p. 46, Dec. 2020.

[109] K. Zhou, Q. Xiea, B. Li et al., "An In-Depth Understanding of The Effect of Aluminum Doping in High-Nickel Cathodes for Lithium-Ion Batteries," *Energy Storage Materials*, vol. 34, pp. 229-240, Jan. 2021.

[110] NISSAN. (2021, Jul. 10). *Accelerating Toward Carbon Neutrality*. [Online]. Available: https://www.nissan-gloobal.com/ENTECHNOLOGY/li on ev.thml

[111] X. Li, Y. Yu, and C. Wang, "Suppression of Jahn-Teller Distortion of Spinel $Limn_2O_4$ Cathode," *Journal of Alloys & Compounds*, vol. 479, pp. 310-313, Jun. 2009.

[112] J. P. Pender, "Electrode Degradation in Lithium-Ion Batteries," *ACS Nano*, vol. 14, pp. 1243-1295, Jan. 2020.

[113] C. Zuo, Z. Hu, R. Qi et al., "Double the Capacity of Manganese Spinel for Lithium-Ion Storage by Suppression of Cooperative Jahn-Teller Distortion," *Advanced Energy Materials*, vol. 10, no. 34, p. 10, Sep. 2020.

[114] A-H. Marincas, F. Goge, S. A. Dorneanu et al., "Review on synthesis methods to obtain $LiMn_2O_4$-Based Cathode Materials for Li-ion Batteries," *Journal Solid State Electrochemistry*, vol. 24, pp. 473-497, Jan. 2020.

[115] S. Lui, B. Wang, X. Zhang et al., "Reviving the Lithium-Manganese -Based Layered Oxide Cathodes for Lithium-Ion Batteries," *Matte*r, vol. 4, no. 5, pp. 1511-1527, May 2021.

[116] L. Yang, K. Yang, and J. Zhang, "Harnessing Surface Structure to Enable High-Performance Cathode Materials for Lithium-Ion Batteries," *Chemical Society Reviews*, vol. 49, pp. 4667-4680, Jan. 2020.

[117] G. Xu, C. Zhang, C. Cui et al., "Strategies for Improving the Cyclability and Thermo-Stability of $LiMn_2O_4$-Based Batteries at Elevated Temperatures," *Journal Materials Chemistry A*, vol. 3, pp. 4092-4123, Feb. 2015.

[118] W. Liu, J. Chen, S. Ji et al., "Enhancing the Electrochemical Performance of the $LiMn_2O_4$ Hollow Microsphere Cathode with $LiNi_{0.5}Mn_{1.5}O_4$ Coated Layer," *Chemistry Europe Journal*, vol. 20, no. 3, pp. 824-830, Jan. 2014.

[119] L. Wen, X. Wang, G. Q. Liu et al., "Novel Surface Coating Strategies for Better Battery Materials," *Surface Innovations*, vol. 6, no. 1-2, pp.13-18, Mar. 2018.

[120] P. Ye, H. Dong, Y. Xu et al., "$Nico_2O_4$ Surface Coating Li [Ni0.03Mn1.97] O_4 Micro-/Nano-Spheres as Cathode Material for High-Performance Lithium-Ion Battery," *Applied Surface Science*, vol. 428, pp. 469-477, Sep. 2018.

[121] T. Kozawa, T. Harata, and M. Naito, "Fabrication of an $LiMn_2O_4$@$LiMnPO_4$ Composite Cathode for Improved Cycling Performance at High Temperatures," *Journal of Asian Ceramic Societies*, vol. 8, no. 2, pp. 309-317, Mar. 2020.

[122] V. Selvamani, N. Phattharasupakun, J. Wutthipron et al., "High-Performance Spinel $LiMn_2O_4$@Carbon Core-Shell Cathode Materials for Li-Ion Batteries," *Sustainable Energy & Fuels,* vol. 3, pp. 1988-1994, May. 2019.

[123] J. Lu, B. Song, H. Xia et al., "High Energy Spinel-Structured Cathode Stabilized by Layered Materials for Advanced Lithium-Ion Batteries," *Journal Power Sources,* vol. 271, pp. 604-613, Dec. 2014.

[124] J. Wu, Z. Cui, J. Wu et al., "Suppression of Voltage-Decay in Li_2MnO_3 Cathode via Reconstruction of Layered-Spinel Co-exist Phases," *Journal Materials Chemistry A*, vol. 8, pp. 18687-18697, Aug. 2020.

[125] S. Liu and H. Yu, "Toward Functional Units Constructing Mn-Based Oxide Cathodes for Rechargeable Batteries," *Science Bulletin*, vol. 66, no. 13, pp. 1260-1262, Jul. 2021.

[126] X. Zhu, F. Meng, Q. Zhang et al., "$LiMnO_2$ Cathode Stabilized by Interfacial Orbital Ordering for Sustainable Lithium-Ion Batteries," *Nature Sustainability*, vol. 4, pp. 392-401, Dec. 2021.

[127] S. Kaewma, N. Wiriya, P. Chantrasuwan, "Multiscale Investigation Elucidating the Structural Complexities and Electrochemical Properties of Layered-Layered Composite Cathode Materials Synthesized at Low Temperatures," *Physical Chemistry Chemical Physics*, vol. 22, no. 10, pp. 5439-5448, Jan. 2020.

[128] D. Andre, S. J. Kim, P. Lump et al., "Future generations of Cathode Materials: An Automotive Industry Perspective," *Journal Material Chemistry A*, vol. 3, pp. 6709-6732, Feb. 2015.

[129] Y. Chen, S. Song, X. Zhang et al., "The Challenges, Solutions, and Development of High-Energy Ni-rich NCM/NCA Lib Cathode Materials," *Journal of Physics: Conference Series*, vol. 1347, p. 9, Jun. 2019.

[130] J. L. Choi, "Recent Progress and Perspective of Advanced High-Energy Co-Less Ni-Rich Cathodes for Li-Ion Batteries: Yesterday, Today and Tomorrow," *Advanced Energy Materials*, vol. 10, p. 31, Sep. 2020.

[131] N. Mohamed and N. K. Allam, "Recent Advances in the Design of Cathode Materials for Li-Ion Batteries," *RSC Advances*, vol. 10, pp. 2162-21685, Jun. 2020.

[132] X. Shen, "Advanced Electrode Materials in Lithium Batteries: Retrospect and Prospect," *Energy Material Advances*, vol. 2021, p. 15, Jun. 2021.

[133] S. W. D. Gourley, T. Or, and Z. Chen, "Breaking Free from Cobalt Reliance in Lithium-Ion Batteries," i*Science*, vol. 23, no. 9, p. 16, Aug. 2020.

[134] K. B-wook. (2021, Jul. 10). *SK Makes World's 1st NCM Battery with 90% Nickel*. [Online]. Available: https//www.koreaherald.com/view.php?ud=20200810000683

[135] H-J. Kim, TNV. Krishna, K. Zeb et al., "A Comprehensive Review of Li-Ion Battery Materials and Their Recycling Techniques," *Electronics*, vol. 9, p. 45, Jul. 2020.

[136] S. Duhnen, J. Betz, M. Kolek et al., "Towards Green Battery Cells: Perspective on Materials and Technologies," *Small Methods*, vol. 4, pp. 1-38, Apr. 2020.

[137] D. Matthews, "Global Value Chains: Cobalt in Lithium-ion Batteries for Electric Vehicles," U.S. International Trade Commission, Washington DC, USA, Rep. ID-067, May 18, 2020.

[138] M. Azevedo, N. Campagnol, and T. Hagenbruch. (2018, Jun 22). *Lithium and Cobalt-A Tale of Two Commodities*. [Online]. Available: https//www.mckinsey.com/industries/metals-and-mining/our-insights/lithium-and-cobalt-a-tale-of-two-commodities

[139] I. Belharouak, J. Nanda, E. Self et al., "Operation, Manufacturing and Supply Chain of Lithium-Ion Batteries for Electric Vehicles," Oak Ridge National Laboratory, Oak Ridge, USA, Rep. ORNL/TM-2020/172955, Jan. 1, 1996.

[140] J. Baars, T. Domenech, R. Bleischwitz et al., "Circular Economy Strategies for Electric Vehicle Batteries to Reduce Reliance on Raw Materials," *Nature Sustainability*, vol. 4, pp. 71-79, Sep. 2021.

[141] UNCTAD, "Commodities at a Glance: Special Issue on Strategic Battery Raw Materials," UNCTAD, Geneva, CH, Rep. No. 13, Jun. 13, 2020.

[142] X. Yu and A. Manthiram, "Sustainable Battery Materials for Next-Generation Electrical Energy Storage," *Advanced Energy Sustainability Research*, vol. 2, pp. 2-12, Jun. 2021.

[143] S-T. Myung, F. Maglia, and K-J. Park "Nickel-Rich Layered Cathode Materials for Automotive Lithium-Ion Batteries: Achievements and Perspectives," *ACS Energy Lett*., vol. 2, no. 1, pp. 196-223, Dec. 2017.

[144] T. Li, X-Z. Yuan, L. Zhang et al., "Degradation Mechanisms and Mitigation Strategies of Nickel-rich NMC-Based Lithium-Ion Batteries," *Electrochemical Energy Reviews*, vol. 3, pp. 43-80, Oct. 2020.

[145] P. Teichert, G. G. Eshetu, H. Jahnke et al., "Degradation and Aging Routes of Ni-Rich Cathode Based Li-Ion Batteries," *Batteries*, vol. 6, no. 8, Jan. 2020.

[146] M. Armand, P. Axmannb, D. Bresser et al., "Lithium-Ion Batteries-Current State of the Art and Anticipated Developments," *Journal of Power Sources*, vol. 479, p. 26, Dec. 2020.

[147] L. Liu, M. Lia, L. Chu et al., "Layered Ternary Metal Oxides: Performance Degradation Mechanisms as Cathodes, and Design Strategies for High-Performance Batteries," *Progress in Mat. Science*, vol. 111, p. 85, Jun. 2020.

[148] L. Song, J. Du, Z. Xiao et al., "Research Progress on the Surface of High-Nickel-Cobalt-Manganese Ternary Cathode Materials: A Mini Review," *Frontiers in Chemistry*, vol. 8, p. 8, Aug. 2020.

[149] A. L. Lipson, J. L. Durham, M. LeResche et al., "Improving the Thermal Stability of NMC622 Li-ion Battery Cathodes Through Doping During Coprecipitation," *ACS Applied Material Interfaces*, vol. 12, pp.18512-18518, Apr. 2020.

[150] X. Chen, F. Ma, Y. Li et al., "Nitrogen-Doped Carbon Coated $LiNi_{0.6}Co_{0.2}Mn_{0.2}O_2$ Cathode with Enhanced Electrochemical Performance for Li-Ion Batteries," *Electrochimica Acta*, vol. 284, pp. 526-533, Sep. 2018.

[151] L. Zhu, T. F. Yan, D. Jia et al., "$LiFePO_4$-Coated $LiNi_{0.5}Co_{0.2}Mn_{0.3}O_2$ Cathode Materials with Improved High Voltage Electrochemical Performance and Enhanced Safety for Lithium-Ion Pouch Cells," *Journal Electrochemical Society*, vol. 166, pp. A5437-A5444, Jan. 2019.

[152] Y. B. Cao, X. Qi, K. H. Hu et al., "Conductive Polymers Encapsulation to Enhance Electrochemical Performance of Ni-rich Cathode Materials for Li-Ion Batteries," *ACS Applied Materials & Interfaces*, vol. 10, pp. 18270-18280, May 2018.

[153] G. L. Xu, Q. Liu, K. K. S. Lau et al., "Building Ultraconformal Protective Layers on Both Secondary and Primary Particles of Layered Lithium Transition Metal Oxide Cathodes," *Nature Energy*, vol 4, pp. 484-494, May 2019.

[154] J. Sagoff. (2019, May 14). *New Argonne Coating Could Have Big Implications for Lithium Batteries*. [Online]. Available: https://www.anl.gov/article/ new-argonne-coating-could-have-big-implications-for-lithium-batteries

[155] T. Wu, X. Liu, X. Zhang et al., "Full Concentration Gradient-Tailored Li-rich Layered Oxides for High-Energy Lithium-Ion Batteries," *Advanced Materials*, vol. 33, no. 2, p. 10, Nov. 2020.

[156] S. Maeng, Y. Chungb, S. Min et al., "Enhanced Mechanical Strength and Electrochemical Performance of Core-Shell Structured High-Nickel Cathode Material," *Journal of Power Sources,* vol. 448, no. 1, p. 227395, Feb. 2020.

[157] P. Yan, J. Zheng, J. Liu et al., "Tailoring Grain Boundary Structures and Chemistry of Ni-rich Layered Cathodes for Enhanced Cycle Stability of Lithium-Ion Batteries," *Natural Energy*, vol. 3, pp. 600-605, Jul. 2018.

[158] C. Wang, R. Yua, S. Hwang et al., "Single Crystal Cathodes Enabling High-Performance All-Solid-State Lithium-Ion Batteries," *Energy Storage Materials*, vol. 30, pp. 98-103, Sep. 2020.

[159] L. Zheng, J. C. Bennett, and M. N. Obrovac, "All-Dry Synthesis of Single Crystal NMC Cathode Materials for Li-Ion Batteries," *Journal Electrochemical Society*, vol. 167, p. 130536, Oct. 2020.

[160] Q. Wu, S. Mao, Z. Wang et al., "Improving $LiNi_xCo_yMn_{1-x-y}$ Cathode Electrolyte Interface Under High Voltage in Lithium-Ion Batteries," *Nano Select*, vol. 1, pp. 111-134, Jun. 2020.

[161] Z. Ahsan, B. Ding, Z. Cai et al., "Recent Progress in Capacity Enhancement of $LiFePO_4$ Cathode for Li-Ion Batteries," *Journal Electrochem, Energy Conservation & Storage*, vol. 18, p. 15, Feb. 2021.

[162] R. Zhao, J. Liu, and F. Ma, "Cathode Chemistries and Electrode Parameters Affecting the Fast Charging Performance of Li-Ion Batteries," *Journal Electrochem, Energy Conservation & Storage*, vol. 17, p. 13, May 2020.

[163] J. Hu, W. Huang, L. Yang et al., "Structure and Performance of The $LiFePO_4$ Cathode Material: From the Bulk to the Surface," *Nanoscale*, vol. 12, pp. 15036-15044, Jun. 2020.

[164] Y-M Xin, H-Y. Xu, J-H Ruan et al., "A Review on Application of $LiFePO_4$ Based Composites as Electrode Materials for Lithium-Ion Batteries," *International Journal of Electrochemical Science*, vol. 16, p. 18, Jun. 2021.

[165] Wall Street Journal. (2021, Jul. 10). *Low-cost EV Battery Wins Fans in China*. [Online]. Available: https//www.wsj.com/article/elon-musk-linkk-this-ev-battery-and-it-costs-lessbut-the-u-s-isnt-on-it-11616929201

[166] E. Els. (2011, Mar. 11). *Cobalt, Nickel Free Electric Car Batteries are a Runaway Success*. [Online]. Available: https://www.mining.com/cobalt-nickel-free-electric-car-batteries-are-a-runaway-success/

[167] ROSKILL. (2020, Jun. 25). *Batteries: The True Drivers Behind LFP Demand-New Safety Standards, Costs, IP Rights, ESG & Simplified Battery Pack Designs*. [Online]. Available: https://roskill.com/news/batteries-the-true-drivers-behind-lfp-demand-new-safety-standards-costs-ip-rights-esg-simplified-battery-pack-designs/

[168] X-G. Yang, T. Liu, and C-Y Wang, "Thermally Modulated Lithium Iron Phosphate Batteries for Mass-Market Electric Vehicles," *Nature Energy*, vol. 6, pp.176-185, Jan. 2021.

[169] N. Tolganbek, Y. Yerkinbekova, S. Kalybekkyzy et al., "Current State of High Voltage Olivine Structured $LiMPO_4$ Cathode Materials for Energy Storage Applications: A Review," *Journal Alloys & Compounds*, vol. 882, p. 16, Nov. 2021.

[170] J. Ma, Y. Li, N. S. Grundish et al., "The 2021 Battery Technology Roadmap," *Journal of Physics D: Applied Physics*, vol. 54, p. 44, Sep. 2021.

[171] A. E. Kharbachi, O. Zavorotynska, M. Latroche et al., "Exploits, Advances, and Challenges Benefiting Beyond Li-Ion Battery Technologies," *Journal Alloys & Compounds,* vol. 817, p. 26, Sep. 2020.

[172] D. Chao, W. Zhou, F. Xie et al., "Roadmap for Advanced Aqueous Batteries: From Design of Materials to Applications," *Science Advances*, vol. 6, no. 21, pp. 1-19, May 2020.

[173] J. Janek and W. G. Zeier, "A solid Future for Battery Development," *Nature Energy*, vol. 1, p. 16141, Sep. 2016.

[174] S. Randau, D. A. Weber, O. Kotz et al., "Benchmarking the Performance of All-Solid-State Lithium Batteries," *Nature Energy*, vol. 5, pp. 259-270, Mar. 2020.

[175] Z. Wang, J, Liu, M, Wang et al., "Toward Safer Solid-State Lithium Metal Batteries," *Nanoscale Advances*, vol. 5, p. 9, Apr. 2020.

[176] S. Ferrari, M. Falco, and A. B. Munoz-Garcia, "Solid-State Post Li Metal Ion Batteries: A Sustainable Forthcoming Reality," *Advanced Energy Materials*, vol. 10, p. 30, Jun. 2021.

[177] Z. Zhang, Y. Shao, B. Lotsch et al., "New Horizons for Inorganic Solid State Ion Conductors," *Energy & Environmental Science*, vol. 11, pp. 1945-1976, Jun. 2018.
[178] G. Yang, C. Abraham, Y. Ma et al., "Advances in Materials Design for All-Solid-State Batteries: From Bulk to Thin Films," *Applied Sciences*, vol. 10, 4727, p. 50, Jul. 2020.
[179] S. Ball, J. Clark, and J. Cookson, "Battery Materials Technology Trends and Market Drivers for Automotive Applications," *Johnson Matthey Technology Review*, vol. 64, no. 3, pp. 287-297, Jul. 2020.
[180] D. Karabelli, K. P. Birke, and M. Weber, "A Performance and Cost Overview of Selected Solid-State Electrolytes: Race between Polymer Electrolytes and Inorganic Sulphides," *Batteries,* vol. 7, no. 18, p. 13, Mar. 2021.
[181] T. Zhang, W. He, W. Zhang et al., "Designing Composite Solid-State Electrolytes for High Performance Lithium Ion or Lithium Metal Batteries," *Chemical Science*, vol. 11, pp. 8686-8707, Jul. 2020.
[182] S. Li, S-Q Zhang, L. Shen et al., "Progress and Perspective of Ceramic/Polymer Composite Solid Electrolytes for Lithium Batteries," *Advanced Science*, vol. 7, p. 22, Jan. 2020.
[183] Z. Ding, J. Li, J. Li et al., "Review-Interfaces: Key Issue to be Solved for All Solid-State Battery Technologies," *Journal Electrochemical Society*, vol. 167, p. 19, Jun. 2020.
[184] S. Lou, F. Zhang, C. Fu et al., "Interface Issues and Challenges in All-Solid-State Batteries: Lithium, Sodium and Beyond," *Advanced Materials*, vol. 33, no. 6, p. 29, Jul. 2020.
[185] C. Singer, J. Schnell, and G. Reinhart, "Scalable processing Routes for the Production of All-Solid-State Batteries-Modeling Interdependencies of Product and Process," *Energy Technologies*, vol. 9, p. 14, Oct. 2021.
[186] K. J. Huang, G. Reder, and E. A. Olivetti, "Manufacturing Scalability Implications of Materials Choice in Inorganic Solid-State Batteries," *Joule*, vol. 5, no. 3, pp. 564-580, Mar. 2021.
[187] E. Sugiura. (2021, May 28). *Can Japan and Toyota win the Solid-State Battery Race?* [Online]. Available: https://asia.nikkei.com/Business/Business-Spotlight/Can-Japan-and-Toyota-win-the-solid-state-battery-raceToyota solid state
[188] K. Chayabuka, G. Moulder, D. L. Danilov et al., "From Li-Ion Batteries Toward Na-Ion Chemistries: Challenges and Opportunities," *Advanced Energy Materials*, vol. 10, p. 11, Aug. 2020.
[189] K. M. Abraham, "How Comparable are Sodium-Ion Batteries to Lithium-Ion Counterparts?," *ACS Energy Letters*, vol. 5, pp. 3544-3547, May 2020.
[190] M. Mirzaelan, Q. Abbas, M. R. C. Hunt et al., "Na-Ion Batteries," in *Encyclopedia of Smart Materials*, A. G. Olabi, Ed. Amsterdam, NLD: Elsevier, 2021, p. 14.
[191] M. Arnaiz, J. L. Gomez-Camer, N. E. Drewett et al., "Exploring Na-ion Technological Advances: Pathways from Energy to Power," *Materials Today Proceedings*, vol. 39, pp. 1118-1131, Apr. 2021.
[192] H. Zhao, N. Deng, J. Yan et al., "A Review on Anode for lithium-Sulphur Batteries: Progress and Prospects," *Chemical Engineering* Journal, vol. 347, pp. 343-365, Sep. 2018.
[193] M. Zhao, B-Q. Li, X-Q. Zhang et al., "A Perspective toward Practical Lithium-Sulphur Batteries," *ACS Central Science,* vol. 6, p. 1095-1104, Jun. 2020.
[194] N. R. Levy and Y. Ein-Eli, "Aluminium-Ion Battery Technology: A Rising Star or a Devastating Fall," *Journal Solid State Electrochemistry*," vol. 24, pp. 2067-2071, Apr. 2020.
[195] S. Hosseini, S. M. Soltani, and Y. Y. Li, "Current Status and Technical Challenges of Electrolytes in Zinc-Air Batteries: An in-Depth Review," *Chemical Engineering Journal*, vol. 408, p. 127241, Mar. 2021.
[196] B. Esser, F. Dolhem, M. Becuwe et al., "A Perspective on Organic Electrode Materials and Technologies for Next Generation Batteries," *Journal Power Sources*, vol. 482, p. 24, Jan. 2021.
[197] G. Karkera, M. A. Reddy, and M. Fichner, "Recent Developments and Future Perspectives of Anionic Batteries," *Journal of Power Sources*, vol. 481, no. 22, p. 17, Jan. 2021.
[198] M. M. Rahman, I. Sultana, Y. Fan et al., "Strategies, Design and Synthesis of Advanced Nanostructured Electrodes for Rechargeable Batteries," *Materials Chemistry Frontiers*, vol. 16, p. 35, Jun. 2021.
[199] D. E. Demirocak, S. S. Srinivasan, and E. K. Stefanakos, "A Review on Nanocomposite Materials for Rechargeable Li-ion Batteries," *Applied Sciences*, vol. 7, no. 7, p. 731, Jul. 2017.
[200] J. E. Knoop and S. Ahn, "Recent Advances in Nanomaterials for High-Performance Li-S Batteries," *Journal Energy Chemistry*, vol. 47, pp. 86-106, Aug. 2020.
[201] J. B. Dunn, L. Gaines, J. C. Kelly et al., "The Significance of Li-Ion Batteries in Electric Vehicle Life-Cycle Energy and Emissions and Recycling's Role in its Reduction," *Energy & Environmental Science*, vol. 8, pp. 158-168, Nov. 2015.
[202] G. Harper, R. Sommerville, E. Kendrick et al., "Recycling Lithium-Ion Batteries from Electric Vehicles," *Nature*, vol. 575, pp. 75-86, Nov. 2019.
[203] L. C. Casals, B. A. Garcia, and C. Canal, "Second Life Batteries Lifespan: Rest of Useful Life and Environmental Analysis," *Journal Environmental Management*, vol. 232, pp. 354-363, Nov. 2019.
[204] J. Bacher, E. Pohjalainen, E. Yli-Rantala et al., "Environmental Aspects Related to the use of Critical Raw Materials in Priority Sectors and Value Chains," European Environment Agency, Copenhagen, DNK, Re. ETC/WMGE 2020/5, Dec. 15, 2020.
[205] H. E. Melin. (2029, Mar. 29). *State-of-the-Art in Reuse and Recycling of Lithium-Ion Batteries*. [Online]. Available: https://www.linkedin.com/pulse/state-of-the-art-lithium-ion-battery-reuse-recycling-research-melin
[206] A. Beaudet, F. Larouche, K. Amouz et al., "Key Challenges and Opportunities for Recycling Electric Vehicle Battery Materials," *Sustainability*, vol. 12, no. 14, p. 12, Jul. 2020.
[207] X. B. Cheng, H. Liu, H. Yuan et al., "A Perspective on Sustainable Energy Materials for Lithium Batteries," *SusMat.* vol. 1, pp. 38-50, Mar. 2021.
[208] X. Yu and A. Manthiram, "Sustainable Battery Materials for Next-Generation Electrical Energy Storage," *Advanced Energy Sustainability Research*, vol. 2, no. 5, p. 12, Jan. 2021.
[209] S. Doose, J. K. Mayer, and P. Michalowski, "Challenges in Ecofriendly Battery Recycling and Closed Materials Cycles: A Perspective on Future Lithium Battery Generations," *Metals*, vol. 11, p. 17, Feb. 2021.
[210] Y. Liu, R. Zhang, J. Wang et al., "Current and Future lithium-Ion Battery Manufacturing," *iScience*, vol. 24, p. 17, Apr. 2021.
[211] P. Cooke, "Gigafactory Logistics in Space and Time: Tesla's Fourth Gigafactory and Its Rivals," *Sustainability,* vol. 12, p. 16, Mar. 2020.
[212] Greenpeace. (2021, Jul. 10). *Greenpeace Report Troubleshoots China's Electric Vehicles Boom, Highlights Critical Supply Risks for Lithium-Ion Batteries*. [Online]. Available: https://www.greenpeace.org/eastasia/press/6175/greenpeace-report-troubleshoots-chinas-electric-vehicles-boom-highlights-critical-supply-risks-for-lithium-ion-batteries/
[213] P. Bhandubanyong and J. T. H. Pearce, "Materials on Wheels: Moving to Lighter Auto-Bodies," *International Scientific Journal of Engineering and Technology*, vol. 2, no.1, pp. 27-36, Jun. 2018.
[214] P. Bhandubanyong and J. T. H. Pearce, "Going Electric: Some Materials Aspects for the Thai Automotive Industry," *Materials Science*, vol. 36, pp. 4-6, Jan. 2019.
[215] A&L. (2020, Nov. 23). *Aluminium for Battery Containers in Electric Cars*. [Online]. Available: https://www.publiteconline.it/ael/aluminium-for-battery-containers-in-electric-cars-3/

[216] F. Lambert. (2021, Jan. 19). *First Look at Tesla's New Structural Battery Pack that will Power its Future Vehicles*. [Online]. Available: https://electrek.co/2021/01/19/tesla-structural-battery-pack-first-picture/
[217] M. Schröder, "Electric Vehicle and Electric Vehicle Component Production in Thailand," ERIA, Jakarta: IDN, Re. FY2021 no. 03, May 7, 2021.
[218] Kasikorn. (2029, Jan. 30). *Thailand is Poised to Produce over 430,000 units of EV Batteries in 5 Years, Becoming 4th Largest Production Base in Asia*. [Online]. Available: https://www.kasikornresearch.com/en/analysis/k-econ/business/Pages/z2960.aspx
[219] Thailand Board of Investment. (2021, Jul. 20). *Thailand Car Makers Ramp Up Electric Vehicle Production Capacity in Thailand, Investment Board Says*. [Online]. Available: https://www.boi.go.th/un/boi_event_detail?module=news&topic_id=125377
[220] Batteries Directive. (2021, Jul. 10). *European Parliamentary Research Service*. [Online]. Available: https://www.europarl.Eu/RegData/etudes/BRIE/2020/654184/EPRBRI(2020)654184_EN.pdf
[221] TGGS. (2021, Jul. 10). *NSTDA in collaboration with KKU KMUTT KMUTNB and EVAT to find Thailand Energy Storage Technology Alliance (TESTA).* [Online]. Available: https://tggs.kmutnb.ac.th/nstda-in-collaboration-with-kku-kmutt-kmutnb-and-evat-to-find-thailand-energy-storage-technology-alliance-testa
[222] EVAT. (2021, Jul. 10). *Thailand's Automotive Industry and Current EV Status*. [Online]. Available: https://www.boi.go.th/upload/content/2.%20[PPT]%20Thailand's%20Automotive%20Industry%20and%20Current%20EV%20Status_5c864c90761f6.pdf

Paritud Bhandhubanyong holds a B. Eng. (1972) and M.Eng. (1976) (Industrial Engineering) from Chulalongkorn University, MBA (1976) from Thammasart University and D.Eng. (Metallurgy) in 1983 from the University of Tokyo. He joined the State Railway of Thailand as a junior engineer then moved to work as an instructor in the Faculty of Engineering, Chulalongkorn University. He was Head of Department of Metallurgical Engineering, Vice Dean of Planning and Development before joining the National Metal and Materials Technology Center as Executive Director. He then moved to be the Executive Director of the Technological Promotion Association Thai-Japan (TPA) before joining the Panyapiwat Institute of Management as Executive Director in the office of the President, acting Head of Department of Automotive Manufacturing Engineering, and Acting Dean of the Faculty of Logistics and Transportation Management. His research interest included Casting Technology, TQM, TPM, TPS, and work-based education (WBE) practices. His recent papers and publication included a chapter in the Report on ASEAN Automotive Industry 2016 (in Japanese), Business Continuity Management (TPA, 2015) and a paper on WBE presented at ISATE 2016.

Dr. Paritud is a member of the Japan Foundry Engineering Society, The Iron and Steel Institute of Japan, former Chairman of the Foundation of TQM Promotion of Thailand, committee member of the Standard and Quality Association of Thailand, advisor to the Thai Foundry Association of Thailand and the Materials and Corrosion Society.

John T. H. Pearce holds a B.Sc. Hons. Degree in Metallurgy (1967) and a Ph.D. in Wear of Abrasion Resistant Materials (1982), both awarded by the University of Aston in Birmingham, England.

Following research and production experience as a Technical Assistant at International Nickel, Rubery Owen Group and British Motor Corporation from 1962 to 1967, he joined British Cast Iron Research Association as a Research Metallurgist.

In 1970 until 1995, he was a Senior Lecturer in Metallurgy and Foundry Technology at Sandwell College FHE. In the West Midlands. He moved to Thailand in 1996 to be a Senior Metals Specialist at the National Metals and Materials Technology Centre (MTEC) until he joined PIM in 2014 as a Lecturer in the School of Engineering. He has contributed to fourteen books/monographs, and is author/co-author of 160 articles, and more than 180 conference papers. His main research & consultancy interests include structure-properties relationships in metal castings, electron microscopy, wear and corrosion resistance, and quality management in metals production.

Dr. Pearce is a Past President of the Birmingham Metallurgical Association and in 1997 received the Voya Kondic Medal from the Institute of Cast Metals Engineers for services to education in the cast metals industry. In the UK, he was a Chartered Engineer, a Fellow of the Institute of Materials and a Member of the Institute of Cast Metals Engineers.

Trend Analysis Based AMDF for Robust Pitch Detection of Speech Signals

Weihua Zhang[1], Yingying Lu[2], and Pingping Xu[3]

[1,2,3]School of Computer and Communication Engineering, Nanjing Tech University Pujiang Institute, Nanjing, China
E-mail: 150916907@qq.com, xhluyingying@163.com, xpp@seu.edu.cn

Received: August 15, 2021 / Revised: September 18, 2021 / Accepted: September 28, 2021

***Abstract*—In this paper, we focus on improving the AMDF pitch detection algorithm (PDA) rather than designing a complete pitch detection system including many complex modification stages. As a hot classical PDA, generating half or multiple pitch errors is a usual defect of AMDF, especially in noisy conditions. Based on a deep analysis of many existing improvements of AMDF, we summarize two modified frameworks and classify the most outstanding improvements into them. Then we propose a novel and simple modified framework for AMDF to conquer the defect of AMDF. For our framework, we also present two kinds of falling trend extraction methods to obtain the proposed Trend Analysis based AMDF (TAAMDF). Finally, Experiments on the *Keele* database are conducted to evaluate our framework. Compared with some outstanding modified AMDFs and well-known ACF, modified AMDF based on our framework shows the best performance especially its robustness to different noises.**

***Index Terms*—Pitch Detection Algorithm, AMDF, Falling Trend Analysis**

I. Introduction

Pitch (or fundamental frequency) plays an important role in many fields of speech signal processing such as speech coding, speech recognition, speech enhancement, etc. This fact has motivated researchers to think of how to detect the pitch from speech signals accurately and effectively. As is known to all, breakthroughs of PDAs emerged decades ago. Since then, there are many classical pitch detection algorithms (PDAs) [1]-[3] and their improvements have been proposed. In spite of this, developing accurate and reliable PDAs is still challenging. There are still many excellent works reported in recent years [4], [5], and one of the most important features we notice is that nowadays researchers devote themselves to designing a complete pitch detection system for high accuracy and noise robustness that adds many pre-processing and post-processing stages to enhance the key part of the system i.e., their PDAs. However, a lot of outstanding software for speech signal analysis still adopts classical PDAs mentioned above to design their pitch detection module. For example, the Autocorrelation Function (ACF) based pitch detection module is included in the Praat [6] software. YIN [7], an excellent pitch estimator, is also based on ACF with some additional modifications. This situation indicates that these classical PDAs are still valuable and powerful. Hence, we hold a viewpoint that it is still meaningful and worthwhile to make these classical PDAs more powerful as well as develop a complete pitch detection system.

In this paper, we pay attention to another classical PDA, namely Average Magnitude Difference Function (AMDF) [2]. AMDF is also one of the most widely used PDAs because of its low computation and high precision. However, Zhang et al. [8] pointed out that a falling trend presents as a global feature in AMDF such that some detection errors that the estimated pitch is half or multiple of the actual sometimes happened. This is not only due to a single cause but a combination of complex factors such as formant, noise, and framing setup of speech signals. Furthermore, noise is the most usual and unavoidable factor for PDA. Therefore, it is important to improve AMDF to eliminate the falling trend and enhance the robustness to noise. To this end, Zhang et al. [8] proposed Circular AMDF (CAMDF) by introducing modulo operation to redefine the calculation AMDF of speech frame at each lag. CAMDF prevents the falling trend and achieves excellent detection performance. Another state-of-the-art modification of AMDF which is worth mentioning is Extended AMDF (EAMDF) presented by Muhammud [9]. EAMDF extends the length of the speech frame to supply the loss of overlap with lag increasing. Thus, EAMDF can overcome the falling trend effectively and outperforms the classical AMDF.

Although these modified AMDFs achieve promising performance, they are not very satisfactory due to changes of either definition or speech frame and will also bring estimated errors sometimes. In this paper, we propose a novel modified framework for AMDF. Different from many existing improvements, this is a simple and distinctive framework that can overcome the shortcoming of AMDF more effectively and is considerably robust to different types of noise.

The rest of this paper is organized as follows: Section 2 reviews AMDF and its representative improvements. Section 3 describes the proposed framework for AMDF. After that, experiments on the *Keele* database are conducted for testing and verifying the proposed framework in Section 4. Finally, the paper is concluded in Section 5.

II. Review and Analysis of Amdf and Its Improvements Amdf

The conventional AMDF [2] is defined as follows:

$$D_{AMDF}(\tau) = \sum_{n=0}^{N-\tau-1} |x(n) - x(n+\tau)| \tag{1}$$

where $x(n)$ denotes a voiced speech frame multiplied by a rectangular window of length N and τ denotes the lag number. For a periodic or quasi-periodic signal with a period of T_p, its AMDF $D_{AMDF}(\tau)$ should exhibit valleys at lag nT_p, where n is an integer. Generally, we can estimate the raw pitch f_p from AMDF according to Equation (2).

$$f_p = fs / \arg\min_{\tau}(D_{AMDF}(\tau)) \tag{2}$$

where fs denotes sample frequency of speech signals. As less data is used to calculate AMDF at higher lags, a falling trend may present as a global feature in the AMDF curve sometimes. Thus, the valley with true pitch information may not be the lowest and the multiple pitch errors may be produced according to Equation (2). Fig. 1 (b) shows a typical example of the double pitch error of classical AMDF. In the figure, the corresponding speech signal is a clean voiced frame (see Fig. 1 (a)).

In order to overcome this shortcoming of AMDF, many outstanding modified AMDFs have been proposed. Among these modifications, CAMDF [8] and EAMDF [9] mentioned in the previous section are two representative ones. CAMDF was proposed to overcome the falling trend by a modulo operation and is defined as follows:

$$D_{CAMDF}(\tau) = \sum_{n=0}^{N-1} |x(\mathrm{mod}(n+\tau, N)) - x(n)| \tag{3}$$

where mod(n + τ, N) represents that n + τ modulo N. Muhammad [9] proposed EAMDF and define it as:

$$D_{EAMDF}(\tau) = \frac{1}{N-\tau} \sum_{n=-N/2}^{N+N/2-\tau} |x(n) - x(n+\tau)| \tag{4}$$

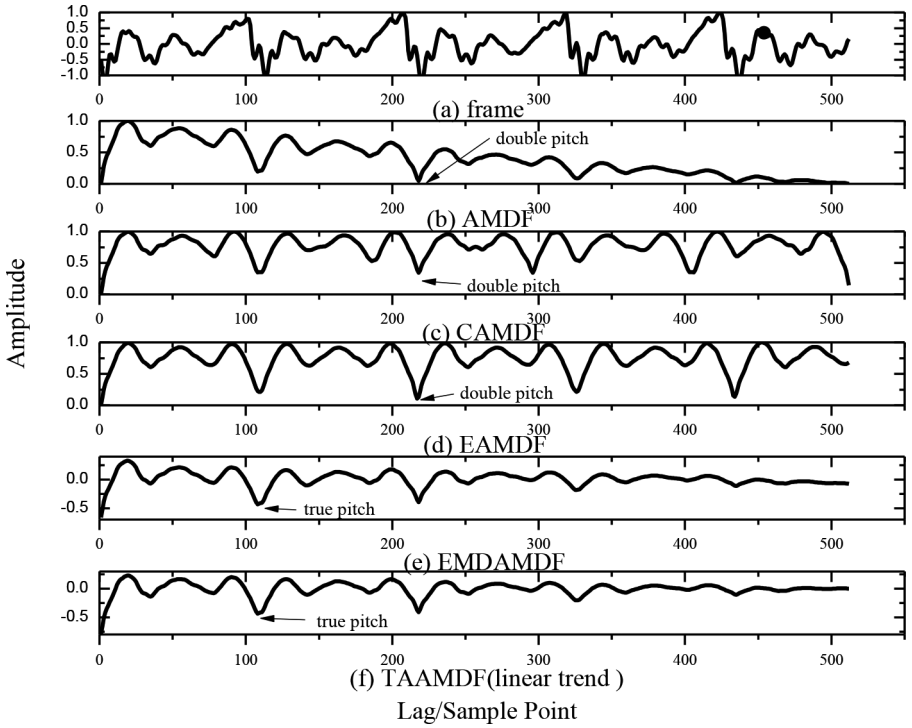

Fig. 1. Comparison between (b) AMDF, (c) CAMDF, (d) EAMDF, (e) EMDAMDF and (f) TAAMDF of (a) a typical speech frame. EMDAMDF and TAAMDF detects the true pitch, while all the other produce double pitch errors.

Actually, it should be noted that compared with the AMDF (Equation (2)), we can clearly find that CAMDF (Equation (3)) is improved by modifying the definition of AMDF whereas EAMDF (Equation (4)) promotes by means of adjusting the length of the speech frame which is used to calculate AMDF. As Fig. 1 (c) and Fig. 1 (d) depict, CAMDF and EAMDF can all achieve eliminating the falling trend. However, they still produce unexpected double pitch errors because of the adverse impact brought by the changes of speech frame or definition. We think that they represent two typical modified frameworks for improving AMDF, namely modifying the definition of AMDF and adjusting the length of the speech frame. Furthermore, our observation is that the vast majority of existing modified AMDFs can all be included in these two frameworks. For example, LVAMDF [10] adjusts the length of the speech frame and HRAMDF [11] both adjusts the frame and redefines AMDF by adding a normalized term.

III. A novel Framework for Improving Amdf

Ideally, we want to find a framework for AMDF that eliminates the falling trend effectively and produces no estimated errors because of adjustment. In our previous work [12], we employ Empirical Mode Decomposition (EMD) [13] to address the problem and improve AMDF. More specifically, let $D_{AMDF}(\tau)$ be AMDF of a voiced speech frame. $D_{AMDF}(\tau)$ can be decomposed into a series of Intrinsic Mode Functions (IMFs) $c_i(\tau)$ and a residue $r_N(\tau)$. Based on the principle of EMD, AMDF can be reconstructed by all IMFs and the residue, which can be expressed as:

$$D_{AMDF}(\tau) = \sum_{i=1}^{N} c_i(\tau) + r_N(\tau) \tag{5}$$

where N is the number of IMFs. We find that the residue $r_N(\tau)$ represents the trend of AMDF data points namely the falling trend which is mentioned in many literatures. Therefore, we spontaneously consider to reconstruct AMDF abandoning the residue, and obtain our EMD-based AMDF (EMDAMDF) [12]:

$$D_{EMDAMDF}(\tau) = \sum_{i=1}^{N} c_i(\tau) \tag{6}$$

It is worth noting that EMDAMDF can also be written as:

$$D_{EMDAMDF}(\tau) = D_{AMDF}(\tau) - r_N(\tau) \tag{7}$$

For the speech frame in Figure 1(a), EMDAMDF can both eliminate the falling trend of AMDF and estimate the true pitch effectively as shown in Fig. 1 (e). It must be emphasized that although the two formulas above turn out the same results, their thoughts are distinct that the former is a reconstruction method and the latter is a removing one.

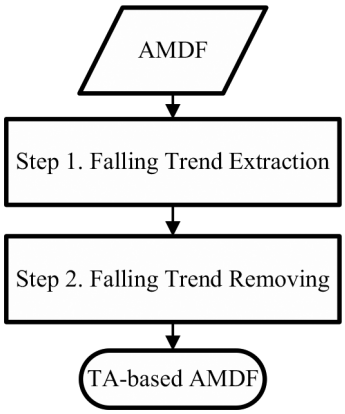

Fig. 2. Trend Analysis-based framework for improving AMDF.

Due to the fine performance of EMDAMDF and inspired by Equation (7) to calculate EMDAMDF, we propose a novel modified framework for AMDF as shown in Fig. 2. This is a simple framework and differs from the two ones mentioned in Section 2. As the figure describes, it consists of two steps, namely, Step 1. falling trend extraction, and Step 2. falling trend removal. More specifically, given an AMDF of speech frame denoted by $D_{AMDF}(\tau)$ we first use some methods such as EMD mentioned above to analyze its mathematical form of the falling trend $r_{trend}(\tau)$ and then remove the falling trend from AMDF to obtain the modified AMDF that we call Trend Analysis based AMDF (TA-based AMDF or TAAMDF) as following:

$$D_{TAAMDF}(\tau) = D_{AMDF}(\tau) - r_{\text{trend}}(\tau) \tag{8}$$

Compared with the other two frameworks mentioned before, our framework aims to analyze the falling trend based on AMDF and then remove it from AMDF instead of modifying the definition of AMDF and changing the length of the speech frame.

It is clear that the key part of our framework is Step 1, i.e., how to extract the falling trend. Therefore, what we focus on is converted to a trend analysis problem in time series analysis. In time series analysis, trend analysis is not an easy question. For many complex uncertain trends, it is difficult to estimate their concrete form. Based on the further analysis of EMDAMDF, we can convince that the falling trend of AMDF is nearly a linear trend and our framework need not pursue preciseness of trend analysis. As shown in Fig. 1 (f) TAAMDF adopting linear trend and least square can eliminate the falling trend and obtain the accurate pitch as well as EMDAMDF. Therefore, we believe that although we do not know the mathematical form of the falling trend of AMDF, many existing conventional trend analysis methods are available for our framework.

As the trend analysis methods for time series analysis have no strict classification, we summarize two types of falling trend analysis methods for the

proposed framework. Generally, one can be called decomposition method such as EMD and the other can be called estimation method such as least square. Fig. 3 is an incomplete list of falling trend extraction methods we summarized. As shown in decomposition methods, we are also able to employ other signal analysis methods such as wavelet analysis to extract the falling trend instead of EMD. In estimation methods, least-square is a representative effective method to estimate the falling trend. Usually, the falling trend is assumed as a specified form such as Linear, Polynomial, Gaussian, etc. Then least square is used to estimate the parameters of the falling trend based on all data points of AMDF such that we can obtain the concrete form of the falling trend of AMDF.

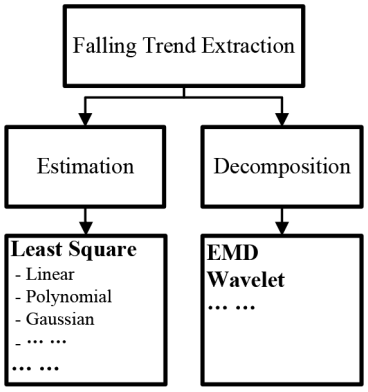

Fig. 3. Two types of falling trend extraction methods for the proposed framework.

For completely understanding our framework, now we describe how to calculate TAAMDF using the estimation method with least square plus polynomial, for example. Suppose we have an AMDF of a voiced speech frame $D(\tau)$ and its lag $\tau = 1, 2, \cdots, n$. Accordingly, all the data points of AMDF are $(1, D(1)), (2, D(2)), \cdots, (n, D(n))$. We use polynomial with the degree m to estimate the falling trend of AMDF and denote it as:

$$r_{trend}(\tau) = a_0 + a_1\tau + a_2\tau^2 + \cdots + a_m\tau^m = \sum_{j=0}^{m} a_j\tau^m \tag{9}$$

Substituting all the data points into (9), we obtain that

$$\begin{cases} D(1) = a_0 \cdot 1^0 + a_1 \cdot 1^1 + a_2 \cdot 1^2 + \cdots + a_m \cdot 1^m \\ D(2) = a_0 \cdot 2^0 + a_1 \cdot 2^1 + a_2 \cdot 2^2 + \cdots + a_m \cdot 2^m \\ \qquad\qquad \cdots\cdots \\ D(n) = a_0 \cdot n^0 + a_1 \cdot n^1 + a_2 \cdot n^2 + \cdots + a_m \cdot n^m \end{cases} \tag{10}$$

Let $A = \begin{bmatrix} 1 & 1 & 1^2 & \cdots & 1^m \\ 1 & 2 & 2^2 & \cdots & 2^m \\ \vdots & \vdots & \vdots & \ddots & \vdots \\ 1 & n & n^2 & \cdots & n^m \end{bmatrix}$, $x = \begin{bmatrix} a_0 \\ a_1 \\ a_2 \\ \vdots \\ a_n \end{bmatrix}$ and $b = \begin{bmatrix} D(1) \\ D(2) \\ \vdots \\ D(n) \end{bmatrix}$ As is known that $rank(A) = m+1<n$ the least square solution of the parameter vector $\hat{x}$ can be calculated by

$$\hat{x} = \begin{bmatrix} \hat{a}_0 \\ \hat{a}_1 \\ \hat{a}_2 \\ \vdots \\ \hat{a}_n \end{bmatrix} = (A^T A)^{-1} A^T b \tag{11}$$

Thus, we obtain the falling trend:

$$\hat{r}_{trend}(\tau) = \hat{a}_0 + \hat{a}_1\tau + \hat{a}_2\tau^2 + \cdots + \hat{a}_m\tau^m = \sum_{j=0}^{m} \hat{a}_j\tau^m \tag{12}$$

Based on the proposed framework in Fig. 2, the TAAMDF can be calculated as:

$$D_{TAAMDF}(\tau) = D(\tau) - \hat{r}_{trend}(\tau) \tag{13}$$

IV. Experiments and Analysis

We test our trend analysis-based framework for AMDF using the *Keele* pitch extraction reference database [14]. The *Keele* database consists of 5 mature females and 5 mature male speakers. Each speaker read a phonetically balanced text. The speech signals are sampled at 20 kHz with 16-bits resolution. The Database provides reference pitch values at 100 Hz frame rate with 26.5 ms rectangular window. Some frames with uncertain reference pitch recorded as '-1' are totally cut down. The whole samples of the database are all employed here.

We choose EMD from decomposition methods and polynomial from estimation methods to extract the falling trend to obtain TAAMDFs based on our framework denoted by TAAMDF (EMD) (*i.e.*, EMDAMDF in [12]) and TAAMDF (Poly) respectively. Note that according to large numbers of experiments and analyses we obtain a reliable formula to determine the degree of the polynomials m for TAAMDF, i.e., m = int ($L_{frame} \cdot f_{raw}/fs$) where int is integer operation, L_{frame} is the frame length, fs is the sampling frequency and f_{raw} is "raw pitch". So-called "raw pitch" here actually refers to the empirical pitch ranges of females and males. Usually, we consider that in our framework it is feasible to set f_{raw} as 100 Hz for male and 200 Hz for female. Therefore, we can set the degree of polynomial of TAAMDF be 3 for male speech and 5 for female speech with regard to the *Keele* database. We compare the TAAMDF with CAMDF and EAMDF which are two state-of-the-art improvements of AMDF belonging to the other two frameworks discussed in the previous section. For showing the excellent performance of our framework, ACF, an outstanding classical PDA

used by lots of speech analysis software, is included in the experiments as well. The experimental results are reported in terms of percentage GPE denoted as % GPE which is short for gross pitch error and defined by Rabiner et al. [15]. The definition of GPE is that the detected pitch period for a frame defers 1ms from the reference value. It should be noted that for fair comparison in all the experiments, both pre-processing and post-processing methods for error prevention and noise robustness such as band-pass filtering, half-wave rectification, center clipping and pitch smooth, are not employed. We want to show the most original performance of all PDAs.

TABLE I
PERFORMANCE OF DIFFERENT ALGORITHMS FOR CLEAN SPEECH OF THE WHOLE KEELE DATABASE

Method	*Keele*
AMDF	17.75
CAMDF	12.30
EAMDF	7.36
ACF	11.07
TAAMDF (EMD)	8.89
TAAMDF (Poly)	**7.13**

Table I gives % GPE of the whole *Keele* database detected by ACF, AMDF, CAMDF, EAMDF, TAAMDF (EMD), and TAAMDF (Poly). It can be observed that CAMDF, EAMDF, and two TAAMDFs all improve AMDF significantly. Although AMDF is not as good as ACF, its modifications can all turn the situation around (CAMDF is an exception but approximate). Besides, we notice that the proposed TAAMDF (Poly) has the least % GPE (7.13%) and owns the overall superiority among all PDAs while EAMDF performs excellently (7.36%) as well. TAAMDF (EMD) also achieves a fewer % GPE (8.89%) than CAMDF and ACF. Finally, from the experimental results, we notice that least square plus polynomial outperforms EMD for the proposed framework.

In order to further evaluate the performance especially the robustness of all PDAs, our experiments are also conducted by adding White, Babble, and Machinegun noise to the database at different Signal-to-Noise Ratio (SNR) set at 10, 5, 0, -5, and -10 dB respectively. Note that SNR is defined as, where S is the average power of the speech signal and N is the average power of the added noise. In our experiments, Babble and Machinegun noise are taken from NOISEX-92 database [16] and White noise is generated by awgn.m in MATLAB. Here we only choose the TAAMDF (poly) as the representative of our framework because of its performance shown in the former experiment. The experimental results are reported in Table II, Table III, and Table IV, respectively.

According to the results, something obvious can be observed. Firstly, different from the outcome for clean speech shown in Table I, ACF has remarkable progress in that it exceeds CAMDF and EAMDF and has a fewer % GPE than them. Then we can also find that although EAMDF has a very similar performance to TAAMDF for clean speech, its robustness to noise is so bad in noisy conditions. As is shown in Table II to Table IV, EAMDF always has the nearly most % GPE among these PDAs except AMDF in three noisy conditions. Finally, it is obvious that TAAMDF outperforms the other PDAs for every noise at any SNR. Besides, according to the definition of ACF, we know that ACF has the robustness to white noise (complete derivation can be seen in [17]). That is why for white noise ACF has a significant advantage over CAMDF and EAMDF. However, TAAMDF still has less % GPE than ACF in noisy conditions, especially for white noise. Therefore, we think that our framework is an efficient and reasonable way to improve AMDF. We also think that TAAMDF based on polynomial and least square within our framework is a more effective PDA than other modified AMDF and ACF.

TABLE II
PERFORMANCE OF DIFFERENT ALGORITHMS FOR THE WHOLE KEELE DATABASE POLLUTED BY WHITE NNOISE AT DIFFERENT SNR

Method	10 dB	5 dB	0 dB	-5 dB	-10 dB
AMDF	30.14	45.29	63.94	82.23	93.06
CAMDF	10.09	13.80	21.18	33.25	51.74
EAMDF	10.32	17.76	30.81	49.83	69.83
ACF	8.83	10.43	14.47	22.28	37.87
TAAMDF	**6.35**	**7.42**	**9.77**	**15.03**	**24.60**

TABLE III
PERFORMANCE OF DIFFERENT ALGORITHMS FOR THE WHOLE KEELE DATABASE POLLUTED BY BABBLE NOISE AT DIFFERENT SNR

Method	10 dB	5 dB	0 dB	-5 dB	-10 dB
AMDF	41.20	54.86	70.41	63.71	88.33
CAMDF	20.38	28.44	42.14	54.36	69.75
EAMDF	18.46	30.89	47.19	81.73	75.18
ACF	16.74	24.15	37.48	57.68	68.01
TAAMDF	**12.68**	**19.00**	**30.86**	**45.92**	**59.42**

TABLE IV
PERFORMANCE OF DIFFERENT ALGORITHMS FOR THE WHOLE KEELE DATABASE POLLUTED BY MACHINEGUN NOISE AT DIFFERENT SNR.

Method	10 dB	5 dB	0 dB	-5 dB	-10 dB
AMDF	30.81	36.37	43.28	50.77	58.64
CAMDF	19.28	23.86	29.71	36.13	42.97
EAMDF	15.94	22.36	29.67	37.74	45.50
ACF	17.15	21.86	28.12	34.99	42.18
TAAMDF	**11.36**	**14.89**	**19.83**	**26.11**	**32.83**

V. Conclusions

In this paper, we address the problem that multiple pitch errors sometimes appear in classical AMDF for pitch detection. We begin with a systematical review and analysis of its existing state-of-art modifications and sum up their improved ways as two kinds of frameworks. Then we propose a novel modified framework and two types of efficient falling trend extraction methods for the framework. Finally, experiments on the *Keele* database are conducted to test and validate the rationality and effectiveness of our modified framework. We can claim that the trend analysis based AMDF which chooses effective falling trend method owns the best performance especially for noisy speech and outperforms obviously modified AMDFs based on the other two frameworks summarized before and ACF which is an outstanding and well-known classical PDA.

Acknowledgement

This work was supported by the Teaching Reform Project of Nanjing Tech University Pujiang Institute under Grants njpj2019-1-03 and njpj2019-1-05.

References

[1] D. A. Krubsack and R. J. Niederjohn, "An Autocerrelation Pitch Detector and Voicing Decision with Confidence Measures Developed for Noise Corrupted Speech," *IEEE*, vol. 39, no. 2, pp. 319-329, Feb. 1991.

[2] M. Ross, H. Shaffer, and R. Freudberg et al., "Average Magnitude Difference Function Pitch Extractor," *IEEE*, vol. 22, no. 5, pp. 353-362, Oct. 1974.

[3] S. Ahmadi and A. S. Spanias, "Cepsrum-Based Pitch Detection Using a New Statistical V/UV Classification Algorithm," *IEEE*, vol. 7, no. 3, pp. 333-338, May. 1999.

[4] F. Kurth, A. Cornaggia-Urrigshardt, and S. Urrigshardt, "Robust F0 estimation in Noisy Speech Signals Using Shift Autocorrelation," in *ICASSP 2014-39th IEEE International Conference on Acoustics, Speech and Signal Processing*, Florence, Italy, 2014, pp. 1468-1472.

[5] P. Pelle and C. Estienne, "A Robust Pitch Detector Based on Time Envelope and Individual Harmonic Information Using Phase Locked Loops and Consensual Decisions," in *ICASSP 2014-39th IEEE International Conference on Acoustics, Speech and Signal Processing*, Florence, Italy, 2014, pp. 1483-1487.

[6] P. Boersma, "Accurate Short-Term Analysis of The Fundamental Frequency and The Harmonics-To-Noise Ratio 0f a Sampled Sound," in *Proc. IFA International Conference*, 1993, pp. 97-110.

[7] A. De Cheveigné and H. Kawahara, "YIN, a Fundamental Frequency Estimator for Speech and Music," *The Journal of the Acoustical Society of America*, vol. 111, no. 4, pp. 1917-1930, Apr. 2002.

[8] W. Zhang, G. Xu, and Y. Wang, "Pitch Estimation Based on Circular AMDF," in *ICASSP 2002*, Orlando, Florida, USA, 2002, pp. I-341-I-344.

[9] G. Muhammad, "Noise Robust Pitch Detection Based on Extended AMDF," in *ISSPIT 2008-IEEE International Symposium on Signal Processing and Information Technology*, Sarajevo, Bosnia and Herzegovina, 2008, pp. 133-138.

[10] L. Gu and R. Liu, "High Performance Mandarin Pitch Estimation," *Acta Electronica Sinica*, vol. 27, no. 1, pp. 8-11, Jan. 1999.

[11] T. E. Tremain, "The Government Standard Linear Predictive Coding Algorithm: LPC-10," *Speech Technology*, vol. 1, no. 2, pp. 40-49, Feb. 1982.

[12] Y. Zong, Y. Zeng, and M. Li et al., "Pitch Detection Using EMD-Based AMDF," in *Proc. ICICIP 2013*, Beijing, China, 2013, pp. 594-597.

[13] N. E. Huang, Z. Shen, S. R. Long et al., "The Empirical Mode Decomposition and the Hilbert Spectrum for Nonlinear and Non-Stationary Time Series Analysis," in *Proc. the Royal Society of London A: Mathematical, Physical and Engineering Sciences*, 1998, pp. 903-995.

[14] G. Meyer, F. Plante, and W. Ainsworth, "A Pitch Extraction Reference Database," in *Proc. European Conference on Speech Communication and Technology*, *EUROSPEECH 1995*, Madrid, Spain, 1995, pp. 827-840.

[15] L. R. Rabiner, M. J. Cheng, and C. A. McGonegal, "A Comparative Performance Study of Several Pitch Detection Algorithms," *IEEE Transactions on Acoustics, Speech and Signal Processing*, vol. 24, no. 5, pp. 399-417, Oct. 1976.

[16] A. Varga and H. J. M. Steeneken, "Assessment for Automatic Speech Recognition: II. NOISEX-92: A Database and an Experiment to Study the Effect of Additive Noise on Speech Recognition Systems," *Speech Communication*, vol. 12, no. 3, pp. 247-251. Jul. 1993.

[17] T. Shimamura and H. Kobayashi, "Weighted Autocorrelation for Pitch Extraction of Noisy Speech," *IEEE*, vol. 9, no. 7, pp. 727-730, Oct. 2001.

Weihua Zhang received a B.S. degree in Electronic Information Engineering from Southeast University, Nanjing, China, and an M.S. degree in Software Engineering from Nanjing University, Nanjing, China. He is currently a Lecturer and the Vice Dean with the School of Computer and Communication Engineering, Nanjing Tech University Pujiang Institute, Nanjing, China. His research interests include signal processing, artificial intelligence, and affective computing.

Yingying Lu received a B.A. degree in Japanese Language and Literature from Nanjing Tech University, Nanjing, China in 2012, and an M.A. degree in Teacher Education from Nanjing Normal University, Nanjing, China in 2016, respectively. From 2016 to 2020, she was a Lecturer with the Department of Humanities, Nanjing Normal University Zhongbei College, Zhenjiang, China. Currently, she has been working as a Lecturer with the School of Computer and Communication Engineering, Nanjing Tech University Pujiang Institute, Nanjing, China. Her research interests include teacher education, psychological health education, and affective computing.

Pingping Xu received the B.S., M.S., and Ph.D. degrees all from Southeast University, Nanjing, China. She is currently a Professor with the National Laboratory of Mobile Communications, School of Information Science and Engineering, Southeast University and the Dean of the School of Computer and Communication Engineering, Nanjing Tech University Pujiang Institute, Nanjing, China. She was working as a guest researcher with the Department of Information and Communication Engineering, Aichi Institute of Technology, Japan in 1997, and with the Mobile Communication Lab, Osaka University, Japan in 2000, respectively. Dr. Xu has published more than 50 scientific papers, 4 books, and 20 patents, and obtained 4 science prizes. Her interests include signal processing, artificial intelligence, and affective computing.

PAPER FORMAT
(IEEE Style)

I. Format

- Your paper must use a paper size corresponding to A 4 which is 210 mm (8.27 inch) Wide and 297 mm (11.69 inch)
- Your paper must be in two column format
- Articles not more than 15 pages in length, single-sided A4 paper, margins (top, bottom, left, right) are 1 inch (2.54 cm)
- Abstract and References and content set to double columns,
- English font is Times New Roman, as follows:

TABLE I
Font Sizes for Papers

Content	Font Size	Labelling
Title (Single column)	18 (CT)	bold
Authors (Single column)	11 (CT)	bold
Authors Information (Single column)	10 (CT)	regular
Abstract	10 (LRJ)	bold
Index Terms (Keywords)	10 (LRJ)	bold
Content	10 (LRJ))	regular
Heading1	10 (CT)	bold (Capitalization)
Heading 2	10 (LJ)	regular
Table Title (Place above the Table)	8 (CT)	regular
Table content	8 (CT)	regular
Figure caption (Place below the figure)	8 (LJ)	regular
Reference Head	10 (CT)	regular (Capitalization)
Reference	8 (LJ)	regular
Author Profiles	10 (LRJ)	bold author name/ profile regular

CT=Centre Text, LJ=Left Justified, RJ=Right Justified, LRJ=Left & Right Justified

II. Composition of the Article

A. Article title

B. Authors information, Write (all) the author's name, affiliation, department, city, country and E-mail (set to Single Column) all.

C. Abstract, Must be under 200 words and not include subheadings or citations. Define all symbols used in the abstract. Do not delete the blank line immediately above the abstract.

D. Index Terms, Enter key words or phrases in alphabetical order, separated by commas.

E. Content

1) Academic article, should include: Introduction, Content, and Conclusion.

2) Research article, should include: introduction, literature review, Materials methods, Results, Discussion, and conclusion.

Clearly summarize the important findings of the paper. It should contain such as objectives, methods and major results.

F. Introduction

The Introduction section of reference text expands on the background of the work (some overlap with the Abstract is acceptable). The introduction should not include subheadings.

G. Pictures, table, etc., Must be use in numerical order in the article, provided the source correctly, cannot use other people' copyright.

Chart should be colored contrastingly or in black and white.

H. Reference

1) Cited in the main text. Indicate the number in the [ ] mark at the end of the text or the name of the referring person. Let the numbers be in the same line of content as [1].

2) Cited after the article. Put all bibliographical reference after articles, and order according to the author's name, please refer IEEE format. The footer reference format is as follows.

III. Rererences

References in research articles and scholarly articles. For academic and research journals, INTERNATIONAL SCIENTIFIC JOURNAL OF ENGINEERING AND TECHNOLOGY (ISJET). The technology defines referrals according to the IEEE format. All references should be listed at the end of the paper using the following.

Basic format for books:

J. K. Author, "Title of chapter in the book," in *Title of His Published Book,* xth ed. City of Publisher, Country if not USA: Abbrev. of Publisher, year, ch. x, sec. x, pp. xxx–xxx.

Examples:

[1] G. O. Young, "Synthetic structure of industrial plastics," in *Plastics,* 2nd ed., vol. 3, J. Peters, Ed. New York: McGraw-Hill, 1964, pp. 15-64.

[2] W.-K. Chen, *Linear Networks and Systems.* Belmont, CA: Wadsworth, 1993, pp. 123-135.

Basic format for periodicals:

J. K. Author, "Name of paper," *Abbrev. Title of Periodical*, vol. x, no. x, pp. xxx-xxx, Abbrev. Month. year.

Examples:

[3] J. U. Duncombe, "Infrared navigation—Part I: An assessment of feasibility," *IEEE Trans. Electron Devices*, vol. ED-11, no. 1, pp. 34-39, Jan. 1959.

[4] E. P. Wigner, "Theory of traveling-wave optical laser," *Phys. Rev*., vol. 134, pp. A635-A646, Dec. 1965.

[5] E. H. Miller, "A note on reflector arrays," *IEEE Trans. Antennas Propagat*., to be published.

Basic format for reports:

J. K. Author, "Title of report," Abbrev. Name of Co., City of Co., Abbrev. State, Rep. xxx, year.

Examples:

[6] E. E. Reber, R. L. Michell, and C. J. Carter, "Oxygen absorption in the earth's atmosphere," Aerospace Corp., Los Angeles, CA, Tech. Rep. TR-0200 (4230-46)-3, Nov. 1988.

[7] J. H. Davis and J. R. Cogdell, "Calibration program for the 16-foot antenna," Elect. Eng. Res. Lab., Univ. Texas, Austin, Tech. Memo. NGL-006-69-3, Nov. 15, 1987.

Basic format for handbooks:

Name of Manual/Handbook, x ed., Abbrev. Name of Co., City of Co., Abbrev. State, year, pp. xxx-xxx.

Examples:

[8] *Transmission Systems for Communications*, 3rd ed., Western Electric Co., Winston-Salem, NC, 1985, pp. 44-60.

[9] *Motorola Semiconductor Data Manual*, Motorola Semiconductor Products Inc., Phoenix, AZ, 1989.

Basic format for books (when available online):

Author. (year, month day). *Title.* (edition) [Type of medium]. *volume (issue).* Available: site/path/file

Example:

[10] J. Jones. (1991, May 10). *Networks.* (2nd ed.) [Online]. Available: http://www.atm.com

Basic format for journals (when available online):

Author. (year, month). Title. *Journal.* [Type of medium]. *volume (issue),* pages. Available: site/path/file

Example:

[11] R. J. Vidmar. (1992, Aug.). On the use of atmospheric plasmas as electromagnetic reflectors. *IEEE Trans. Plasma Sci.* [Online]. *21(3),* pp. 876-880. Available: http://www.halcyon.com/pub/journals/21ps03-vidmar

Basic format for papers presented at conferences (when available online):

Author. (year, month). Title. Presented at Conference title. [Type of Medium]. Available: site/path/file

Example:

[12] PROCESS Corp., MA. Intranets: Internet technologies deployed behind the firewall for corporate productivity. Presented at INET96 Annual Meeting. [Online]. Available: http://home.process.com/Intranets/wp2.htp

Basic format for reports and handbooks (when available online):

Author. (year, month). Title. Comp any . City, State or Country. [Type of Medium]. Available: site/path/file

Example:

[13] S. L. Talleen. (1996, Apr.). The Intranet Archi-tecture: M anaging information in the new paradigm. Amdahl Corp., CA. [Online]. Available:http://www.amdahl.com/doc/products/bsg/intra/infra/html

Basic format for computer programs and electronic documents (when available online):

ISO recommends that capitalization follow the accepted practice for the language or script in which the information is given.

Example:

[14] A. Harriman. (1993, June). Compendium of genealogical software. *Humanist.* [Online]. Available e-mail: HUMANIST @NYVM.ORG Message: get GENEALOGY REPORT

Basic format for patents (when available online):

Name of the invention, by inventor's name. (year, month day). *Patent Number* [Type of medium]. Available: site/path/file

Example:

[15] Musical toothbrush with adjustable neck and mirror, by L.M.R. Brooks. (1992, May 19). *Patent D 326 189* [Online]. Available: NEXIS Library: LEXPAT File: DESIGN

Basic format for conference proceedings (published):

J. K. Author, "Title of paper," in *Abbreviated Name of Conf.*, City of Conf., Abbrev. State (if given), year, pp. xxxxxx.

Example:

[16] D. B. Payne and J. R. Stern, "Wavelength-switched pas- sively coupled single-mode optical network," in *Proc. IOOC-ECOC,* 1985, pp. 585-590.

Example for papers presented at conferences (unpublished):

[17] D. Ebehard and E. Voges, "Digital single sideband detection for interferometric sensors," presented at the 2nd Int. Conf. Optical Fiber Sensors, Stuttgart, Germany, Jan. 2-5, 1984.

Basic format for patents:

J. K. Author, "Title of patent," U.S. Patent x xxx xxx, Abbrev. Month. day, year.

Example:

[18] G. Brandli and M. Dick, "Alternating current fed power supply," U.S. Patent 4 084 217, Nov. 4, 1978.

Basic format for theses (M.S.) and dissertations (Ph.D.):

J. K. Author, "Title of thesis," M.S. thesis, Abbrev. Dept., Abbrev. Univ., City of Univ., Abbrev. State, year.

J. K. Author, "Title of dissertation," Ph.D. dissertation, Abbrev. Dept., Abbrev. Univ., City of Univ., Abbrev. State, year.

Examples:

[19] J. O. Williams, "Narrow-band analyzer," Ph.D. dissertation, Dept. Elect. Eng., Harvard Univ., Cambridge, MA, 1993.

[20] N. Kawasaki, "Parametric study of thermal and chemical nonequilibrium nozzle flow," M.S. thesis, Dept. Electron. Eng., Osaka Univ., Osaka, Japan, 1993.

Basic format for the most common types of unpublished references:

J. K. Author, private communication, Abbrev. Month, year.

J. K. Author, "Title of paper," unpublished.

J. K. Author, "Title of paper," to be published.

Examples:

[21] A. Harrison, private communication, May 1995.

[22] B. Smith, "An approach to graphs of linear forms," unpublished.

[23] A. Brahms, "Representation error for real numbers in binary computer arithmetic," IEEE Computer Group Repository, Paper R-67-85.

Basic format for standards:

Title of Standard, Standard number, date.

Examples:

[24] IEEE Criteria for Class IE Electric Systems, IEEE Standard 308, 1969.

[25] Letter Symbols for Quantities, ANSI Standard Y10.5-1968.

First A. Author and the other authors may include biographies at the end of regular papers. Biographies are often not included in conference related papers. The first paragraph may contain a place and/or date of birth (list place, then date). Next, the author's educational background is listed. The degrees should be listed with type of degree in what field, which institution, city, state, and country, and year the degree was earned. The author's major field of study should be lower-cased.

The second paragraph uses the pronoun of the person (he or she) and not the author's last name. It lists military and work experience, including summer and fellowship jobs. Job titles are capitalized. The current job must have a location; previous positions may be listed without one. Information concerning previous publications may be included. Try not to list more than three books or published articles. The format for listing publishers of a book within the biography is: title of book (city, state: publisher name, year) similar to a reference. Current and previous research interests end the paragraph.

The third paragraph begins with the author's title and last name (e.g., Dr. Smith, Prof. Jones, Mr. Kajor, Ms. Hunter). List any memberships in professional societies. Finally, list any awards and work for committees and publications. If a photograph is provided, the biography will be indented around it. The photograph is placed at the top left of the biography, and should be of good quality, professional-looking, and black and white (see above example). Personal hobbies will be deleted from the biography. Following are two examples of an author's biography.

Second B. Author was born in Greenwich Village, New York City, in 1977. He received the B.S. and M.S. degrees in aerospace engineering from the University of Virginia, Charlottesville, in 2001 and the Ph.D. degree in mechanical engineering from Drexel University, Philadelphia, PA, in 2008. From 2001 to 2004, he was a Research Assistant with the Princeton Plasma Physics Laboratory. Since 2009, he has been an Assistant Professor with the Mechanical Engineering Department, Texas A&M University, College Station. He is the author of three books, more than 150 articles, and more than 70 inventions. His research interests include high-pressure and high-density nonthermal plasma discharge processes and applications, microscale plasma discharges, discharges in liquids, spectroscopic diagnostics, plasma propulsion, and innovation plasma applications. He is an Associate Editor of the journal *Earth*, *Moon*, *Planets*, and holds two patents.

Mr. Author was a recipient of the International Association of Geomagnetism and Aeronomy Young Scientist Award for Excellence in 2008, the IEEE Electromagnetic Compatibility Society Best Symposium Paper Award in 2011, and the American Geophysical Union Outstanding Student Paper Award in Fall 2005.

Third C. Author received the B.S. degree in mechanical engineering from National Chung Cheng University, Chiayi, Taiwan, in 2004 and the M.S. degree in mechanical engineering from National Tsing Hua University, Hsinchu, Taiwan, in 2006. He is currently pursuing the Ph.D. degree in mechanical engineering at Texas A&M University, College Station.

From 2008 to 2009, he was a Research Assistant with the Institute of Physics, Academia Sinica, Tapei, Taiwan. His research interest includes the development of surface processing and biological/ medical treatment techniques using nonthermal atmospheric pressure plasmas, fundamental study of plasma sources, and fabrication of micro- or nanostructured surfaces.

Mr. Author's awards and honors include the Frew Fellowship (Australian Academy of Science), the I. I. Rabi Prize (APS), the European Frequency and Time Forum Award, the Carl Zeiss Research Award, the William F. Meggers Award and the Adolph Lomb Medal (OSA).

Remark: More detail information, Pleases read Preparation of Papers for INTERNATIONAL SCIENTIFIC JOURNAL OF ENGINEERING AND TECHNOLOGY (ISJET), https://ph02.tci-thaijo.org/index.php/isjet/index

Panyapiwat Institute of Management (PIM)
85/1 Moo 2, Chaengwattana Rd,
Bang Talat, Pakkred, Nonthaburi 11120, Thailand
Tel. +66 2855 1560 Fax. +66 2855 0392
https://www.tci-thaijo.org/index.php/isjet/index
https://isjet.pim.ac.th
E-mail: isjet@pim.ac.th